University of Applied Sciences Hamburg

Life Science Faculty

Development of uptake assays for proton-coupled nutrient transporters

Master's thesis

Pharmaceutical Biotechnology

Submitted by

Josi Steinke

[redacted]

Hamburg, 31.08.2021

Thesis evaluator: Prof. Dr. Birger Anspach (HAW Hamburg)

Thesis evaluator: Dr. Katharina Jungnickel (EMBL Hamburg)

The work presented in this thesis was performed in the group of Dr. Christian Loew at the European Molecular Biology Laboratory (EMBL) in Hamburg.

Abstract

A wide range of membrane transporters play an essential role in providing cells with nutrients, maintaining cell homeostasis and mediating signaling processes. Since they were found to contribute in certain diseases and are able to transport selected drug molecules, many transporters were studied with the aim to gain knowledge about the transport mechanisms. Aside from the determination of the protein structure, functional assays provide a valuable tool for transporter characterization. The presented study focused on using label-free functional assays to detect substrate uptake into proteoliposomes driven by proton-coupled membrane transporters. For this purpose, the di- and tripeptide transporter DtpB from *E. coli* was used, which is a member of the Major Facilitator Superfamily. DtpB co-transports protons to drive uptake of small peptides against their concentration gradient. This proton-coupling was used in the functional assays shown here, by directly measuring proton-influx as a result of substrate translocation.

The first assay established for DtpB was based on incorporating the pH-sensitive fluorescent dye pyranine into proteoliposomes and measuring the decrease in fluorescence upon proton-influx. Here, a charge-gradient was applied across the liposomal membrane to facilitate proton-coupled transport. A range of di- and tripeptides was screened for uptake by DtpB using this assay and 11 apparent substrates as well as one peptide with an inhibiting effect were identified. The collected transport data were further plotted against the respective K_D values, which were determined for each peptide by nanoDSF (low volume differential intrinsic tryptophan scanning fluorimetry), to investigate the correlation between affinity and transport activity. This analysis showed that apparent substrates of DtpB clustered in the affinity range of 0.1 mM ≤ K_D ≤ 4 mM and for most peptides outside this range no transporter mediated proton-influx was measured. Furthermore, the pyranine-based assay was also established for the Anion:Cation symporters LgoT and DgoT, as previously shown by Bartels (2020) and Leano et al. (2019), to further verify the assay and stereospecificity of both transporters was shown. Also, the K_D and V_{max} values were determined for selected substrates of all three transporters.

The second uptake assay used here was a Solid Supported Membrane approach from the company Nanion, where proteoliposomes were attached onto a lipid bilayer on a gold coated sensor. Electrodes measured proton-flux into the liposomes as a change in current due to capacitive coupling of the liposomes to the sensor. With this assay, the transport of selected substrates identified in the pyranine-based assay was verified in absence of a membrane potential.

In the frame of the presented work, both assays were shown to reliably detect transporter mediated proton-uptake and allow screening of a large number of compounds.

Acknowledgements

Firstly, I want to thank Prof. Dr. Birger Anspach from HAW Hamburg for supervising my work and supporting me during my studies.

Furthermore, I want to acknowledge Dr. Christian Loew for giving me the opportunity to work in his research group at EMBL Hamburg and for his professional advice.

Special thanks go to Dr. Katharina Jungnickel, who supervised my work in the lab and shared her expertise with me. I am grateful for her continuous support and helpful advice, whenever I needed it.

Moreover, I want to thank Kim Bartels for sharing her knowledge with me and helping me to get started at EMBL.

A great thanks to Dr. Vadim Kotov for his work in data processing and to Maxime Killer and Giada Finocchio for sharing their data with me.

Furthermore, I want to express my gratitude to Florian Gabriel, who helped me with tips and advice during the writing process.

Finally, I am thankful for the support of Jo and my family, who always believe in me and motivate me.

Table of Content

List of abbreviations

%	percent
°C	degree celsius
μ_{c+}/μ_{c+}	mean positive/negative control
µL	microliter
µm	micrometres
µM	micomolar
α	amplitude of the exponent
ACS	Anion:Cation symporter
ADP	Adenosine diphosphate
ATP	Adenosine triphosphate
Ca^{2+}	calcium ion
Ca^{2+}-ATPase	calcium adenosine triphosphatase
CCCP	Carbonyl Cyanide m-Chlorophenylhydrazone
Cl^-	chloride ion
CMC	critical micelle concentration
Cs^+	cesium ion
CV	column volumes
DDM	n-Dodecyl-β-D-Maltoside
DM	n-Decyl-β-D-Maltopyranoside
DMSO	Dimethyl sulfoxide
Dnase	deoxyribonuclease
DPhPC	1,2-diphytanoyl-sn-glycero-3-phosphocholine
Dtp	Di- and tripeptide
E. coli	Escherichia coli
EDTA	Ethylenediaminetetraacetic acid
F	Faraday constant
F_{crit}	critical value
g	gram
h	hour
H^+	hydrogen atom
HEPES	4-(2-hydroxyethyl)-1-piperazineethanesulfonic acid
IC_{50}	half maximal inhibitory concentration
IPTG	Isopropyl β-D-1-thiogalactopyranoside
K^+	potassium ion
K_D	dissociation constant
kDa	kilodalton
kJ	kilojoule
K_M	michaelis constant
L	Liters
LB	lysogeny broth
m	electrical charge
M	Molar
mAU	milli absorption units

MFS	Major Facilitator Superfamily
mg	Milligramme
MilliQ water	ultrapure water
min	minutes
mL	millilitre
mM	millimolar
mV	millivolt
MWCO	molecular weight cutt-off
nA	nanoampere
Na^+	sodium ion
Na+/K+-ATPase	sodium-potassium adenosine triphosphatase
nanoDSF	low volume differential intrinsic tryptophan scanning fluorimetry
nF	nanofarad
ng	nonogram
$NH4^+$	ammonium ion
Ni-IMAC	Nickel-immobilized metal affinity chromatography
nm	nanometre
nm	nanometer
nS	nanosiemens
OD optical density	optical density
PBS	Phosphate-buffered saline
pKa	negative base-10 logarithm of the acid dissociation constant
pK_D	negative base-10 logarithm of the dissociation constant
POPE	1-palmitoyl-2-oleoyl-sn-glycero-3-phosphoethanolamine
POPG	1-palmitoyl-2-oleoyl-sn-glycero-3-phospho-(1'-rac-glycerol)
POT	proton-dependent oligopeptide transporter
psi	Pound-force per square inch
R	molar gas constant
Rb^+	rubidium ion
RFU	relative fluorescence
rpm	rotations per minute
RSS	squared sum of the residuals
RT	room temperature
SDS-PAGE	Sodium Dodecyl Sulfate Polyacrylamide Gel Electrophoresis
sec	second
SEC	Size Exclusion Chromatography
SLC	Solute Carriers
SSM	Solid Supported Membrane
T	absolute temperature
t_0	starting time point
TB	Terrific Broth
TCEP	tris(2-carboxyethyl)phosphine
TEV	Tobacco Etch Virus protease
TM	transmembrane helix
V_{max}	maximum reaction velocity
V-type ATPase	Vacuolar-type ATPase
w/v	weight per volume

xg	times gravity
Δμ	electrochemical membrane potential
$\Delta\mu_{H}+$	proton electrochemical gradient
ΔG	Gibbs energy change
ΔH	change in enthalpy
Δp	protonmotive force
ΔpH	concentration difference of protons
ΔS	change in entropy
ΔΨ	difference in electrical potential
σ_{c+}/σ_{c-}	standard deviation positive/negative control
τ	time constant

List of Figures

List of Tables

1 Introduction

Cellular membranes are lipid bilayers with a hydrophobic interior and hydrophilic surface forming a physical barrier around cells, nuclei and cell organelles (Shi, 2013). This barrier is semipermeable for biologically important molecules and therefore enables a controlled environment inside the cell (Daniel et al., 2006). To maintain cell homeostasis and facilitate cell growth, metabolism and signal transduction, a wide range of highly specific transporters play an essential role (Drew et al., 2021). They are integral membrane proteins and specifically transport molecules like ions, sugars, lipids, nucleobases and amino acids across biological membranes (Shi, 2013). Membrane transporters have distinct features that separate them from membrane channels (Shi, 2013). In an activated state, a membrane channel simultaneously allows permeation of molecules from both sides of the membrane with a turnover rate close to the limit of diffusion (Shi, 2013). Molecules can only move down their concentration gradient, which is also described as passive transport (Shi, 2013). Opposed to that, a transporter undergoes conformational changes to complete one transport cycle, transferring a molecule from one side of the membrane to the other (Drew et al., 2021). The transporter is never accessible from both sides at the same time (Drew et al., 2021). This type of transport can be directed against the concentration gradient of the substrate and therefore requires energy input, which is also termed active transport (Yan, 2015). The mechanism of transport is not yet fully understood and depends on the type of transporter (Shi, 2013).

To examine the transport mechanism, the structures of many transporters were determined e.g., by X-Ray crystallography or cryogenic electron microscopy (Quistgaard et al., 2016; Cheng, 2018). Structures of transport proteins in different states of the transport cycle can give meaningful insights into the transport process (Quistgaard et al., 2016). Also, the ability of a transporter to bind to different molecules can be tested to get an estimation about potential substrates (Quistgaard et al., 2016). Structures of transport proteins with a ligand in the binding site can give information on how the binding site interacts with different molecules and how substrates might be recognized (Newstead et al., 2011). However, binding of a ligand does not necessarily mean that it is transported (Drew et al., 2021). Functional assays are an essential addition to structural information in understanding the mechanisms of membrane transporters (Volpe, 2016). They can be used to find substrates or inhibitors of a transporter, which is useful to understand the function of a transporter *in vivo* (Volpe, 2016). Also, this information can improve drug development, e.g. with the aim of increasing uptake of a drug molecule by a certain transporter (Drew et al., 2021). Optimising the structure of a drug molecule to be recognised by a membrane transporter can improve absorption and bioavailability of the drug (Drew et al., 2021).

1.1 The Major Facilitator Superfamily

All membrane transporters used in this project belong to the Major Facilitator Superfamily (MFS), the largest family of secondary active transporters (Drew et al., 2021). The family is divided into more than 80 subfamilies, all transporting a different set of compounds (Drew et al., 2021). MFS transporter substrates include ions, nucleosides, amino acids, short peptides, vitamins and lipids (Reddy et al., 2012). As they are responsible for nutrient uptake, metabolite extrusion and also multidrug resistance, MFS transporters play a crucial role in cell growth, metabolism and homeostasis (Yan, 2015). Some are also involved in signalling processes between cells and intracellular compartments or in neurotransmission (Yan, 2015). Human solute carriers (SLCs) that belong to the MFS family are mostly found in the intestine, liver, kidney and brain (Yan, 2015). Dysfunctions of these transporters can be related to cancer, Alzheimer's disease and different metabolic diseases, which makes them potential drug targets (Yan, 2015). Furthermore, MFS transporters that are involved in multidrug resistance in bacteria or fungi might be useful in the development of antimicrobial drugs (Drew et al., 2021). For example, in *E. coli* 19 out of 37 putative multidrug resistance transporters belong to the MFS (Drew et al., 2021). Also, MFS transporters can be candidates for delivery of orally administered drugs, as some have been found to transport toxins and drug molecules (Drew et al., 2021).

1.1.1 Protein structure and transport mechanism

MFS transporters are between 40-60 kDa in size and show a sequence similarity of approximately 12-18 % (Reddy et al., 2012). They generally consist of 12 transmembrane helices (TMs) (approx. 75 %) organised into an N- and a C-domain, but also members with 13-16 TMs are known (Reddy et al., 2012). The domains are connected by an unstructured loop or α-helices and show a quasi-twofold symmetry axis perpendicular to the membrane plane (Yan, 2013). All members share this MFS-fold (Drew et al., 2021). Each domain contains six TMs that might either originate from two inverted repeats of 3 TMs or a triplicate of 2 TMs but no clear evolutionary proof has yet been provided for one of the two theories (Drew et al., 2021). The substrate-binding cavity is located between the two domains halfway into the membrane (Yan, 2013).

Regarding the transport mechanism of MFS transporters, the alternating access model has been proposed already in 1966 (Jardetzky, 1966).

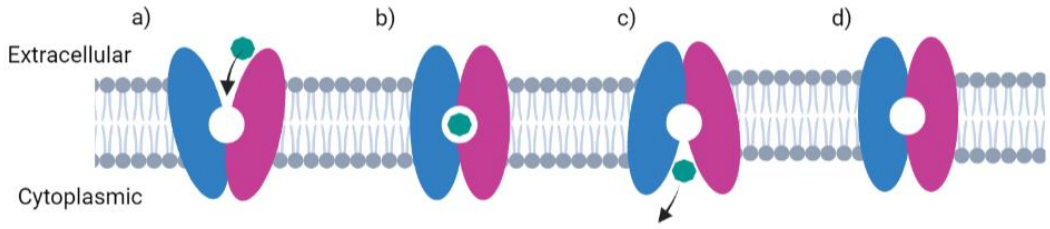

Figure 1: Schematic illustration of the alternating access mechanism in membrane transporters. *Substrate is bound to the transporter in the outward-open conformation (a), then it changes to the occluded conformation with the substrate caught in the binding site (b). In the inward-open conformation (c) the substrate is released, and the apo-form of the transporter returns to the occluded state (d) to begin a new transport cycle from the outward-open state. Created in BioRender.com.*

It has been well established that a transporter undergoes conformational changes adopting at least three different conformational states during the transport process (Figure 1) (Quistgaard et al., 2016). The substrate binding site is never exposed to both sides of the membrane simultaneously, but alternatively to one side only (Yan, 2013). When a transporter is in its outward-open state, the binding site is exposed to the extracellular space and a substrate can bind (Quistgaard et al., 2016). Rigid body rotation then leads to the occluded state, where the binding site is not accessible from either side and the substrate is trapped inside the protein (Yan, 2013; Quistgaard et al., 2016). To maintain electrochemical gradients over the membrane, the occluded state is crucial (Drew et al., 2021). The inward-open conformation is induced by further conformational changes and the binding site gets exposed to the cytoplasm where the substrate is released (Quistgaard et al., 2016). The apo-form of the transporter then returns back to the outward-open conformation (Quistgaard et al., 2016). Structures of different MFS transporters have been identified, that reveal the inward- and outward-open conformations (Quistgaard et al., 2013). The proton-dependent xylose/H+ symporter was the first MFS transporter with structures of both conformations available (Figure 2) (Quistgaard et al., 2013).

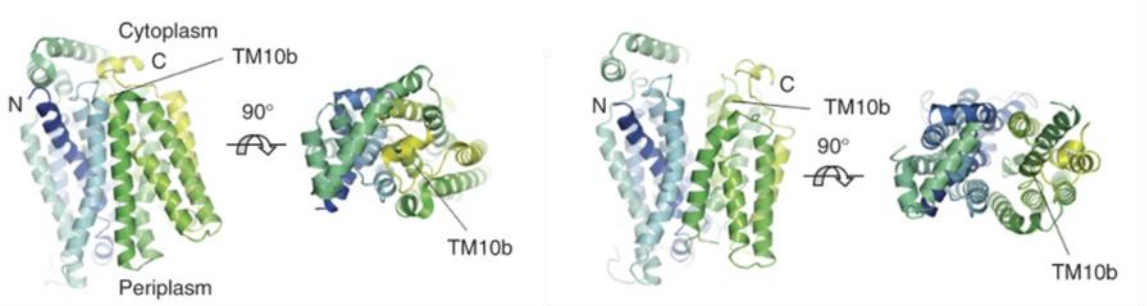

Figure 2: structure of the xylose transporter XylE from E. coli in partially occluded outward state (left, PDB 4GBY) and inward open state (right, PDB 4JA4). *Both structures are shown in cartoon representation, in the same orientation. Transmembrane helix 10b is labelled and N- and C-terminus are indicated, respectively (modified from Quistgaard et al., 2013).*

Still, not all details regarding the transport mechanism are known, in particular how transport is induced and which molecular interactions are crucial for conformational changes of the transporter (Quistgaard et al., 2016). Different models have been proposed to describe the rotation of the two domains but it yet remains a mystery how exactly a transporter moves within the biological membrane (Drew et al., 2021).

1.2 Membrane potential as a driving force for transport

Electrochemical membrane potentials play a crucial role in signal transduction, energy production and solute transport in a cell (Hammond, 2015). In mitochondria, for example, electron transport is coupled to the translocation of protons from the matrix into the intermembrane space to generate an electrochemical proton gradient (Esteras et al., 2020). The energy from this gradient is used for the generation of ATP from ADP by the ATP-synthase (Esteras et al., 2020). Furthermore, a stable electrochemical gradient is maintained across the plasma membrane of a cell by different ion pumps and transporters (Ramahi and Ruff, 2014). This potential is determined by two compounds, the electrical membrane potential and the concentration difference of an ion (Ramahi and Ruff, 2014). The latter one forces ions to diffuse towards the side of the membrane with a lower concentration of the respective ion (Hammond, 2015). The electrical potential attracts positively charged ions towards the negatively charged side of the membrane and vice versa (Hammond, 2015). Under physiological conditions a cell has a negative intracellular potential, with higher extracellular concentrations of sodium (Na^+), calcium (Ca^{2+}) and chloride (Cl^-) ions and a higher intracellular concentration of potassium (K^+) ions (Ramahi and Ruff, 2014). These concentration gradients are mainly maintained by the Na^+/K^+-ATPase and the Ca^{2+}-ATPase, which are primary-active transporters driven by the energy obtained from ATP hydrolysis (Hammond, 2015). The Na^+/K^+-pump exports three sodium ions in exchange for two potassium ions, while the Ca^{2+}-ATPase exports Ca^{2+} ions out of the cell (Hammond, 2015). For *E. coli* cells (K12) during the exponential growth phase, the membrane potential ranges between -220 mV and -140 mV depending on the age of the cells (Bot and Prodan, 2010).

Transporters that use the energy stored in the electrochemical membrane potential ($\Delta\tilde{\mu}$) to move substrates against their concentration gradient are called secondary-active transporters (Shi, 2013). MFS transporters can co-transport ions or solutes, either together with the substrate (symport) or in the opposite direction (antiport) (Figure 3) (Drew et al., 2021).

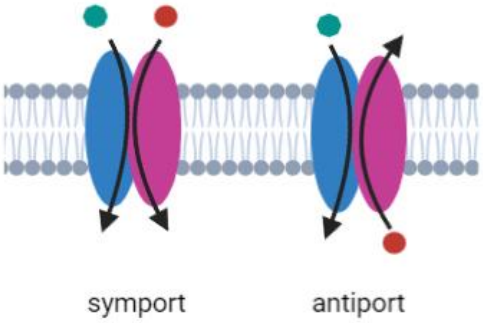

Figure 3: Schematic illustration of symport and antiport mechanisms in membrane transporters. *Two molecules can either be co-transported across the cell membrane in the same direction (symport) or in the opposite direction (antiport). Created in BioRender.com.*

They can perform electrogenic transport, meaning they transport a net charge over the membrane, or electroneutral transport, where no net charge is transported (Drew et al., 2021). Cotransport of ions enables transport against the substrate gradient because the transport direction is defined by the charge gradient (Nicholls and Ferguson, 2013). This coupling is necessary as a driving force for solute transport uphill a concentration gradient because it is energetically unfavourable to concentrate a solute or e.g. for a negatively charged solute to be transported into a negatively charged interior (Nicholls and Ferguson, 2013). Consequently, MFS transporters have the ability to accumulate a substrate inside the cell or deplete it (Quistgaard et al., 2016). This is especially important for bacteria to survive in varying environments because in the external medium nutrients are mostly present at low concentrations, but they are needed in higher concentrations in the cytoplasm to maintain metabolism (Nicholls and Ferguson, 2013). The majority of MFS families cotransport protons as the driving force but also sodium-coupled transporters are known (Drew et al., 2021).

Generally, there are two components involved in a proton electrochemical gradient ($\Delta\tilde{\mu}_{H^+}$), the difference in electrical potential (ΔΨ) and the concentration difference of protons (ΔpH) (Nicholls and Ferguson, 2013). $\Delta\tilde{\mu}_{H^+}$ is expressed in kJ/mol but can be converted into the protonmotive force (Δp) in mV (Nicholls and Ferguson, 2013). The energy that is stored in an electrochemical potential can be calculated as the Gibbs energy change (ΔG) (Nicholls and Ferguson, 2013). The Gibbs-Helmholtz equation (eq. 1) describes this energy change taking into account the changes in enthalpy (ΔH) and entropy (ΔS) of a system, with T being the absolute temperature (Nicholls and Ferguson, 2013).

$$\Delta G = \Delta H - T\Delta S \quad (1)$$

A variant of the Gibbs energy change specifically allows determination of an electrochemical ion gradient (Nicholls and Ferguson, 2013). Therefore, both ΔΨ and the concentration gradient of ions need to be taken into consideration (Nicholls and Ferguson, 2013). The transfer of 1 mol of a solute

from concentration $[X]_A$ to $[X]_B$ in the absence of a membrane potential is defined by equation (2), with R being the molar gas constant (Nicholls and Ferguson, 2013).

$$\Delta G = 2.3RT \log_{10} \frac{[X]_B}{[X]_A} \quad (2)$$

For the transport of 1 mol of a cation X^{m+} driven by a membrane potential ΔG is described by the equation:

$$\Delta G = -mF\Delta\Psi \quad (3)$$

with F being the Faraday constant and m being the electrical charge of the ion (Nicholls and Ferguson, 2013). Taken together, the transport of a cation down an electrical potential from concentration $[X^{m+}]_A$ to $[X^{m+}]_B$ can be calculated using equation (4) (Nicholls and Ferguson, 2013).

$$\Delta G = -mF\Delta\Psi + 2.3RT \log_{10} \left\{ \frac{[X^{m+}]_B}{[X^{m+}]_A} \right\} \quad (4)$$

If the ion gradient is a proton electrochemical gradient, this can be simplified to equation (5) (Nicholls and Ferguson, 2013).

$$\Delta\tilde{\mu}_{H^+} = -F\Delta\Psi + 2.3RT\Delta pH \quad (5)$$

For the determination of ΔΨ the equilibrium Nernst equation (eq. 6) can be used, which is derived from equation (4) in the equilibrium state with ΔG = 0 (Nicholls and Ferguson, 2013).

$$\Delta\Psi = 2.3 \frac{RT}{mF} \log_{10} \left\{ \frac{[X^{m+}]_B}{[X^{m+}]_A} \right\} \quad (6)$$

This results in the Nernst potential for an ion gradient at its equilibrium state, which can be used for ion gradients resulting from redistribution of an ion by electrical uniport across the membrane to restore their electrochemical equilibrium (Nicholls and Ferguson, 2013). One way to reach this is to add a salt to one side of a membrane, which is semi-permeable and only allows the anion or the cation of the salt, but not both, to permeate the bilayer (Nicholls and Ferguson, 2013).

1.3 Uptake assays for membrane transporters

To date, different methods have been established for measuring the uptake of various substances by a membrane transporter. Often cells overexpressing the transporter of interest or membrane preparations of these are used for transport or inhibition assays (Volpe, 2015). Using cells for *in vivo*

assays can provide valuable information on substrate-transporter interactions because the transporter is studied in its physiologic environment (Volpe, 2015). However, due to the presence of other membrane transporters with overlapping activities in a cell, the transport activity might not be clearly assigned to one transporter (Volpe, 2015). This approach is also not suitable for transporters localised to organelle membranes (Drew et al., 2021). Alternatively, liposomes containing purified protein can be used for *in vitro* assays (Drew et al., 2021). Liposomes are vesicles consisting of a lipid bilayer with an aqueous phase inside and can be composed of various lipid compositions (Torchilin, 2005). Proteoliposomes are generated by mixing lipid vesicles with a pure protein solubilised in detergent (Rigaud and Lévy, 2003). The protein will incorporate into the liposomes together with the detergent, forming mixed lipid-protein-detergent micelles (Rigaud and Lévy, 2003). Removal of detergent should leave the protein in the lipid vesicle, which stabilises the protein in the absence of detergent (Rigaud and Lévy, 2003). This approach is considered as the golden standard in uptake assays because it enables a complete control of the conditions inside and outside the vesicle and to specifically examine the activity of one transporter protein (Drew et al., 2021). Also, it is possible to apply an electrochemical potential across the lipid bilayer and thus investigate the influence of a pH- or ion-gradient on the transporter (Drew et al., 2021).

For most functional studies on MFS transporters, *in vivo* uptake assays in *E. coli* with labelled substrates were utilized (Volpe, 2015). For this, a certain amount of cells overexpressing the protein of interest is transferred into a well plate and mixed with buffer containing a fluorescent or radiolabelled substrate (Harder et al., 2008). The substrate is taken up by the engineered cells but in theory significantly less by cells not overexpressing the protein (Harder et al., 2008). The transport reaction is allowed to continue for a defined time and then stopped by separating the cells from the supernatant (Harder et al., 2008). The amount of transported substrate can then be determined by measuring the fluorescent or radioactivity signal within the cells (Harder et al., 2008; Ernst et al., 2009). To determine transport inhibition by other substances, a mixture of the labelled substrate and an unlabelled ligand is added to the cells and uptake is measured as before (Ernst et al., 2009). Using different concentrations of the new ligand, an IC_{50} value can be determined, or uptake rates can be calculated taking the substrate concentration at different time points of a reaction (Ernst et al., 2009). This type of assay provides information on the uptake of the labelled substrates but not on transport of the unlabelled ligands (Ernst et al., 2009). For these, only competition with the binding site can be reported (Ernst et al., 2009). Alternatively, uptake assays with labelled substrates can also be performed in liposomes or vesicles containing purified protein instead of using whole cells (Harder et al., 2008). An advantage of using a radiolabelled substrate is the high sensitivity of the assay (Shen and Karner, 2021). However, this method bares safety hazards due to the radiation the experimenter is

exposed to (Yamamoto et al., 2011). Also, the availability of suitable isotope-labelled substrates is limited and they are mostly relatively costly (Yamamoto et al., 2011).

In the recent years, also methods to measure uptake without using any labelled or fluorescent substrates were developed (Drew et al., 2021). For this, mostly purified protein reconstituted into bacterial membranes or liposomes are used because their internal environment can be controlled (Drew et al., 2021). A method that was established for different transporters is to load the liposomes with a fluorescent dye, that is sensitive to a certain molecule or ion, and changes its fluorescent behaviour upon substrate uptake into the liposome (Parker et al., 2014). An example for this is the pH-sensitive dye pyranine (Trisodium 8-hydroxypyrene-1,3,6-trisulfonate, Figure 4), which was used for functional characterisation of the proton-dependent oligopeptide transporter (POT) $PepT_{St}$ (Kano and Fendler, 1977; Parker et al., 2014). Pyranine is not able to permeate the bilayer and its spectral properties are well characterised (Kano and Fendler, 1977).

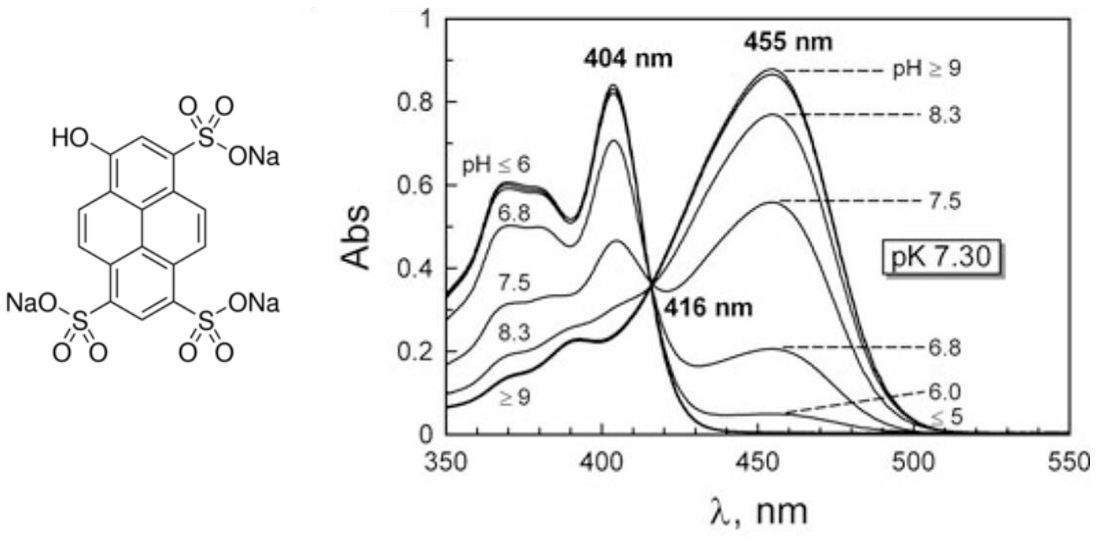

Figure 4: Structural formula of pyranine in protonated form (left; Pyranine Sigma-Aldrich, 2021) and absorbance spectra of pyranine (right). *Pyranine is a negatively charged pH sensitive fluorescent dye. Its three sulfonate groups are all ionized over the entire pH range. The absorbance of 40 µM pyranine was measured in aqueous buffer solutions at different pH (Fedosov et al., 2012).*

The absorbance spectrum of pyranine in Figure 4 indicates a stable absorbance value over a pH range from 5.0 to 9.0 at a wavelength of 416 nm. Opposed to that, absorbance maxima at 404 nm and 455 nm are pH dependent. At pH 5.0 only the excitation maximum at 404 nm exists, while pH 9.0 only shows an excitation maximum at 455 nm. These characteristics make pyranine a suitable dye for detection of proton influx into the liposome (Kano and Fendler, 1977). Absorbance at 416 nm can be used as a reference signal that represents the pyranine concentration in the sample, as long as the pH is in the range from 5.0 to 9.0. Normalising absorbance at 455 nm to the absorbance at 416 nm provides a measure for pH independently of the pyranine concentration. Additionally, pyranine is

highly available and detectable in low concentrations, below the µM range (Kano and Fendler, 1977). The downside of using pyranine in liposomal uptake assays is that the buffer capacity has to be kept low in order to allow detection of small changes in pH and it is only suitable for transporters inducing a pH change upon substrate transport. Also, this method is an indirect measurement of substrate transport as a function of proton movement and does not detect a substrate directly (Parker and Newstead, 2014).

To test proton-coupling of a transporter, an artificial membrane potential can be generated in liposome-based assays (Harder et al., 2008). Therefore, proton permeability of the liposomes should be as small as possible to maintain a proton-gradient over a defined time span (Tsai and Miller, 2013). One way to generate a potential is to apply a pH-gradient across the liposomal membrane (Foucaud, 1992). This principle was applied in 1992 for the functional characterisation of the Lactose transport system of *Streptococcus thermophilus* (Foucaud, 1992). Apart from that, V-type ATPases can be reconstituted into the liposomes in addition to the protein of interest to generate a proton-gradient (Harder et al., 2008). An example would be, the cytochrome c oxidase which is able to transport protons across biological membranes in presence of ascorbate (Harder et al., 2008).

Ionophores present another way for induction of a membrane potential by selectively transporting ions across membranes (Nicholls and Ferguson, 2013). An example for this is valinomycin, a natural antibiotic from *Streptomyces*, which acts as a mobile carrier for Cs^+, Rb^+, K^+ or $NH4^+$ (Figure 5) (Nicholls and Ferguson, 2013).

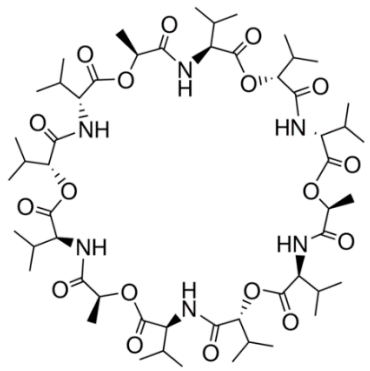

Figure 5: Structural formula of valinomycin, a neutral cyclic dodecadepsipeptide antibiotic *(Valinomycin Sigma-Aldrich, 2021). Valinomycin consists of a 36-member ring and selectively transports potassium ions across cell membranes by binding them in the centre of the ring structure (Nicholls and Ferguson, 2013).*

Valinomycin can diffuse across the membrane in complexed and uncomplexed form (Nicholls and Ferguson, 2013). Opposed to other K^+ uniporters, it has a high selectivity for K^+ over Na^+ (Nicholls and Ferguson, 2013). Applying a higher KCl concentration inside the liposomes than outside leads to an

inward directed charge-gradient upon addition of valinomycin because only K^+ can permeate the membrane but not Cl^- (Nicholls and Ferguson, 2013).

Another method to study electrogenic ion-coupled transporters is the Solid Supported Membrane (SSM) based method, where currents induced by ion transport are measured (Bazzone et al., 2017). There, liposomes are attached to a gold coated sensor chip, which is placed into a Faraday cage (Bazzone et al., 2017). An inward or outward directed substrate gradient can be generated by rinsing the sensor with a respective buffer (Bazzone et al., 2017). Electrogenic uptake of the substrate changes the potential inside the liposomes and the charging current can be detected (Bazzone et al., 2017). This current is used as an indirect measure for ion-coupled substrate uptake (Bazzone et al., 2017). The method has been successfully applied to investigate the function of different ATP-dependent ion pumps but also symporters, including PepT1 and bacterial POTs (Bazzone and Barthmes, 2020). The SSM-based technology provides a sensitive method for rapid and automated compound screening as various compounds can be tested on one sensor (Gerbeth-Kreul et al., 2021). This makes it suitable for pharmaceutical drug screening processes and it can be useful as a validation method in combination with other uptake assay methods (Gerbeth-Kreul et al., 2021). A general disadvantage of the method´s dependence on ion-coupled transport is that the amount of substrate that was taken up into the liposome is not measured directly (Bazzone et al., 2017).

1.4 Aim of project

The main aim of this study was to develop label-free liposomal uptake assays for proton-coupled transporters as an alternative to using radiolabelled substrates. First, an uptake assay using the fluorophore pyranine as a reporter dye was established for DtpB (di- and tripeptide transporter B), a POT from *E. coli* (Newstead, 2015). The POT family is a subfamily of the MFS and POT members can be found in mammals, bacteria, fungi, plants and yeast (Parker et al., 2014). They are known to transport di- and tripeptides with a high promiscuity, meaning a transporter can recognise a variety of different peptides in the same binding site (Parker et al., 2014). The human POTs PepT1 and PepT2 are some of the most promiscuous transporters known and are potential drug targets as they were found to transport peptide-like drug molecules, for example ß-lactam antibiotics, angiotensin converting enzyme inhibitors or antiviral nucleoside prodrugs (Guettou et al., 2013; Parker et al., 2014). The structure of DtpB was recently solved in the Loew group (Jian Lei and Maxime Killer, EMBL Hamburg) and structures with different peptides located in the binding site were obtained. Additionally, binding affinity of various ligands was determined with the aim of identifying the

mechanisms underlying promiscuity of the transporter. From these data the question arose whether the ligands obtained in the structures are also substrates of the transporter and whether there is a correlation between ligand binding and transport activity. It was hypothesised that affinity measurements could be used to predict whether a peptide is transported or not. To address this, several peptides with known affinity were tested for transport in the pyranine-based uptake assay with DtpB. The transport data could also help to identify specific peptide characteristics that are essential for transport activity. Furthermore, testing various peptides gave an estimation of the suitability of this assay for high-throughput screening and of its reproducibility.

The SSM-based uptake assay was established for DtpB as a second label-free approach. This technique is suitable for high-throughput screening with a high degree of automation. Here, substrate driven transport was tested for some peptides that previously showed transport activity in the pyranine-based uptake assay, as a verification. Opposed to the pyranine-based assay, this one was performed in the absence of a membrane potential.

For further validation of the pyranine-based uptake assay a second MFS transporter from *E.* coli, the putative L-galactonate transporter (LgoT), was studied. LgoT belongs to the subfamily of ACS (Anion:Cation symporter) transporters and the structure of the empty transporter was recently solved in the Loew group (Kim Bartels, EMBL Hamburg) (Bartels, 2020). The structure and function of the proton-coupled D-galactonate transporter DgoT were previously investigated, revealing its high specificity for D-galactonate (Leano et al., 2019). In this study, both LgoT and DgoT were examined in the pyranine-based uptake assay to probe their stereospecificity and at the same time assess suitability of the uptake assay for different transporter types. As L-galactonate is not commercially available as a radioactively labelled molecule, a label-free alternative was especially important for functional studies of LgoT.

2 Materials

2.1 Chemicals

Table 1: chemicals used in the described experiments.

Chemical	Supplier	Cat number
1-octadecanthiol	Sigma-Aldrich	8.14444
CCCP	Sigma-Aldrich	C2759-250MG
Trichlomethan/chloroform	Carl Roth GmbH +Co KG	3313.4
DDM	Anatrace Products	D310S
D-galactonate	Sigma-Aldrich	44511-100MG
DM	Anatrace Products	D322S
D(+)-Galactose >98%	Carl Roth GmbH +Co KG	4987.2
Glycerol	Carl Roth GmbH +Co KG	4043.1
HEPES	Carl Roth GmbH +Co KG	9105.3
Imidazole	Carl Roth GmbH +Co KG	X998.4
IPTG	Carl Roth GmbH +Co KG	2316.4
2-Propanol	Carl Roth GmbH +Co KG	AE73.1
K_2HPO_4	Carl Roth GmbH +Co KG	P749.2
kanamycinsulfat	Carl Roth GmbH +Co KG	T832.4
KCl	Carl Roth GmbH +Co KG	6781.1
KH_2PO_4	Carl Roth GmbH +Co KG	3904.1
L-galacto-1,4-lactone	Carbosynth Ltd.	R620 6NE
$MgSO_4$	Carl Roth GmbH +Co KG	0261.1
NaCl	Carl Roth GmbH +Co KG	3957.2
NaOH	Carl Roth GmbH +Co KG	6771.1
NaH_2PO_4	Carl Roth GmbH +Co KG	K300.2
Na_2HPO_4	Carl Roth GmbH +Co KG	X987.2
n-decane	Sigma-Aldrich	8.03405
pentane	Sigma-Aldrich	C5H12
proteinase inhibitor (EDTA-free)	Roche Diagnostics GmbH	43203100
pyranine	Sigma-Aldrich	H1529-1G
TCEP	Soltec Ventures	M115
Triton-X 100	Carl Roth GmbH +Co KG	3051.4
valinomycin	Sigma-Aldrich	V0627-10MG

2.2 Peptides and amino acids

Table 2: peptides and amino acids used in the described experiments.

Name	Supplier
AA	Sigma-Aldrich
AAAA	Bachem
AAA	Bachem
AAY	Bachem
AD	Bachem
AF	Sigma-Aldrich
AI	Bachem
AL	Sigma-Aldrich
ALA	Bachem
APF	Bachem
AV	Bachem
AW	Bachem
βAβA (bAbA)	Bachem
EK	Bachem
GG	Sigma-Aldrich
GGG	Sigma-Aldrich
GH	Sigma-Aldrich
KA	Bachem
KV	Bachem
L-alanine	Fluka
L-Valine	Sigma-Aldrich
MS	Sigma-Aldrich
NV	Bachem
PR	Bachem
SL	Bachem
SY	Bachem
TF	Bachem
WG	Sigma-Aldrich
YQ	Bachem

2.3 Lipids

Table 3: lipids used in the described experiments.

Lipid	Supplier	Cat number
1-palmitoyl-2-oleoyl-sn-glycero-3-phosphoethanolamine (POPE)	Avanti Polar Lipids, Inc.	850757P
1-palmitoyl-2-oleoyl-sn-glycero-3-phospho-(1'-rac-glycerol) (sodium salt) (POPG)	Avanti Polar Lipids, Inc.	840457P
1,2-diphytanoyl-sn-glycero-3-phosphocholine (DPhPC)	Merck	850356C

2.4 Enzymes

Table 4: enzymes used in the described experiments.

Enzyme	Supplier	Cat number
Dnase	AppliChem	A3778 0500
Lysozyme, from chicken egg	Sigma-Aldrich	62971-106-F
TEV protease	EMBL Hamburg	-

2.5 Medium

Table 5: chemicals used in the described experiments.

Medium	Supplier	Cat number
LB	Carl Roth GmbH +Co KG	6669.2
LB-Agar	Carl Roth GmbH +Co KG	6671.1
TB	Carl Roth GmbH +Co KG	3556.2

2.6 Plasmids

Table 6: plasmids used in the described experiments.

Protein name	Base vector	Tag	Cleavage site
DtpB	pNIC-CTHF	C-terminal 6xHis-tag	TEV protease
DgoT	pBAD_MCS	C-terminal 6xHis-tag	TEV protease
LgoT	pNIC28-Bsa4	C-terminal 6xHis-tag	TEV protease

2.7 Buffers

Table 7: Composition of buffers used in the described experiments.

Name	Composition
1 x PBS	137 mM NaCl 2.7 mM KCl 10 mM Na2HPO4 1.8 mM KH2PO4
NaPi, 0.5 M, pH 8.0	0.46 M Na_2HPO_4 0.04 M NaH_2PO_4
Lysis buffer, DtpB	1xPBS 15 mM Imidazole, 300 mM NaCl
Lysis buffer, ACS	20 mM NaPi 15 mM Imidazole 300 mM NaCl 5 % Glycerol
wash buffer 1, DtpB	1xPBS 150 mM NaCl 0.1 % DDM, 20 mM Imidazole
wash buffer 1, ACS	20 mM NaPi 150 mM NaCl 5 % Glycerol 0.03% DDM
wash buffer 2, DtpB	1xPBS 150 mM NaCl 0.1 % DDM 30 mM Imidazole
wash buffer 2, ACS	20 mM NaPi 150 mM NaCl 5 % Glycerol 0.03% DDM 10 mM Imidazole
elution buffer, DtpB	1xPBS 150 mM NaCl 0.1 % DDM 0.2 250 mM Imidazole
elution buffer, ACS	20 mM NaPi 150 mM NaCl 5 % Glycerol 0.03% DDM 200 mM Imidazole
dialysis buffer, DtpB	20 mM HEPES pH 7.5 150 mM NaCl 0.03 % DDM
dialysis buffer, ACS	20 mM HEPES pH 7.0 200 mM NaCl 5 % Glycerol

	0.3% DM
Gel filtration buffer, DtpB	20 mM HEPES pH 7.5 150 mM NaCl 0.3 % DM
Gel filtration buffer, ACS	20 mM HEPES pH 7.0 200 mM NaCl 5 % Glycerol 0.3% DM
KPi, 50 mM, pH 7.0	30.75 mM K2HPO4 19.25 mM KH2PO4
inside buffer	5 mM HEPES pH 6.8 120 mM KCl 2 mM MgSO4
outside buffer	5 mM HEPES pH 6.8 120 mM NaCl 2 mM MgSO4

2.8 Bacterial strains

Table 8: bacterial strains used in the described experiments.

Name	Organism	Supplier
C41 (DE3)	E. coli	EMBL Hamburg

2.9 Equipment and Consumables

Table 9: equipment and consumables used in the described experiments.

Name	Supplier
Tecan Spark 20M	TECAN
rotator SB3	Stuart
Avanti JXN-26 centrifuge	Beckman Coulter
Optima XE-90	Beckman Coulter
Optima MAX-XP	Beckman Coulter
SevenCompact pH/Ion (pH meter)	Mettler Toledo
SURFE^{2}R	Nanion
UVPChemStudio	analytic jena
MicroSpin G-25 Columns	Cytiva
Polycarbonate membrane, 400 nm	Avestin, Inc.
LiposoFast	Avestin, Inc.
SnakeSkin Dialysis tubing, 10,000 MWCO	Thermo Scientific
Spectra/Por 6 dialysis membrane, pre-wetted	Spectrum Laboratories

Spin-X UF6, 50k MWCO	Corning
Ni-NTA Agarose	invitrogen
Centrifuge 5810R	eppendorf
Bio-beads SM2, adsorbent media	Bio-Rad
Bis-Tris Protein Gels – RunBlue, 4-12 %	Biozol / expedeon
nanodrop 2000c	ThermoScientific
Rotary Evaporator Rotavapor R-114	Büchi
Superdex® 200 Increase 10/300 GL	GE Healthcare
Sonicator waterbath	Elmasonic
MiniSpin® centrifuge	Eppendorf

2.10 Computational resources

Table 10: software used in the described experiments.

Name	**Source**
VisionWorks	https://developer.nvidia.com/
Microsoft office	https://www.microsoft.com/de-de/
Prism GraphPad	https://www.graphpad.com/scientific-software/prism/
Python3	https://www.python.org/download/releases/3.0/

3 Methods

3.1 Cell culture and protein purification

Transformation was performed by mixing 50 µl of chemically competent cells (*E. coli*, C41), with approximately 50 ng of the respective plasmid (see Table 11) followed by a heat shock at 42 °C for 45 sec. Plasmid constructs used here were previously cloned by other members of the Loew group (EMBL Hamburg).

Table 11: overview of plasmids used in this study for transformation of E. coli C41 cells.

Protein name	Base vector	Tag	Cleavage site
DtpB	pNIC-CTHF	C-terminal 6xHis-tag	TEV protease
DgoT	pBAD_MCS	C-terminal 6xHis-tag	TEV protease
LgoT	pNIC28-Bsa4	C-terminal 6xHis-tag	TEV protease

Together with 300 µl LB medium, the cells were incubated at 37°C for 1 h and then plated on an LB-Agar plate supplemented with 0.03 mg/mL kanamycin and incubated at 37 °C overnight. The next day, 50 mL LB medium supplemented with 0.03 mg/mL kanamycin were inoculated with a single colony and incubated at 37 °C and 220 rpm overnight. The starting culture was diluted in 1 L TB medium supplemented with 0.03 mg/mL kanamycin to an optical density (OD) of 0.1 - 0.15 and kept at 37 °C shaking at 220 rpm. IPTG was added to a final concentration of 0.2 mM when the OD reached 0.6 – 0.8. After induction the incubator temperature was lowered to 18 °C for overnight growth. The cells were harvested at 10,000 xg and 20 °C for 15 min (Avanti JXN-26, Beckman Coulter, JLA 8.1 rotor) and the pellet was resuspended in 5 mL lysis buffer (Table 12) per gram wet cell pellet weight. Additionally, 5 units/mL DNase, 1 tablet proteinase inhibitor (EDTA-free) per 100 mL, 1 mg/mL lysozyme and 0.5 mM TCEP were added and the solution stirred for 1 h at 4°C until the pellet was fully resuspended. Cell lysis was performed by passing the suspension through an emulsifier (EmulsiFlex-C3, Avestin) at 10,000 – 15,000 psi pressure for three times. Subsequent centrifugation of the suspension at 10,000 xg and 4 °C for 12 min (Optima XE-90, Beckman Coulter) removed the cell debris and unbroken cells. By ultracentrifugation of the supernatant for 50 min at 95,000 xg and 4 °C, the membrane fraction was pelleted. The membrane pellet was then resuspended in 3 mL lysis buffer per gram initial wet cell pellet weight and incubated for 1 h at 4 °C together with 1 tablet proteinase inhibitor (EDTA-free) per 100 mL, 0.5 mM TCEP and 1 % n-Dodecyl-β-D-Maltoside (DDM, Anatrace) (w/v). As a detergent, DDM

leads to solubilisation of the membrane proteins by forming a micelle around them and with this is removing them from the lipid bilayer (Stetsenko and Guskov, 2017). Another ultracentrifugation step at 70,000 xg and 4 °C for 50 min removed the insoluble proteins from the solution and the supernatant was applied to Nickel-immobilized metal ion affinity chromatography beads (Ni-NTA Agarose, Invitrogen). The His-tag on the protein of interest forms a complex with the chelated nickel ions on the beads and thus can be separated from the remaining proteins in the soluble fraction (Spriestersbach et al., 2015). After incubation of the supernatant with Ni-IMAC beads for 45 min, the solution was applied onto a gravity column and the beads were washed twice with 2 column volumes (CV) wash buffer (Table 12) containing 20 mM Imidazole in the first wash and 30 mM Imidazole in the second wash. Imidazole competes with the His-tag for binding to the Nickel ion and in low concentrations removes unspecifically bound proteins (Spriestersbach et al., 2015). For elution of the bound proteins, an Imidazole concentration of 250 mM was used and the elution fractions were combined and mixed with 0.5 mg TEV protease to cleave the His-tag from the protein of interest (Block et al., 2007). The solution was then transferred into a dialysis tube (Spectra/Por 6 dialysis membrane, Spectrum Laboratories) and dialysis was performed overnight in 3 L gel filtration buffer (Table 12) at 4 °C to remove the Imidazole.

Table 12: Compositions of buffers used for purification of DtpB and ACS transporters.

buffer name	DtpB	ACS transporters
lysis buffer	1xPBS, 15 mM Imidazole, 300 mM NaCl	20 mM NaPi, 15 mM Imidazole, 300 mM NaCl, 5 % Glycerol
wash buffer 1	1xPBS, 150 mM NaCl, 0.1 % DDM, 20 mM Imidazole	20 mM NaPi, 150 mM NaCl, 5 % Glycerol, 0.03% DDM
wash buffer 2	1xPBS, 150 mM NaCl, 0.1 % DDM, 30 mM Imidazole	20 mM NaPi, 150 mM NaCl, 5 % Glycerol, 0.03% DDM, 10 mM Imidazole
elution buffer	1xPBS, 150 mM NaCl, 0.1 % DDM, 250 mM Imidazole	20 mM NaPi, 150 mM NaCl, 5 % Glycerol, 0.03% DDM, 200 mM Imidazole
dialysis buffer	20 mM HEPES pH 7.5, 150 mM NaCl, 0.03 % DDM	20 mM HEPES pH 7.0, 200 mM NaCl, 5 % Glycerol, 0.3% DM
Gel filtration buffer	20 mM HEPES pH 7.5, 150 mM NaCl, 0.3 % DM	20 mM HEPES pH 7.0, 200 mM NaCl, 5 % Glycerol, 0.3% DM

After dialysis, 15 mM Imidazole and Ni-beads were added to the solution and incubated for 30 min at 4 °C. The mixture was again applied onto a column and the flowthrough collected, which should contain the cleaved protein of interest (negative IMAC). As the His-tag was removed by TEV, the protein should no more bind to the beads but to make sure there was no unspecific binding the remaining beads were washed with dialysis buffer containing 15 mM Imidazole. Both, flowthrough and washing step were combined and concentrated using a 50 kDa MWCO concentrator (Spin-X UF6, Corning).

Before the protein could be used for reconstitution, a Size Exclusion Chromatography (SEC) was performed to test the purity of the protein and change the detergent from DDM to n-Decyl-β-D-Maltopyranoside (DM, Anatrace). The concentrated protein was loaded onto a Superdex 200 Increase 10/300 GL column (GE Healthcare), pre-equilibrated in gel filtration buffer. The protein was eluted at a flow rate of 0.5 mL/min in 500 µl fractions. Selected fractions were additionally loaded onto an SDS-PAGE gel to further check their purity and protein concentrations were measured using NanoDrop (NanoDrop 2000c, ThermoScientific). Fractions that contained the protein of interest were directly flash frozen in liquid nitrogen and stored at -80 °C until needed.

3.2 Liposome preparation and reconstitution

Liposomes for uptake assays were composed of 1-palmitoyl-2-oleoyl-sn-glycero-3-phosphoethanolamine (POPE) and 1-palmitoyl-2-oleoyl-sn-glycero-3-phospho-(1'-rac-glycerol) (sodium salt) (POPG) in a 3:1 ratio (w/w), since this combination has proven to be suitable for application of electrochemical or pH gradients and mimics the composition of the *E. coli* membrane (Figure 6) (Tsai and Miller, 2013).

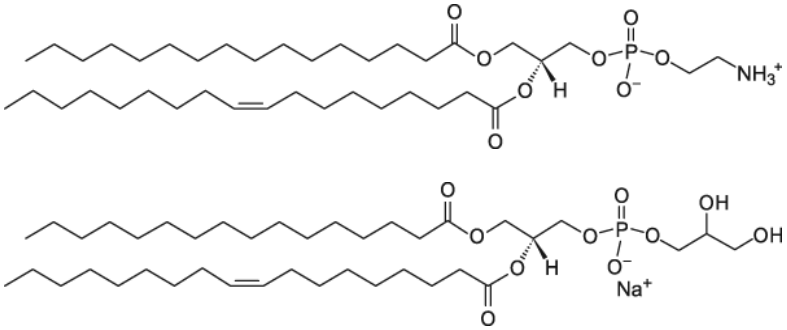

Figure 6: Structural formula of 1-palmitoyl-2-oleoyl-sn-glycero-3-phosphoethanolamine (POPE) on top and 1-palmitoyl-2-oleoyl-sn-glycero-3-phospho-(1'-rac-glycerol) (sodium salt) (POPG) below. *Lipids were mixed in a 3:1 ratio for formation of liposomes. (Avanti Polar Lipids, 2021a; Avanti Polar Lipids, 2021b)*

In a round-bottom glass flask, 200 mg lipids (150 mg POPE, 50 mg POPG) were dissolved in 10 mL chloroform. A rotary evaporator (Rotary Evaporator Rotavapor R-114, Büchi) was used to remove the

solvent (Figure 7). This led to formation of a dry lipid cake on the wall of the flask, which was then washed twice with 10 mL pentane, to remove residual chloroform, and again dried under vacuum. Afterwards, the dry lipids were resuspended in degassed 50 mM KPi buffer pH 7.0 (Table 13) to a final lipid concentration of 20 mg/mL. Two freeze-thaw cycles in liquid nitrogen were performed in order to achieve the same buffer conditions inside and outside the liposomes. Liposomes were then aliquoted, flash frozen in liquid nitrogen and stored at -80°C for reconstitution of membrane proteins.

Table 13: Composition of 50 mM KPi buffer for liposome preparation and reconstitution.

buffer composition: KPi	
50 mM KPi, pH 7.0	30.75 mM K_2HPO_4 19.25 mM KH_2PO_4

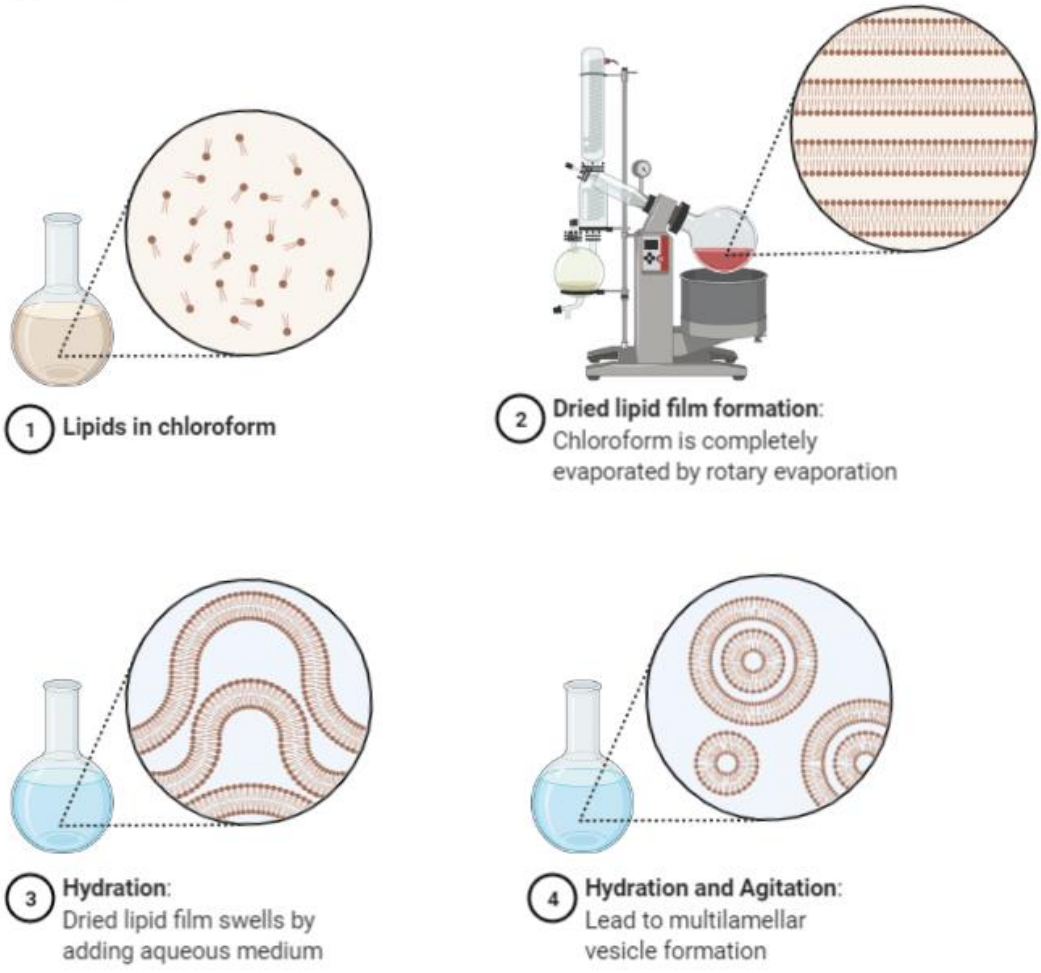

Figure 7: Schematic illustration of the thin layer method for liposome production. *Lipids are dissolved in chloroform and then dried using a rotary evaporator to form a lipid cake on the wall of the glass flask. This is hydrated by adding buffer to the flask and multilamellar liposomes form under agitation. Created in BioRender.com*

For reconstitution of a protein into the liposomes it is crucial to remove the detergent micelles around the protein (Rigaud and Lévy, 2003). Co-micellization of the purified protein solubilised in detergent and phospholipids leads to formation of mixed lipid-protein-detergent micelles (Rigaud and Lévy,

2003). Detergents interfere with the vesicle formation and increase liposome permeability (Rigaud and Lévy, 2003). When the detergent is removed from the solution, the protein eventually incorporates into the liposomes. For this, different methods can be employed (Rigaud and Lévy, 2003).

3.2.1 Rapid dilution method

One reconstitution method used in this project was the rapid dilution technique, which is suitable for proteins dissolved in a detergent with high critical micelle concentration (CMC). DM has a higher CMC (1.6 mM) than DDM (0.17 mM) and can therefore faster be reduced below its CMC by dilution, without having to remove the detergent completely. This is advantageous during reconstitution into liposomes when the protein has to be removed from the micelles and integrated in the liposomes.

The thawed liposomes were diluted in 50 mM KPi buffer to 5 mg/mL lipid concentration and preformed liposomes were prepared by extrusion (LiposoFast, Avestin) through a 400 nm filter (Polycarbonate membrane, Avestin) leading to unilamellar vesicles with a homogenous size distribution (Rigaud and Lévy, 2003). Extruded vesicles were then mixed with protein at 0.5 mg/mL to reach a protein to lipid ratio of 1:60 or 1:10 (w/w) and incubated at room temperature for 1 h. Approximately 60 mL of precooled 50 mM KPi buffer (pH 7.0) were used to dilute the mixture by a factor of 20 for liposomes at a ratio of 1:60 and by a factor of 75 for liposomes at a ratio of 1:10 by slowly adding the mixture to the buffer. The aim of this was to reduce the detergent concentration below its CMC, so the membrane transporter integrates into the liposome bilayer. Proteoliposomes were pelleted at 45,000 rpm and 4 °C for 2 h, resuspended in 0.5 mL KPi buffer (50 mM, pH 7.0) and then dialysed (SnakeSkin Dialysis tubing, Thermo Scientific) against 3 L of the same buffer for another two days with two buffer exchanges each day to further remove any residual detergent. Proteoliposomes were then harvested at 100,000 xg and 4 °C for 30 min (Optima MAX-XP, Beckman Coulter), resuspended in KPi buffer (50 mM, pH 7.0) to a final theoretical protein concentration of 0.5 mg/mL and freeze-thawed twice before storage at -80 °C. To check the reconstitution efficiency, 4 µl proteoliposomes were applied onto an SDS-PAGE together with three protein samples (0.5 µg, 1 µg and 2 µg) as reference. After staining the gel, a densiometry analysis (VisionWorks, Nvidia) was performed and the total density of the protein samples was used for a linear calibration, which enabled estimation of the protein concentration in the proteoliposomes. Here, a reconstitution efficiency of 100 % would correspond to 2 µg protein in 4 µl proteoliposomes solution.

3.2.2 Biobead method

Another established method for reconstitution of membrane proteins into liposomes is using biobeads to remove the detergent. This method has been proven to result in liposomes with very low ionic permeability because the detergent is removed more effectively than by dialysis (Rigaud and Lévy, 2003). Additionally, it can also be used for detergents with low CMC (Rigaud and Lévy, 2003). Liposomes were prepared as described above, by diluting them to 0.5 mg/mL followed by extrusion through a 400 nm (Polycarbonate membrane, Avestin) filter. They were then mixed with Triton-X 100 to disrupt the liposomes and thus make them more accessible for the protein (Rigaud and Lévy, 2003). The suitable concentration of Triton-X 100 for a 3:1 POPE/POPG lipid mixture was determined by measuring the amount that is needed to decrease the absorbance value of empty liposomes by 15 % (Parker and Newstead, 2014). Therefore, 200 µL of liposomes at 0.5 mg/mL lipid concentration were transferred into a transparent 96-well plate and the initial absorbance measured at 540 nm (Tecan Spark 20M). Then 10 % Triton-X 100 was added in steps of 0.5 µL and the absorbance measured until approximately 85 % of the initial value were reached. Here, 1.5 µL of 10 % Triton-X 100 were necessary, which corresponds to a final concentration of 0.075 % of Triton-X 100.

Incubation of the liposomes for reconstitution with Triton-X 100 was allowed for 10 min and then protein at 0.5 mg/mL was added to reach the protein to lipid ratio of 1:30 or 1:60. The mixture was incubated for 30 min at room temperature, mixing it occasionally, and then incubated at 4 °C for another 30 min on a rotation wheel. Afterwards, biobeads (Bio-beads SM2, Bio-Rad) were added to the solution in three steps depending on the Triton-X 100 amount in the solution. In the first step, 10 mg biobeads were used per 10 µl of 10 % Triton-X 100 and then incubated for 2 h at 4 °C. Then 20 mg of biobeads were added in the second step, again followed by 2h incubation at 4 °C. In the last step 40 mg of biobeads were added to the mixture, followed by an incubation overnight at 4°C. Proteoliposomes were harvested the next day by transferring the solution with a syringe onto 1 mL gravity columns to remove any remaining biobeads. Residual biobeads in the tube were washed twice with 300 µL KPi buffer (50 mM, pH 7.0) for complete liposome recovery. The proteoliposome solution was then centrifuged at 100,000 xg and 4 °C for 30 min (Optima MAX-XP, Beckman Coulter), the supernatant was removed and the pellet resuspended in fresh KPi buffer (50 mM, pH 7.0) to a final protein concentration of 0.5 mg/mL. After two freeze-thaw cycles, 4 µL were loaded onto an SDS-PAGE gel to check reconstitution efficiency as described before and liposomes were stored at -80 °C.

3.3 Pyranine assay

This uptake assay was based on trapping pyranine, a pH sensitive fluorescent dye, in the lumen of proteoliposomes containing reconstituted proton-coupled membrane transporters (Kano and Fendler, 1977). Buffer conditions on both sides of the liposomes were kept the same, except from using potassium ions on the inside and sodium ions on the outside. By adding valinomycin a negative inward membrane potential is created, which in turn drives substrate uptake of the proton-coupled transporters used in this study (Figure 8). The resulting pH-shift in the liposomes was detected by measuring a decrease in pyranine fluorescence. Emission was measured at a wavelength of 510 nm for the excitation wavelengths of 415 nm and 460 nm. The excitation at 415 nm was used as a reference signal to detect dilution effects independent of pH during the measurement because it is stable over the pH range of 4 to 10, as described before (Kano and Fendler, 1977). Excitation at 460 nm is close to a pH dependent maximum in the pyranine spectrum and therefore suitable to measure pH changes (Kano and Fendler, 1977). An important requirement for this assay is that proteoliposomes are relatively tight and show only little proton leakage over the time course of the assay. Furthermore, a low buffer concentration (5 mM HEPES, pH 6.8) was used in order to detect low proton fluxes and reach a high sensitivity.

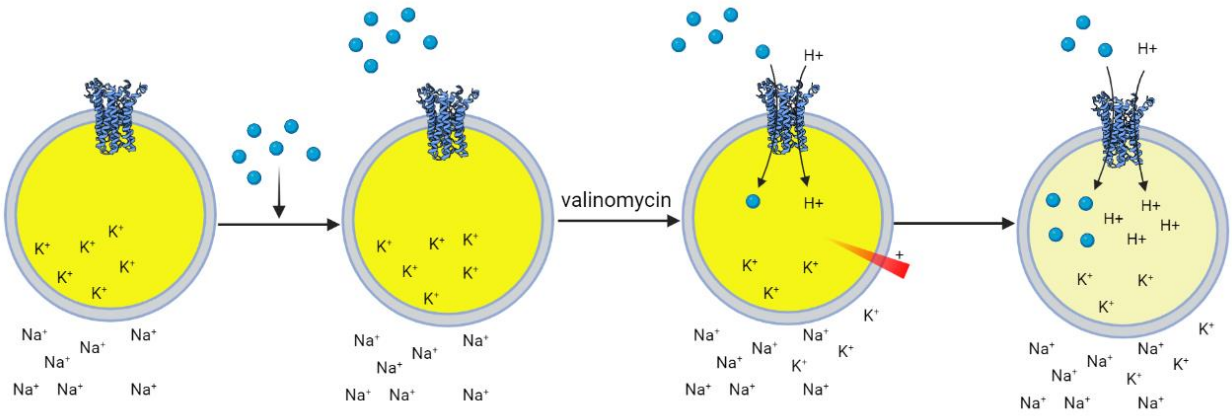

Figure 8: Schematic illustration of the liposome-based uptake assay for proton-coupled membrane transporters using pyranine as a fluorescent dye. *Liposomes are loaded with a buffer containing pyranine and potassium ions. To equalise ionic strength on both sides of the liposome, sodium ions are added to the outside buffer. Addition of valinomycin increases the membrane permeability of potassium ions and generates an inward directed negative charge gradient. Substrate transport by the membrane protein is driven by the membrane potential and substrate is taken up into the liposome accompanied by protons. The proton-influx reduces the internal pH and decreases pyranine fluorescence. Created in BioRender.com.*

For pyranine assays, proteoliposomes with the respective membrane transporter reconstituted in POPE:POPG lipid mixture, and liposomes without protein (empty liposomes) were used. For a single measurement, 5 µg of reconstituted protein were used. First, the appropriate amount of liposomes were harvested at 100,000 xg for 30 min at 4 °C (Optima MAX-XP, Beckman Coulter) and the remaining pellet resuspended in 450 µl of inside buffer (Table 14) containing 1 mM pyranine. Liposomes were

exposed to 7 freeze-thaw cycles to adjust buffer conditions inside and outside the liposomes and encapsulate pyranine molecules. Afterwards, the liposomes were extruded through a 400 nm filter (Polycarbonate membrane, Avestin) 11 times to achieve homogenous unilamellar vesicles. The liposomes were pelleted again at 60,000 xg and 15 °C for 30 min (Optima MAX-XP, Beckman Coulter), the supernatant discarded and the pellet overlayed with 100 µl inside buffer to remove remaining pyranine. Additionally, the 150 µL of resuspended liposomes were applied to an equilibrated G-25 spin column (MicroSpin G-25 Columns, Cytiva) and spun at 800 xg for 1 min to remove any residual pyranine. Another ultracentrifugation step (Optima MAX-XP, Beckman Coulter) was performed (60,000 xg, 30 min, 15 °C) to recover the proteoliposomes and then resuspend them in a final volume of 4 µl inside buffer per measurement.

Table 14: compositions of buffers used for liposomal uptake assays with pyranine as a pH-sensitive dye

buffer name	composition
inside buffer	5 mM HEPES pH 6.8, 120 mM KCl, 2 mM $MgSO_4$
outside buffer	5 mM HEPES pH 6.8, 120 mM NaCl, 2 mM $MgSO_4$

For a single measurement 4 µl of proteoliposomes and 190 µl outside buffer (Table 14) were transferred into a black flat-bottom 96-well plate, which was inserted in a microplatereader (Tecan Spark 20M). The device was set to measuring emission at 510 nm for excitation wavelengths of 415 and 460 nm simultaneously over a time period of 5 min. For the addition of substrate and valinomycin to a sample, the measurement was stopped, one compound added by mixing the solutions quickly and the measurement was then continued. For transport assays with DtpB, a substrate concentration of 2.5 mM and a valinomycin concentration of 10 µM were used, respectively. Valinomycin was previously prepared as a 10 mM stock in DMSO and then diluted to 100 µM in water. Substrate stock solutions were prepared as 50 mM stocks dissolved in outside buffer, for peptides and sugar acids equally. The stock solution of L-galactonate had to be obtained from L-galacto-1,4-lactone dissolved in outside buffer by adjusting the pH in steps. In solution, lactone has an acidic pH, which was at approximately pH 5 for a 100 mM solution. Increasing the pH to 7.0 leads to formation of L-galactonate by hydrolysis since it is the conjugate base of L-galactonic acid (PubChem, 2021). As the pKa of L-galactonic acid is at 3.5, the acid deprotonates at neutral pH and therefore the pH decreases again leading to a shift of the equilibrium towards the acid. Titration with NaOH continued over a period of five weeks until the solution stabilized at pH 7.0, meaning most of the lactone was converted into L-galactonate.

After measuring the pyranine fluorescence over 5 minutes, the fluorescence values for excitation at 460 nm were divided by the values at 415 nm and the data was normalized against the average fluorescence ratio of the first 25-28 sec before substrate addition. This way, the initial relative fluorescence started around a value of 1 for every measurement and was not dependent on the total amount of pyranine incorporated in the liposomes, which can differ between liposome preparations. The transport signal was determined starting from the time point after addition of valinomycin to the sample. As a reference signal, the slope of the empty liposome signal was determined by linear curve fitting for each measurement. This slope was subtracted from the proteoliposome signal to obtain the corrected curve that indicates transport by the respective protein without unspecific interactions. The corrected curve was either fitted with a linear or exponential fit. For an exponential fit the following equation was applied for the corrected relative fluorescence (RFU_{corr}) with the initial relative fluorescence at the starting time point ($RFU_{corr}(t_0)$), the amplitude of the exponent (a), the starting time point (t_0) and the time constant (τ). The time constant gives the time that is required for the signal to decrease by 1/e of the initial value (eq. 7).

$$RFU_{corr}(t) = RFU_{corr}(t_0) - a * \left(1 - e^{\frac{-(t-t_0)}{\tau}}\right) \quad (7)$$

For each corrected transport curve, the residuals of both fits were calculated and examined for normality using the D'Agostinos K^2 test with a significance of 0.05. If both fits showed normally distributed residuals, the F-test was applied to decide which fit better describes the curve. Otherwise, the F-test could not be applied and the exponential fit was selected. The F-statistic was calculated using the equation below (eq. 8).

$$F = \frac{(RSS_{linear} - RSS_{exp})/(p_{exp} - p_{linear})}{RSS_{exp} - (n - p_{exp})} \quad (8)$$

Here, RSS is the squared sum of the residuals, p is the number of fit parameters (2 for linear, 3 for exponential) and n is the number of datapoints in a curve. The critical value F_{crit} was computed from the F distribution with 0.01 statistical significance and degrees of freedom determined from (p_{exp} - p_{linear}) and (n-p_{exp}). For all curves with an F-statistic above F_{crit} the exponential model was selected, otherwise the linear fit. In the case of a negative F-statistic the linear model was chosen because the exponential model could not fit the curve sufficiently well. For comparison of linear and exponential transport curves, the initial slope at the starting time of a measurement (t_0) was calculated. The t_0 slope of a linear fit equals the slope of the fit, while for the exponential fit it was calculated as the ratio of a to τ. Finally, the relative initial slope was calculated as follows:

(9)

$$t_{0\_slope\_rel} = \frac{t_{0\_slope_{substrate}} - t_{0\_slope_{buffer}}}{t_{0\_slope_{positive\ control}} - t_{0\_slope_{buffer}}}$$

The respective buffer signal was subtracted from each substrate signal and signals were normalised to the respective signal of the positive control for comparison of t_0 slopes from different experiment days. Curve fitting and data manipulation were performed in Phyton3 (Python, 2019) by Vadim Kotov (EMBL Hamburg) with the following modules: numpy (Jones et al., 2001), scipy (van der Walt and Jarrod, 2010), pandas (McKinney, 2010), matplotlib (Hunter, 2019) and seaborn (Wascom et al., 2020).

3.4 SSM-based assay

The Nanion SURFE^{2}R N1 was utilized in this assay to measure uptake of substrate into liposomes by proton-coupled membrane transporters. Opposed to the pyranine assay, no fluorescent signal but a current induced by proton-flux was used as a measure of transport. For this, proteoliposomes were attached onto a gold coated sensor, which had an additional 1,2-diphytanoyl-sn-glycero-3-phosphocholine (DPhPC) layer on the surface (Figure 9). The sensor was then located in a Faraday cage with one electrode coupled to the gold sensor and one electrode connected to the surrounding buffer of the proteoliposomes. For uptake measurements, a substrate gradient was generated by rinsing the sensor with an activating solution containing the substrate, which was then transported into the liposomes accompanied by proton transport. Proton-flux was measured by the electrodes according to the principle of capacitive coupling of the liposomes to the sensor. Changes in current were recorded by the system and plotted on the display of the SURFE^{2}R N1 user interface. If proton-coupled uptake occurs, a positive current is induced, which declines once the charge gradient approaches the potential of the substrate gradient (Figure 9). In order to restore the initial conditions, the sensor was then rinsed with a deactivating solution which generated a substrate-gradient in the opposite direction. Information that can be obtained from the transport signal is the rise time, the decay time, the peak current (amplitude) and the peak integral. The latter two can automatically be determined by the SURFE^{2}R N1 software.

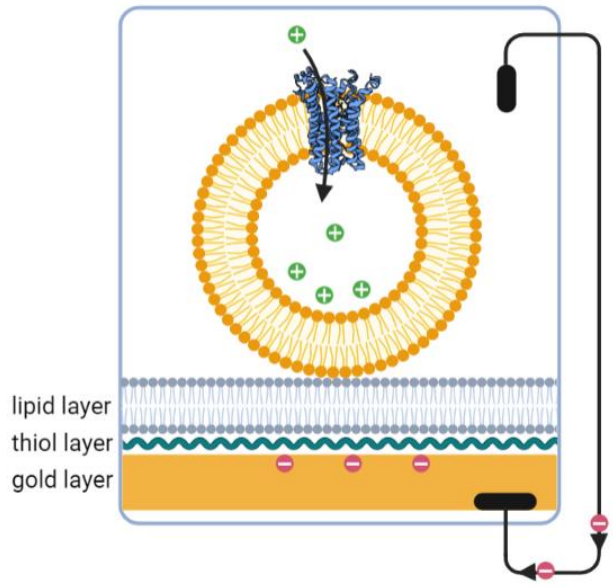

Figure 9: Schematic illustration of the measuring principle of SSM-based uptake assays in the Nanion SURFE²R. *The gold coated sensor chip is covered by a thiol layer connected to a lipid layer. Liposomes are attached to the lipid layer and proton flux into the liposomes can be measured according to the principle of capacitive coupling. The change in current between the two electrodes is measured and displayed. Created in BioRender.com*

To enable SSM formation, first 50 µL of a 0.5 mM 1-octadecanthiol solution in isopropanol was added to the sensor and incubated for a minimum of 30 min. Afterwards, the solution was removed by tapping the sensor on a tissue and rinsing the sensor with 5 mL isopropanol and 5 mL MilliQ water, respectively. The water had to be completely removed from the sensor before applying 1.5 µL of DPhPC (7.5 ug/uL), dissolved in n-decane, onto it and immediately covering it with 50 µL of SURFE^{2}R buffer (20 mM HEPES pH 6.8, 120 mM KCL, 2 mM MgSO4). During this process, the sensor surface may not be touched by the pipette tip to keep it functional. Previously prepared liposomes with a 1:10 protein to lipid ratio were thawed at RT and diluted in 50 mM KPi buffer (pH 7.0, see section 3.2) to a lipid concentration of 1 mg/mL. The liposome solution was sonicated for 30 sec (Sonicator waterbath, Elmasonic) and 10 µL of it were added to the buffer surface on a sensor. After centrifugation of the sensor for 30 min at 3000 xg (Centrifuge 5810R, Eppendorf) at room temperature, it was ready to be used. As a quality control, the capacity and conductance values of a sensor were checked using the "CapCon" function of the SURFE^{2}R. Sensors with a capacitance in the range of 15-30 nF and a conductance below 5 nS were used for transport assays according to the manufacturer's instructions (Barthmes and Bazzone, 2017). Measurements were performed using the workflow "BAB_B 2s", meaning the sensor was rinsed with the deactivating solution (B) followed by the activating solution (A) and then again deactivating solution, each for a duration of 2 sec (Figure 10). After the measurement, another rinse with deactivating solution was done to completely restore the initial conditions and improve the baseline for the next measurement.

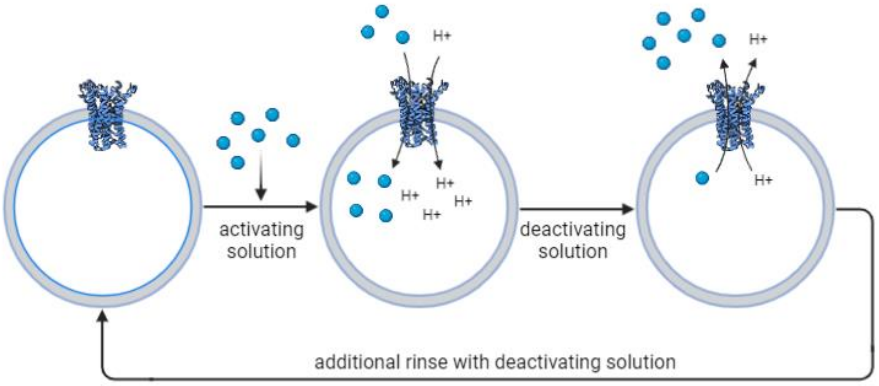

Figure 10: Schematic representation of an uptake experiment using SSM-based electrophysiology. *The sensor is alternately rinsed with activating and deactivating solution. The activating solution contains a substrate, which is taken up into the liposomes by the transporter protein due to the inward directed substrate gradient. Deactivating solution reverses this substrate gradient and initiates substrate flux out of the liposome until the initial state is restored. Created in BioRender.com*

To prevent artefacts related to the substrate to occur, an inert and structurally similar substance was added to the deactivating solution. Artifact signals were examined and reduced before starting transport measurements, using liposomes with no transporter protein (empty liposomes) as a negative control. Generally, transport measurements can only directly be compared when they were performed on the same sensor, since sensors can vary in the amount of vesicles attached. It is possible to perform several measurements on one sensor in a row, depending on the stability of the transporter and the membrane preparation (Bazzone et al., 2017). To check the stability of a sensor, a positive control with high amplitude was included as first and last measurement on each sensor. In case the control signal changed by more than 20 % over the course of the measurement, the data was not deemed reliable because changes in the peak current might be caused by a loss of transporter activity. To assure reproducibility of the obtained data, measurements were performed in triplicates on one sensor and then repeated on two more sensors. The data from one sensor was normalised to a reference signal to compare the signals from different sensors without including the variation in adsorption efficiency (Bazzone et al., 2017).

3.5 Data analysis and quality control

The Michaelis-Menten model describes the kinetic properties of an enzymatic reaction, catalysing the transition of a substrate to a product (Berg et al., 2002). Here, substrate and enzyme form a complex, from which the product is released (eq. 10) (Berg et al., 2002). This reaction pathway can also be applied for the transport process of a substrate by a membrane transporter. The substrate first binds to the transporter and then gets released on the other side of the membrane.

$$E + S \underset{k_{-1}}{\overset{k_1}{\rightleftharpoons}} ES \xrightarrow{k_2} E + P \quad (10)$$

For determination of K_M and V_{max} the processed transport signals of different concentrations of a substrate were fitted in Prism GraphPad according to the Michaelis-Menten equation (eq. 11) (GraphPad, 2020).

$$Y = \frac{V_{max} * X}{K_M + X} \quad (11)$$

With X being the substrate concentration and Y the transport signal. V_{max} is the maximum transport activity reached at substrate saturation and is characteristic for an enzyme at a certain concentration (Berg et al., 2002). K_M is the substrate concentration that is needed to reach half maximum transport activity (Berg et al., 2002). Assuming that the rate constant for dissociation of the complex (k_{-1}) is much larger than the rate constant for product formation (k_2), the K_M value is a measure for affinity of the substrate to the protein (Berg et al., 2002). A high K_M indicates weak binding while a low K_M indicates high affinity (Berg et al., 2002).

Relative IC_{50} was determined as the concentration of inhibitor required to reach half of the maximum inhibition effect possible with this inhibitor (Software, GraphPad, 2020b).

To judge the quality of an assay, the dimensionless coefficient termed Z'-factor was used. It is widely used in assay development and optimisation and describes the capability of an assay to identify hits (Zhang et al., 1999). The Z'-factor is based on the positive and negative control and considers the dynamic range and data variation of an assay (Zhang et al., 1999). It was calculated according to the equation below (eq. 12) (Zhang et al., 1999). (12)

$$Z' = 1 - \frac{(3\sigma_{c+} + 3\sigma_{c-})}{|\mu_{c+} - \mu_{c-}|}$$

Here, σ_{c+} and σ_{c-} are the standard deviations of the positive and negative control, respectively, defining the data variability band (Zhang et al., 1999). The mean values are represented by μ_{c+} and μ_{c-} and their difference defines the dynamic range of the assay (Zhang et al., 1999). The Z'-factor can range from negative infinity to one, but is only meaningful in the range from -1 to 1 (Zhang et al., 1999). An ideal assay has a Z'-factor of 1, meaning there is a large separation band between positive and negative control data (Figure 11) (Zhang et al., 1999).

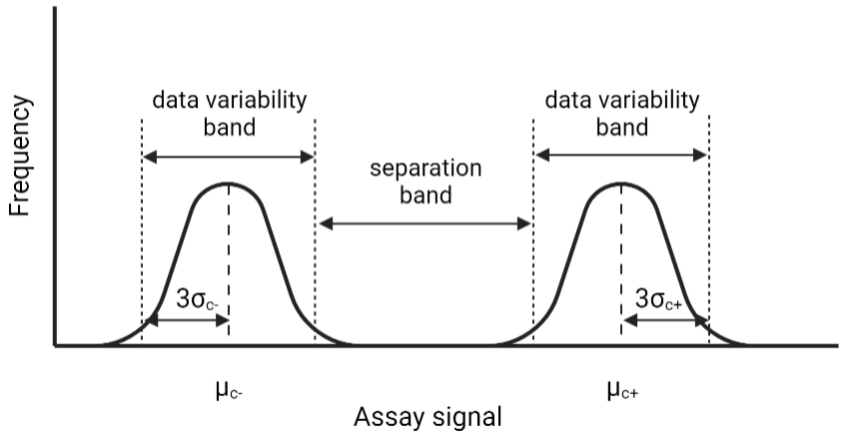

Figure 11: Graphical definition of the separation band between positive and negative control signals for determination of assay quality. *The Figure shows a hypothetical frequency distribution of positive and negative control data, assuming a normal distribution profile. The mean values for positive (μ_{c+}) and negative control (μ_{c-}) are indicated together with the respective data variability band defined by three times standard deviation (σ_{c+}, σ_{c-}).*

A large separation band can be achieved by a large dynamic range, a small data variability or a combination of both (Zhang et al., 1999). An assay with a Z'-factor between 1 and 0.5 is defined as an excellent assay and below 0.5 as an acceptable assay with small separation band (Zhang et al., 1999). If the Z'-factor is at zero the variability bands touch, but the assay can still be used for yes/no specifications (Zhang et al., 1999). A Z'-factor below zero makes screening impossible because the variability bands overlap (Zhang et al., 1999). Similar to the Z'-factor also the Z-factor referring to the separation band between control and sample data can be calculated. Therefore, the same equation is used, replacing one of the controls by the sample data. This allows an evaluation of the performance of the assay on different samples.

Data visualisation was performed in Prism GraphPad (Prism – GraphPad, 2021).

4 Results

4.1 Expression and purification

Expression in *E. coli* C41 cells and purification of membrane proteins was carried out according to an established protocol (Ural-Blimke et al., 2019). *E. coli* C41 cells are especially suitable for overexpression of membrane proteins because they are less influenced by the toxic effect of membrane protein overexpression than BL21(DE3) cells (Miroux and Walker, 1996). They were transformed by heat shock, then plated onto agar plates and grown in LB medium. Expression in TB medium was induced by IPTG (Miroux and Walker, 1996). For purification, cells were homogenised and the cell membranes isolated. Solubilisation of membrane proteins in detergent and subsequent IMAC were used for purification of the proteins of interest.

In the following, exemplary results for each protein purified during this project are shown.

4.1.1 DtpB

DtpB was expressed in 2 L cell culture and yielded approximately 40 g total wet cell pellet mass. Samples from several steps of the purification process were loaded on an SDS-PAGE gel (Figure 12). The purified protein was concentrated to 1 mL and 500 µL were run on the SEC column in DM containing buffer.

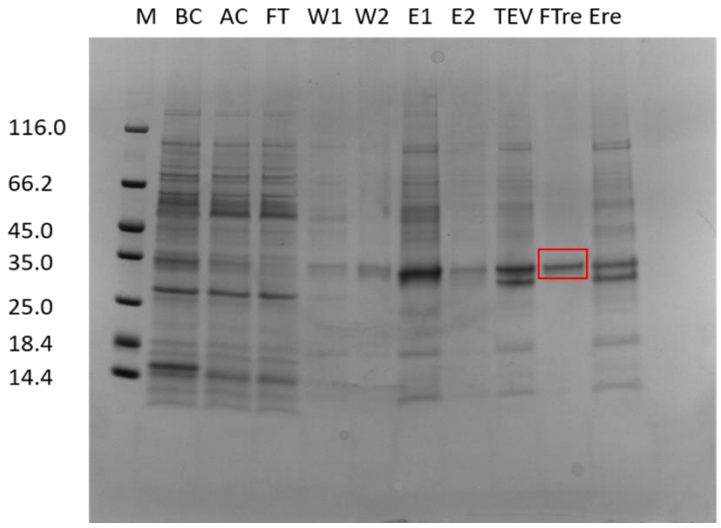

Figure 12: SDS-PAGE gel to monitor the purification process of DtpB showing individual steps of the IMAC. *Molecular weight of the marker proteins is indicated on the left. The final purified protein band is marked in red.*
M: protein marker, BC & AC: membrane preparation incubated with detergent before centrifugation (BC) and in the supernatant (AC), FT: flow-through, W1 &W2: wash 1 and 2, E1 & E2: elution 1 and 2, TEV: after incubation with TEV o/n, FTre: flow-through negative IMAC, Ere: elution negative IMAC.

The gel shows several different proteins in the membrane preparation of the C41 cells (Figure 12, lane BC). The number is reduced after solubilisation with DDM, only leaving the soluble proteins in the supernatant after centrifugation (Figure 12, lane AC). Most of these proteins are also present in the flow-through of the IMAC, as they do not bind to the Ni-beads (Figure 12, lane FT). In the two wash fractions with increasing Imidazole concentration, faint bands of most proteins from the flow-through can be observed (Figure 12, lanes W1 and W2). The first elution step with high Imidazole concentration shows one dominant band of the protein of interest and faint bands of other proteins interacting with the Ni-beads (Figure 12, lane E1). In the second elution step, mainly a thin band of DtpB can be found (Figure 12, lane E2). DtpB was expected at a molecular weight of 53 kDa but appears at roughly 35 kDa on the gel. Incubation with TEV adds a band of TEV molecules (theoretical molecular weight 27 kDa) to the protein mixture of the elution steps (Figure 12, lane TEV). Subsequent negative IMAC led to a single band of DtpB in the flow-through with the rest of the proteins in the elution step (Figure 12, lanes FTre and Ere).

The chromatogram below shows the UV absorption of the purified sample on a Superdex 200 10/300 GL column and an SDS-PAGE of the peakfractions (Figure 13).

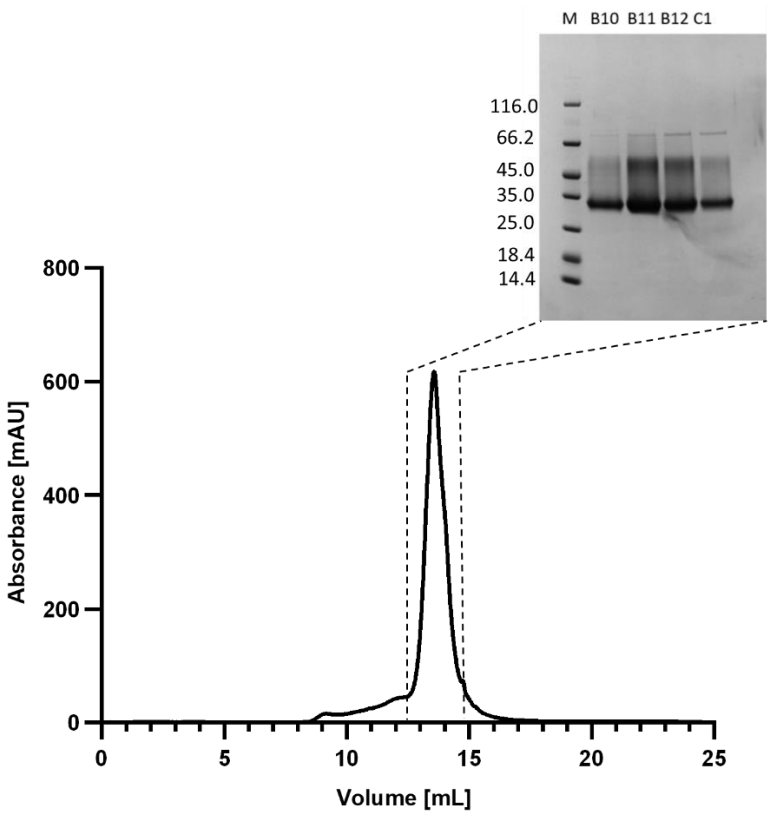

Figure 13: Chromatogram of purified DtpB run on Superdex 200 Increase 10/300 GL column (GE Healthcare) *in HEPES buffer (20 mM, pH 6.8) with addition of 150 mM NaCl and 0.3 % DM. Elution volume was one column volume at a flow rate of 0.5 mL/min and 500 µL fractions were collected. The Figure indicates UV absorption of the sample and the insert shows an SDS-PAGE gel of peakfractions B10 – C1 with weight of marker proteins (M) indicated on the left.*

Table 15: protein concentrations of peakfractions containing purified DtpB from SEC on Superdex 200 Increase 10/300 GL column (GE Healthcare), measured using NanoDrop.

fraction name	protein concentration [mg/mL]
B10	0.750
B11	1.841
B12	1.442
C1	0.696

DtpB eluted at a retention volume of 13.5 mL in a sharp peak with smaller overlapping peaks in front. These small peaks might contain aggregates or dimers of the protein. Peakfractions B10 to C1 were selected and loaded onto an SDS-PAGE gel to test purity of the sample. All four fractions show a thick band of DtpB below 35.0 kDa without major impurities (Figure 13). Additionally, the protein concentrations in the selected fractions were measured using NanoDrop (see Table 15). DtpB was successfully purified and directly used for reconstitution into liposomes, the remaining fractions were stored at -80°C.

4.1.2 LgoT

A 2 L expression of LgoT yielded 50 g wet cell pellet mass and was processed in the same way as DtpB except for using DM in the dialysis buffer instead of DDM.

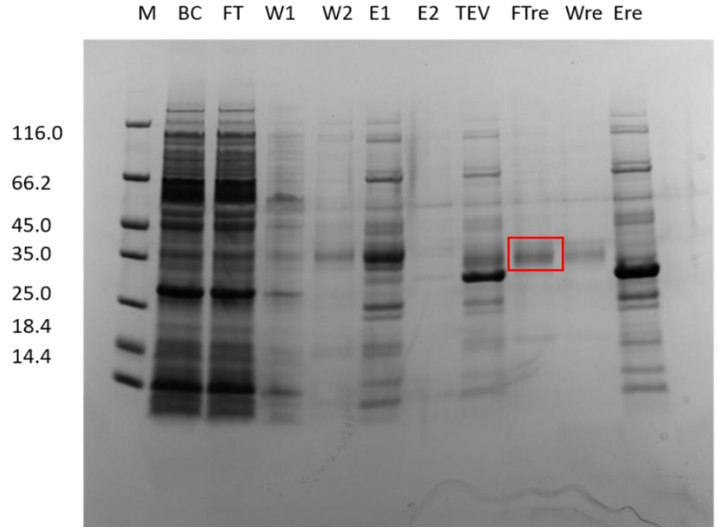

Figure 14: SDS-PAGE gel to monitor the purification process of LgoT showing individual steps of the IMAC. *Molecular weight of the marker proteins is indicated on the left.*
M: protein marker, BC: membrane preparation incubated with detergent before centrifugation (BC), FT: flow-through, W1 & W2: wash 1 and 2, E1 & E2: elution 1 and 2, TEV: after incubation with TEV o/n, FTre: flow-through negative IMAC, Ere: elution negative IMAC.

SDS-PAGE of the purification steps shows several membrane proteins in the flow-through of the IMAC, which are washed off the column in the washing steps (Figure 14). A thick band of LgoT can be observed in the first elution step, accompanied by other proteins that bound to the Ni-beads (Figure 14, lane E1). After TEV cleavage LgoT is eluted relatively pure from the IMAC column (Figure 14, lanes FTre and Wre). LgoT has a theoretical molecular weight of 49.4 kDa but was observed on the gel at roughly 35 kDa, as already seen for DtpB. The combined elution and wash fractions were concentrated and run on a Superdex 200 10/300 GL column.

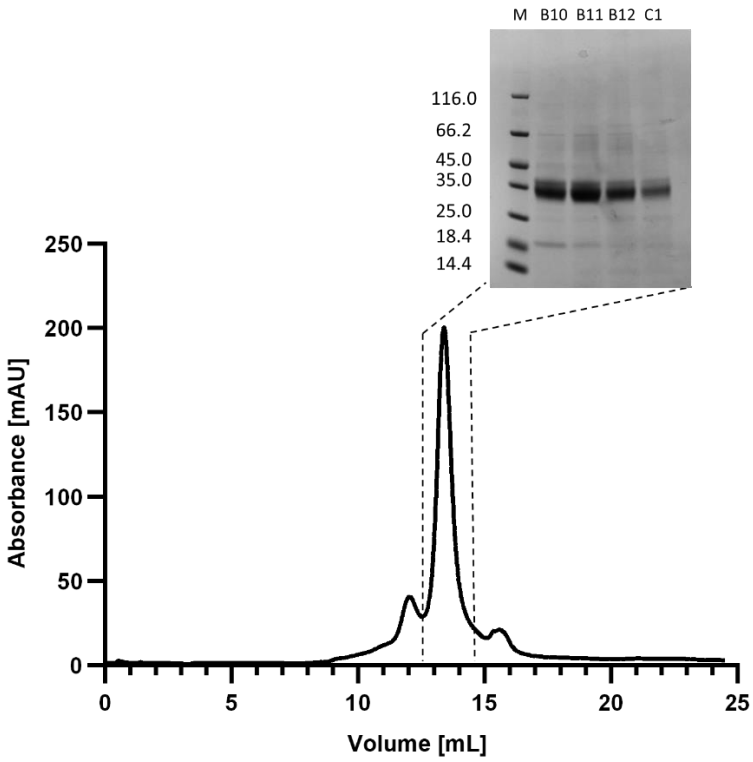

Figure 15: Chromatogram of purified LgoT run on Superdex 200 Increase 10/300 GL column (GE Healthcare) *in HEPES buffer (20 mM, pH 6.8) with addition of 200 mM NaCl and 0.3 % DM. Elution volume was one column volume at a flow rate of 0.5 mL/min and 500 µL fractions were collected. The Figure indicates UV absorption of the sample and the insert shows an SDS-PAGE gel of peakfractions B10 – C1 with weight of marker proteins (M) indicated on the left.*

Table 16: protein concentrations of peakfractions containing purified LgoT from SEC on Superdex 200 Increase 10/300 GL column (GE Healthcare), measured using NanoDrop.

fraction name	protein concentration [mg/mL]
B10	0.560
B11	0.783
B12	0.503
C1	0.286

The chromatogram shows a homogenous peak for LgoT at a retention volume of 13.5 mL with smaller peaks overlapping on the sides (Figure 15). These peaks might contain aggregates of the protein or impurities. Peakfractions (B10 - C1) were loaded onto an SDS-PAGE gel, displayed in Figure 15. All selected fractions show a clear band of LgoT without impurities. Protein concentrations of the fractions are given in Table 16. LgoT was directly used for reconstitution into liposomes and the remaining fractions stored at -80 °C.

Purified DgoT, which was used for reconstitution into liposomes, was previously expressed and purified by other members of the lab (Loew group, EMBL Hamburg) using the same procedure as for LgoT.

4.2 Liposome preparation and reconstitution

POPE/POPG (3:1) liposomes were prepared in the rotary evaporator according to an established protocol (Bartels, 2020) by drying the dissolved lipids in a round bottom glass flask to form a dry lipid layer and then hydrating it with KPi buffer. This lipid composition was chosen because it has been shown to be suitable to form liposomes, which are able to maintain a pH-gradient of 3 units and a 1,000-fold K^+-gradient (Tsai and Miller, 2013). Prior to reconstitution the liposomes were extruded through a 400 nm filter to obtain small unilamellar vesicles with a homogenous size distribution (Parker and Newstead, 2014). Two different methods were applied for reconstitution of membrane transporters into liposomes, the rapid dilution and biobead method.

4.2.1 Rapid dilution method

This method was performed similar to Parker et al. (2014), where it was used for reconstitution of $PepT_{So}$. The sufficient amount of DtpB was mixed with extruded liposomes, incubated for one hour and then transferred into approximately 60 mL KPi buffer (pH 7.0) to dilute the detergent below its CMC. Additionally, dialysis was performed over two days to further decrease the detergent concentration. If detergent integrated into the liposomes together with the protein, this would lead to a higher permeability of the liposomes (Rigaud and Lévy, 2003). This method is not suitable for detergent with a low CMC because the dilution effect reached here would not be sufficient to dilute the detergent below its CMC (Rigaud and Lévy, 2003). Depending on the assay that should be performed with the proteoliposomes and the reconstituted protein, either a 1:60 or 1:10 protein to lipid ratio was used. After harvest of the liposomes, the reconstitution efficiency was checked on an SDS-PAGE, as similarly performed by Parker and Newstead (2014) for $PepT_{So}$. An exemplary result for reconstitution of DtpB can be seen below (Figure 16).

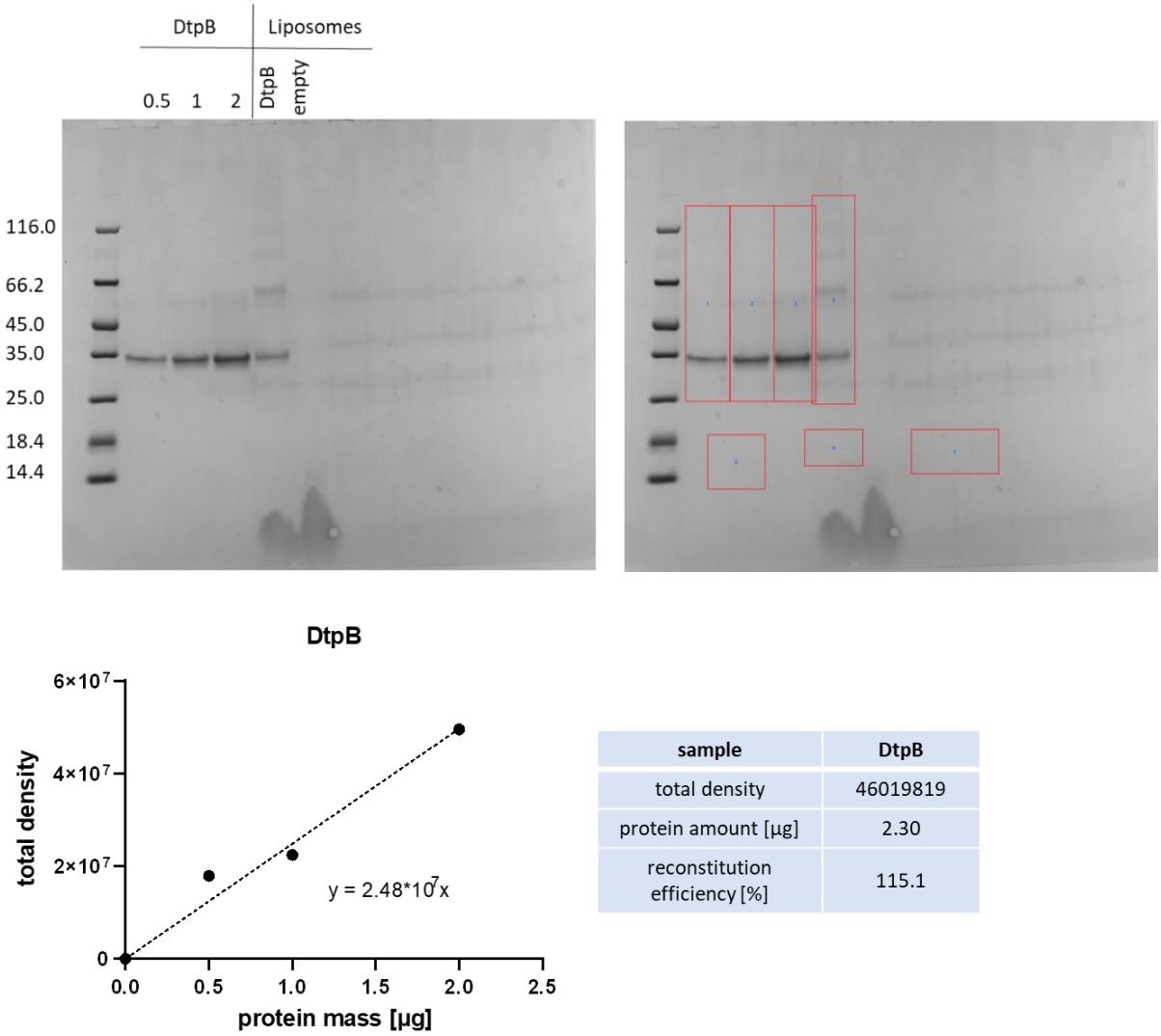

sample	DtpB
total density	46019819
protein amount [µg]	2.30
reconstitution efficiency [%]	115.1

Figure 16: Analysis of reconstitution efficiency for DtpB in POPE/POPG liposomes. *Top: SDS-PAGE gel loaded with samples of DtpB and proteoliposomes, molecular weight of marker proteins is indicated on the left. Lane 2-4: 0.5, 1 and 2 µg DtpB, respectively, lane 5: 4 µL DtpB liposomes, lane 6: empty liposomes. Areas for density analysis are marked in red on the right gel. Bottom: calibration curve for densiometric analysis is shown on the left including the respective formula for the linear fit. The linear fit was performed in Prism GraphPad. The Table on the right displays the total density of the proteoliposome sample with DtpB and the calculated protein amount and reconstitution efficiency.*

DtpB was applied to the gel in amounts of 0.5, 1 and 2 µg together with 4 µL of the proteoliposomes. A reconstitution efficiency of 100 % would correspond to 2 µg protein in the liposome sample. For densiometry analysis the total density of each lane on the gel was determined and a calibration curve generated (Figure 16). From this, the protein mass in the proteoliposomes could be determined. Here, the efficiency was at roughly 100 %.

4.2.2 Biobead method

The biobead reconstitution method was utilized for the sugar acid transporters examined in this project because very tight liposomes were necessary for uptake assays with these transporters and

this way also protein solubilised in DDM (low CMC) could be used for reconstitution (Rigaud and Lévy, 2003).

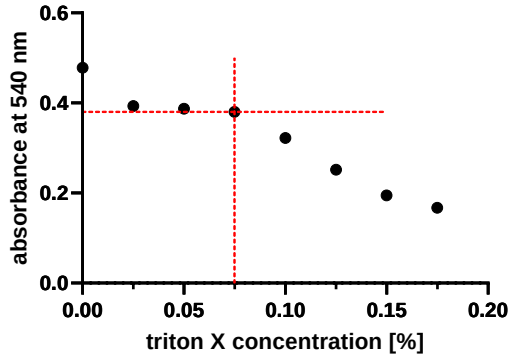

Figure 17: Liposome destabilisation by Triton-X 100. *Absorbance of 200 µL of empty liposomes at a lipid concentration of 0.5 mg/mL was measured at a wavelength of 540 nm. Triton-X 100 (10%) was added in steps of 0.5 µL and absorbance measured for each step to determine the amount that was required to decrease the initial absorbance by 20 %. The respective absorbance and concentration values are marked by red dashed lines.*

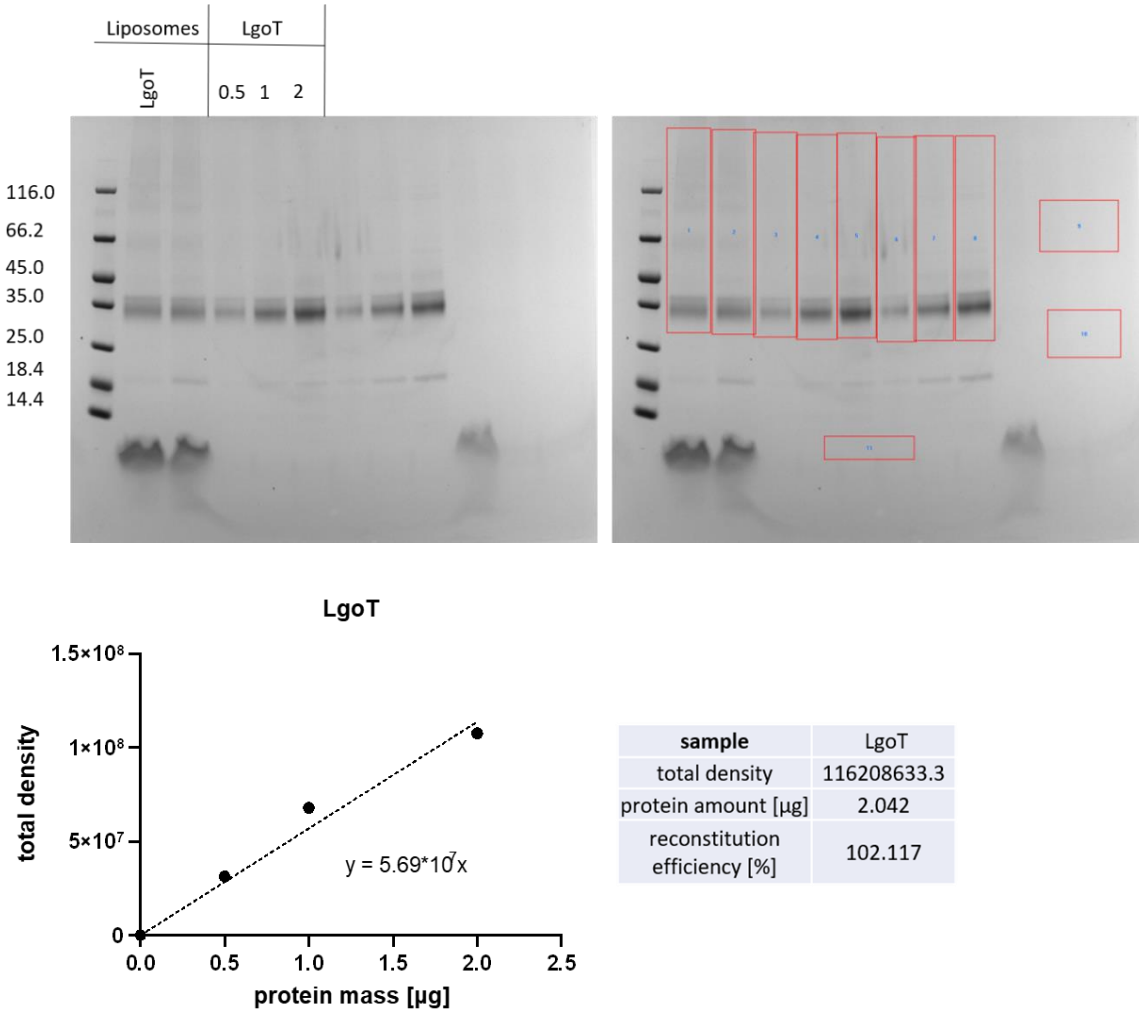

sample	LgoT
total density	116208633.3
protein amount [µg]	2.042
reconstitution efficiency [%]	102.117

Figure 18: Analysis of reconstitution efficiency for LgoT in POPE/POPG liposomes. *Top: SDS-PAGE gel loaded with samples of LgoT and proteoliposomes, molecular weight of marker proteins is indicated on the left. Lane 2: 4 µL proteoliposomes with LgoT, lane 4-6: 0.5, 1 and 2 µg LgoT. Areas for density analysis are marked in red on the right gel. Bottom: calibration curve for densiometric analysis is shown on the left including the respective formulas for the linear fit. The Table on the right displays the total density of the proteoliposome sample and the calculated protein amount and reconstitution efficiency.*

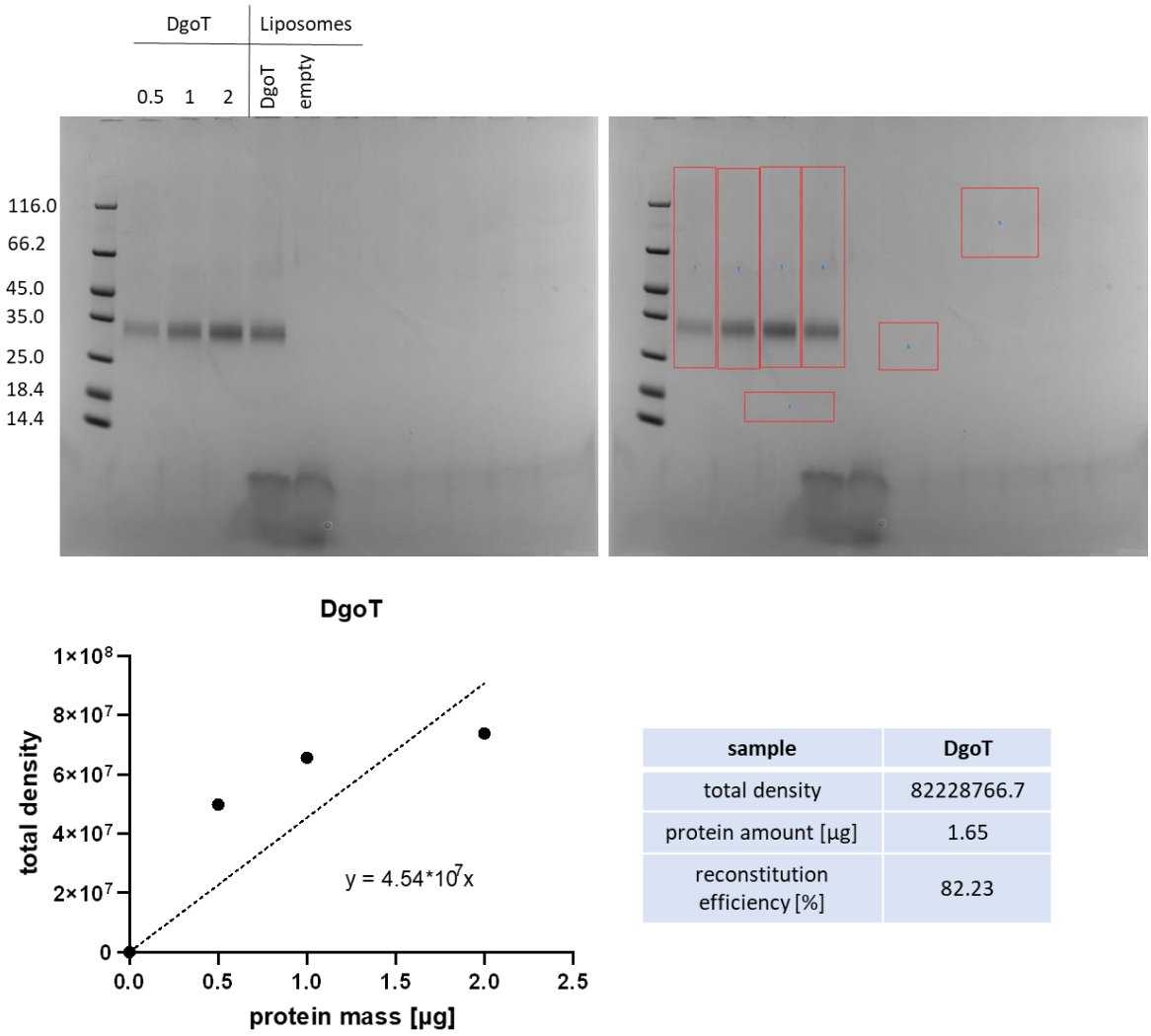

sample	DgoT
total density	82228766.7
protein amount [µg]	1.65
reconstitution efficiency [%]	82.23

Figure 19: Analysis of reconstitution efficiency for DgoT in POPE/POPG liposomes. *Top: SDS-PAGE gel loaded with samples of DgoT and proteoliposomes, molecular weight of marker proteins is indicated on the left. Lane 2-4: 0.5, 1 and 2 µg DgoT, lane 5: 4 µL DgoT liposomes, lane 6: 4 µL empty liposomes. Areas for density analysis are marked in red on the right gel. Bottom: calibration curve for densiometric analysis is shown on the left including the respective formula for the linear fit. The Table on the right displays the total density of the proteoliposome sample with DgoT and the calculated protein amount and reconstitution efficiency.*

The procedure was adapted from Parker and Newstead (2014), where it was used for reconstitution of NRT1.1. Previously extruded liposomes were destabilised by addition of Triton-X 100, then mixed with protein and incubated for 30 min at room temperature and 30 min at 4°C. Removal of the detergent was carried out by mixing the liposome solution with defined amounts of biobeads in three steps. Results of the Triton-X 100 titration to find the right concentration for destabilisation of liposomes are shown in Figure 17. The initial absorbance of the liposomes was at 0.48 and a decrease by 20 % to an absorbance of 0.38 was observed after addition of 1.5 µL of 10 % Triton-X 100, which corresponds to a Triton-X concentration of 0.075 %. The two Figures 18 and 19 display the analysis of the reconstitution efficiency for DgoT and LgoT. The reconstitution efficiency was checked the same way as for the rapid dilution method. Both ACS transporters were reconstituted with a high efficiency of 82 % for DgoT and 100 % for LgoT.

4.3 Pyranine uptake assays

The most common way of performing liposomal uptake assays is using radiolabelled substrates to directly measure the substrate amount inside the liposome after a given time. This method bares safety hazards due to the radiation the experimenter is exposed to and also the availability of suitable isotope-labelled substrates is limited (Yamamoto et al., 2011). Therefore, finding an alternative system to study proton-coupled transporters is paramount. One such alternative is the indirect read out of proton-flux upon substrate translocation. In this study, pyranine was entrapped into liposomes to detect proton influx. The advantages of pyranine include its high availability, high sensitivity and detectability in low concentrations (Kano and Fendler, 1977).

To perform uptake assays as close to the physiological environment of the transporter as possible, they can be conducted in whole cells, which overexpressed the target protein (Volpe, 2015). For examination of a single transporter this could give a rough characterisation of the transport activity but other transporters recognising the same substrates could interfere (Volpe, 2015). For example, in *E. coli* three more di- and tripeptide transporters besides DtpB are known that could hinder the *in vivo* characterisation of DtpB (Ernst et al., 2009). Liposomal uptake assays have the advantage of a fully controlled environment to specifically examine the function of one transporter (Drew et al., 2021).

As all transport proteins tested in this study are known or putative proton-coupled transporters, an electrochemical proton gradient was applied across the liposome bilayer to facilitate transport activity (Harder et al., 2008; Leano et al., 2019). Therefore, a higher KCl concentration was used inside the liposomes and the ionic strength was balanced with NaCl on the outside. Addition of valinomycin led to a negative inward potential, as described before. The difference in electrical potential (ΔΨ) across the liposomal membrane was calculated as follows (eq. 13 and 14), assuming a temperature of 20 °C. The concentration of potassium ions inside the liposomes was at 120 mM (inside buffer). As the liposomes were resuspended in 4 µL of inside buffer per measurement and then diluted with 200 µL of outside buffer (not containing potassium), the concentration of potassium ions outside the liposomes was at 2.35 mM.

$$\Delta\Psi = 2.3\frac{RT}{mF}\log_{10}\left\{\frac{[X^{K+}]_B}{[X^{K+}]_A}\right\} \tag{13}$$

$$\Delta\Psi = 2.3\frac{8.314\ \frac{J}{K\ mol} * 293.15\ K}{1 * 96485.332\frac{C}{mol}}\log_{10}\left\{\frac{2.35mM}{120mM}\right\} = -99.3\ mV \tag{14}$$

The negative inward electrical potential was at roughly -100 mV.

4.3.1 Determining the substrate profile of DtpB

DtpB, a known di- and tripeptide transporter in *E. coli,* was tested with a variety of peptides to examine the specificity of this transporter and better understand its function. Here, proteoliposomes with a protein to lipid ration of 1:60 were used, as this was shown to be a suitable ratio for liposomal uptake assays with $PepT_{St}$ (Parker et al. 2014). As di-alanine (AA) showed significant competition for the binding site of DtpB in a previous study (Harder et al., 2008) the pyranine assay was first established for this dipeptide. Tetra-alanine (AAAA) was used as a negative control since tetrapeptides should not be transported (Harder et al., 2008). Also, measurements with addition of buffer not containing any peptide were performed as a reference signal, showing potential proton permeability of the proteoliposomes not associated with transporter activity. Moreover, the generation of a membrane potential after valinomycin addition was tested by adding CCCP (Carbonyl Cyanide m-Chlorophenylhydrazone) to the solution. CCCP is a protonophore and therefore able to translocate protons across the membrane, uncoupling the membrane potential. It can be seen in Figure 20 that the fluorescence measured at 460 nm in empty liposomes is stable during addition of buffer and valinomycin but immediately decreases to nearly zero when CCCP is added. This means the protonophore caused a strong proton influx indicating a negative inward membrane potential was present in the liposomes. Absorbance measured at 415 nm stays constant, as this is not pH dependent, and only slightly decreases due to dilution effects, when solutions are added.

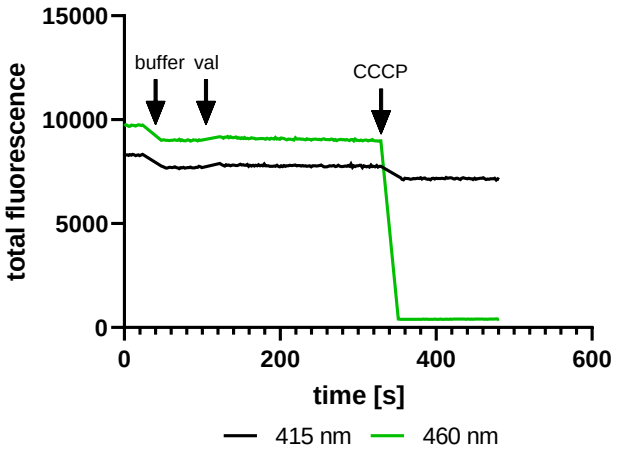

Figure 20: Measurement of pyranine fluorescence in empty liposomes at 415 and 460 nm with addition of CCCP. *To test generation of a membrane potential liposomes were mixed with buffer and valinomycin (val) and CCCP was added after roughly 300 s. CCCP transports protons across the liposomal membrane and therefore disrupts the membrane potential.*

Figure 21 shows the raw data of an exemplary experiment with AA in empty and DtpB liposomes, indicating absorption at 415 and 460 nm.

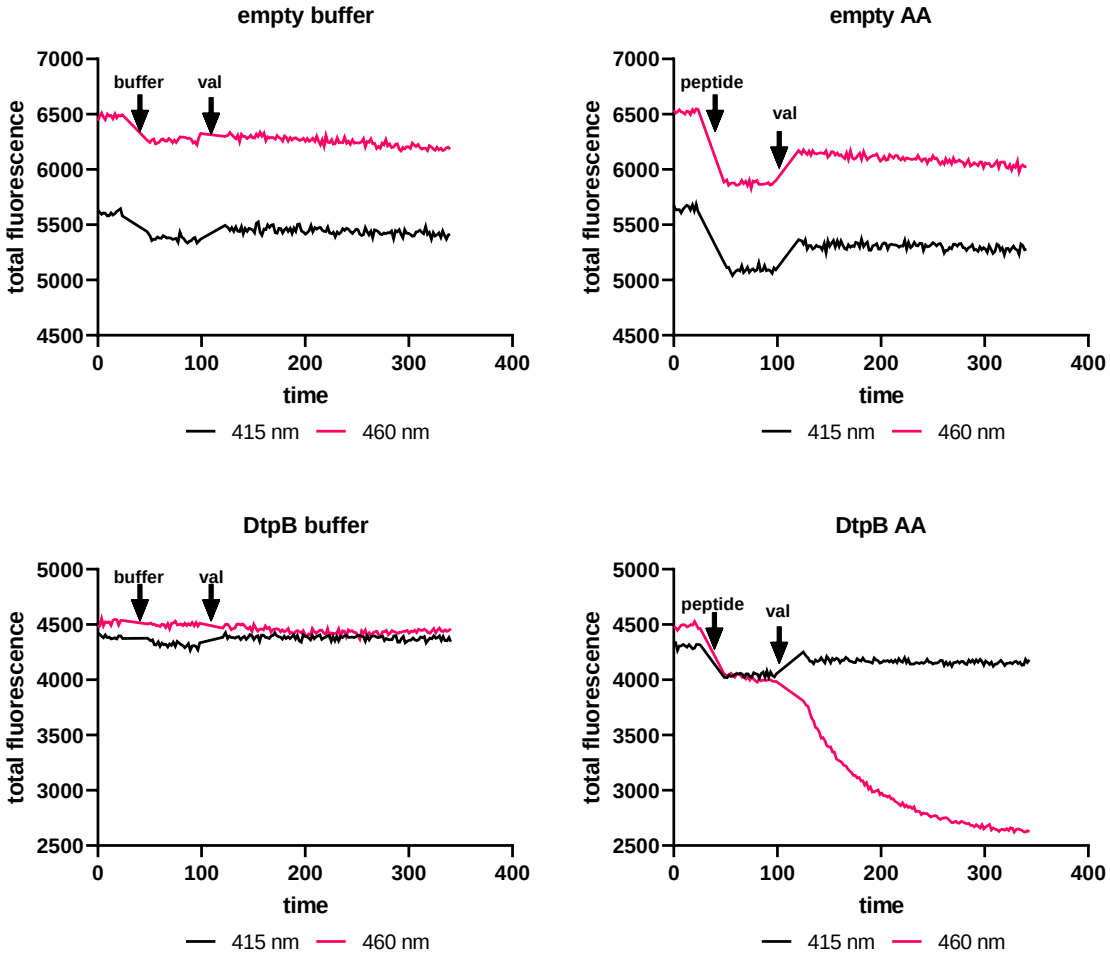

Figure 21: Raw data of a liposome-based uptake assay using the fluorescent dye pyranine as a reporter for proton influx. Empty liposomes and proteoliposomes with DtpB were tested for uptake of di-alanine. *As a reference also the buffer signal was recorded. Absorption was measured at 415 and 460 nm. The total fluorescence is shown over the time course of a measurement. Arrows indicate the time point of substrate and valinomycin (val) addition.*

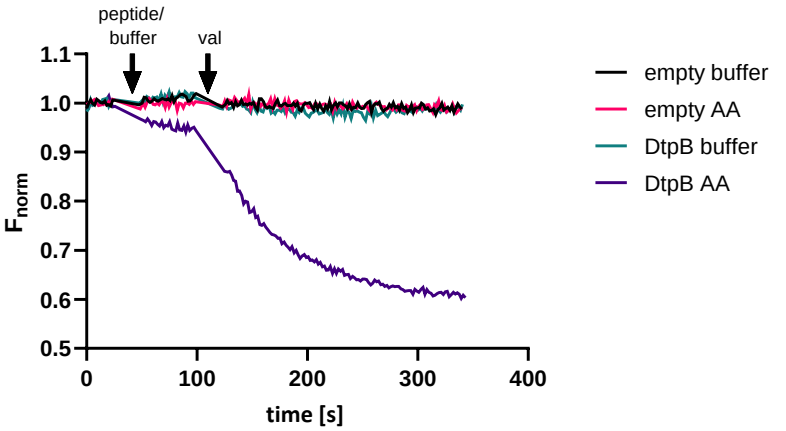

Figure 22: Normalised transport signal for uptake measurement with empty and DtpB liposomes using the pyranine assay. Uptake was tested for buffer (reference) and AA. *Normalised fluorescence is shown over the time course of the measurement. Arrows indicate the time point of substrate and valinomycin (val) addition.*

The data was pre-processed by dividing the fluorescence values for excitation at 460 nm by the ones at 415 nm and then normalised to the average initial value before addition of any compound. The normalised curves are displayed in Figure 22.

In order to rule out transport artefacts due to ions or pH in the substrate solution, the empty transport curve (bck_norm) was fit with a line (bck_norm_fit) and the slope subtracted from the transport curve with DtpB proteoliposomes (Figure 23). This led to the corrected transport curve (norm_corr) shown in Figure 23, which was then fitted with either a linear or exponential fit (norm_corr_fit).

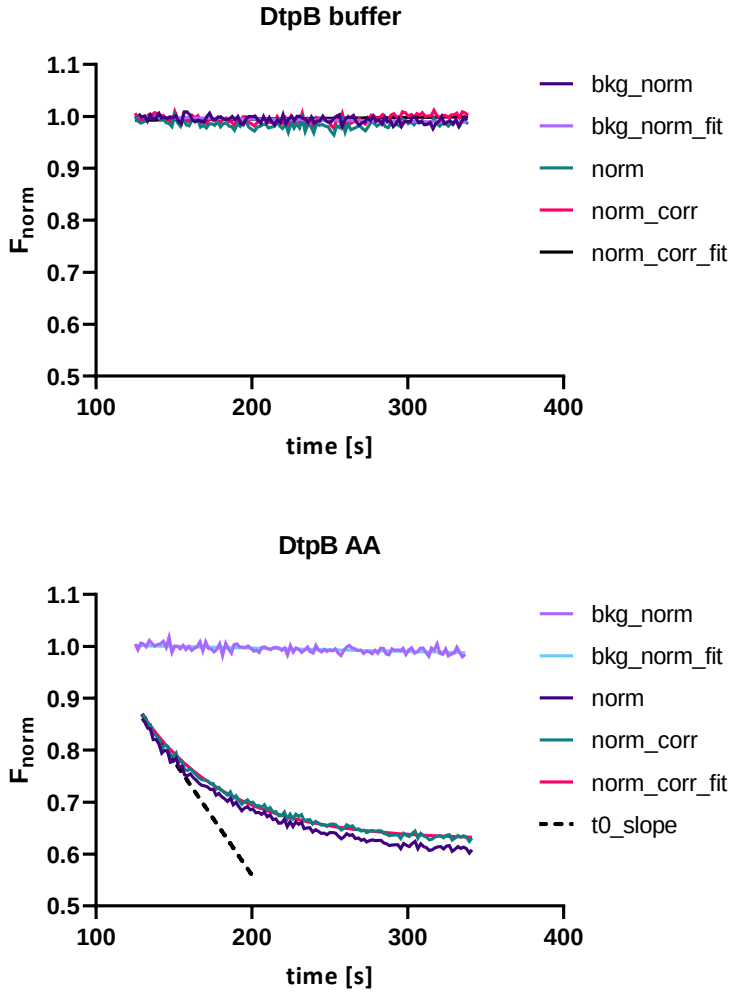

Figure 23: Curve fitting and corrected curves for uptake of buffer and AA by empty and DtpB liposomes using the pyranine assay. *The normalised signals for empty liposomes (bkg_norm) were fitted with a line (bkg_norm_fit) and the slope was subtracted from the normalised DtpB signal (norm) to obtain the corrected curve (norm-corr). This was fitted with an exponential fit (norm_corr_fit) and the initial slope was determined (t0_slope).*

Figure 23 shows exemplary fittings of a buffer control and a di-alanine transport curve. After normalisation and correction of the transport signal by the empty signal, the residuals for linear and exponential fits were calculated and the F-test was used to decide which fit describes the datapoints best. If the F-statistic value was above the critical value F_{crit}, the exponential model was selected,

otherwise the linear model was used. For each transport signal the t_{0_slope} was calculated using the parameters of the fit, as described before.

As can be seen in Figure 24, there was a relatively high variability of the transport signal for the positive control AA between different proteoliposome batches. To assure reproducibility of the measurements and reduce the error of the fits, only batches were used, which showed an AA signal with an amplitude ≥ 0.1 and a tau value ≤ 150 s. Also, for each peptide the transport signal was normalised to the AA signal measured the same day, to make data of different days and batches comparable.

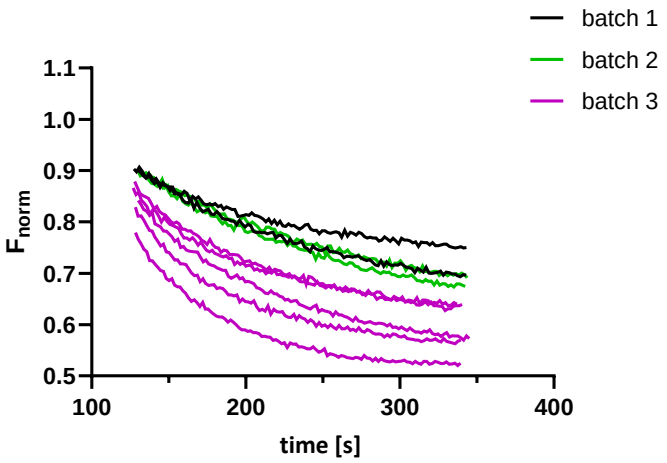

Figure 24: Variability of transport curves for AA transport by DtpB in different proteoliposome batches using the pyranine assay. *Measurements from three different batches, indicated by colour, are shown. Each curve corresponds to a different experiment day indicating the normalised and corrected transport signal.*

For all tested peptides, triplicate measurements were performed on three individual days. This gave a realistic estimation of variability of the assay due to liposome preparation and transporter functionality. For all triplicate measurements, a substrate concentration of 2.5 mM and a valinomycin concentration of 1 µM was used for 5 µg of protein.

Figure 25 shows examples of peptides leading to high proton uptake into proteoliposomes, therefore resulting in an exponential curve. Different examples of peptides causing no, or little proton transport are displayed in Figure 26.

The complete set of raw data for all peptides tested for uptake by DtpB can be found in the annex (section 9.1) and a summary of the results is displayed in Figure 27. It gives the relative initial slopes ($t_{0\_slope\_rel}$) of all three measurements for each peptide and the median value with the median absolute deviation shown as error bars.

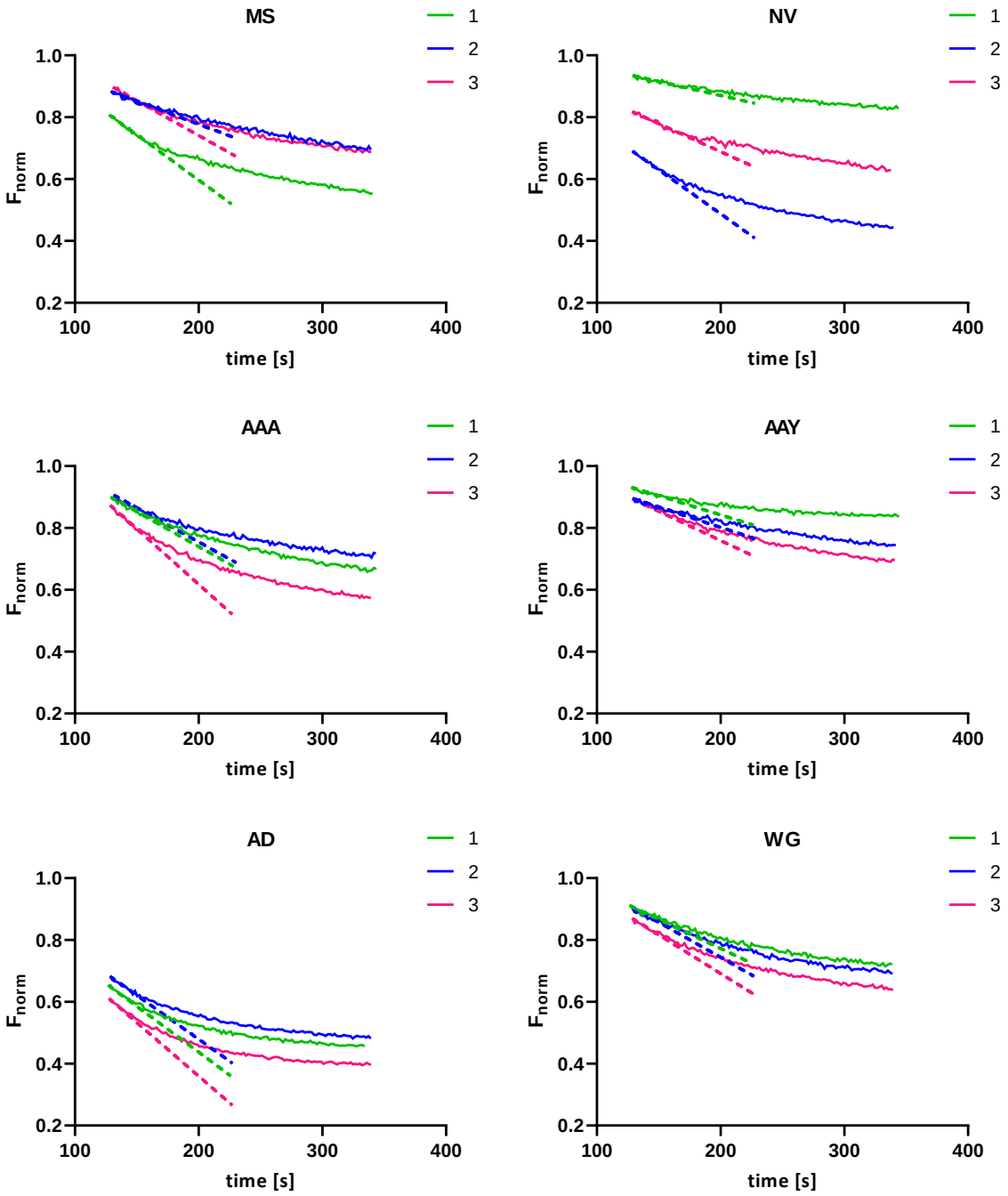

Figure 25: corrected transport curves (solid line) and t_0 slopes (dashed line) for triplicate measurements of MS, NV, AAA, AD, WG and AAY in a concentration of 2.5 mM. *Uptake assays were performed with DtpB proteoliposomes on three different days for each peptide using the fluorescent dye pyranine as a reporter for proton influx.*

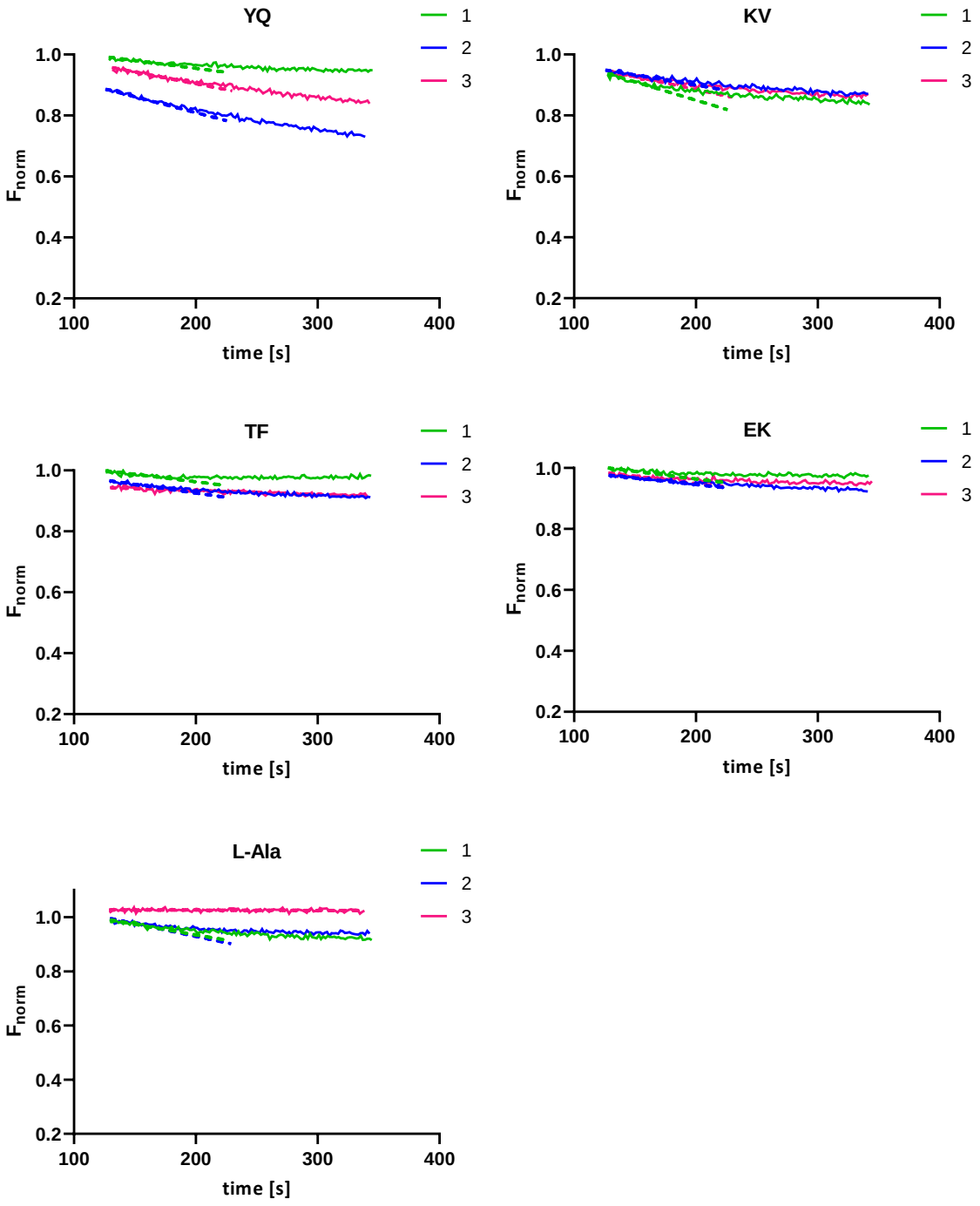

Figure 26: Corrected transport curves (solid line) and t_0 slopes (dashed line) for triplicate measurements of YQ, KV, TF, EK and L-Ala in a concentration of 2.5 mM. *Uptake assays were performed with DtpB proteoliposomes on three different days for each peptide using the fluorescent dye pyranine as a reporter for proton influx.*

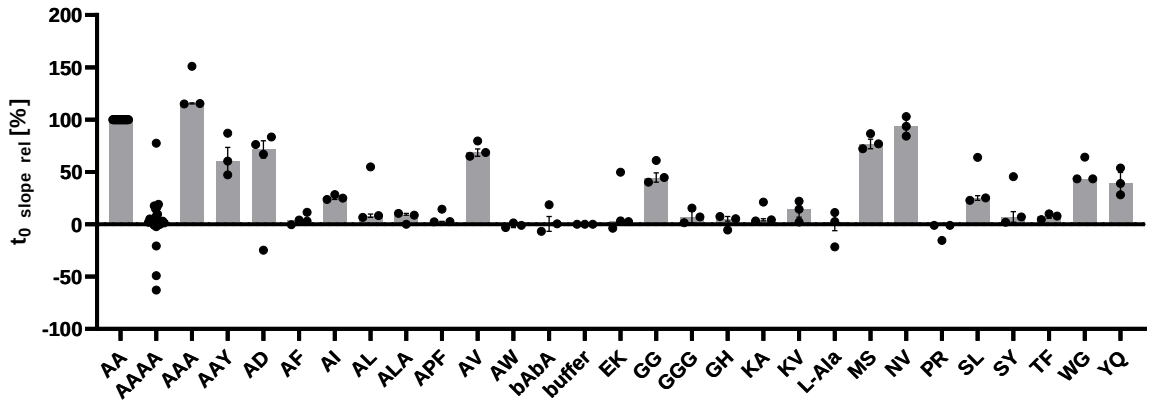

Figure 27: Relative initial slopes ($t_{0\_slope\_rel}$) of all peptides measured in triplicates for uptake by DtpB using the pyranine assay. *All peptides were tested in a concentration of 2.5 mM. The individual datapoints, the median value and the median absolute deviation are displayed for each peptide.*

It can be observed from Figure 27 that the peptides AA, MS, NV, AD, AV and AAA caused the highest proton influx into the liposomes (~ 70 – 125 %) and therefore might be strongly transported. Less proton influx was induced by peptides such as GG, AAY, WG and YQ with a range of 40 -60 % relative transport signal. For many other peptides a relative decrease in fluorescence of less than 10 % was observed (Figure 27).

The Z'-factor between AA and AAAA was calculated to evaluate the quality of this assay. Instead of using the mean and standard deviation of the relative t_0 slopes, the median and the median absolute deviation were utilized here because these are robust statistics, more resistant to outliers. This approach was better suited due to the variability of the proteoliposome batches, e.g. to account for the few outliers that were observed for AAAA (Figure 27). It improved the Z'-factor of the assay and was therefore continued for all further data evaluation. The Z'-factor was calculated as follows:

$$Z'_{DtpB} = 1 - \frac{(3\sigma_{AA} + 3\sigma_{AAAA})}{|\mu_{AA} - \mu_{AAAA}|} = 1 - \frac{(0 + 10.8)}{|100 - 3.1|} = 0.89 \quad (15)$$

The resulting Z'-factor is above 0.5 and can therefore be classified as an excellent assay with a sufficient separation band.

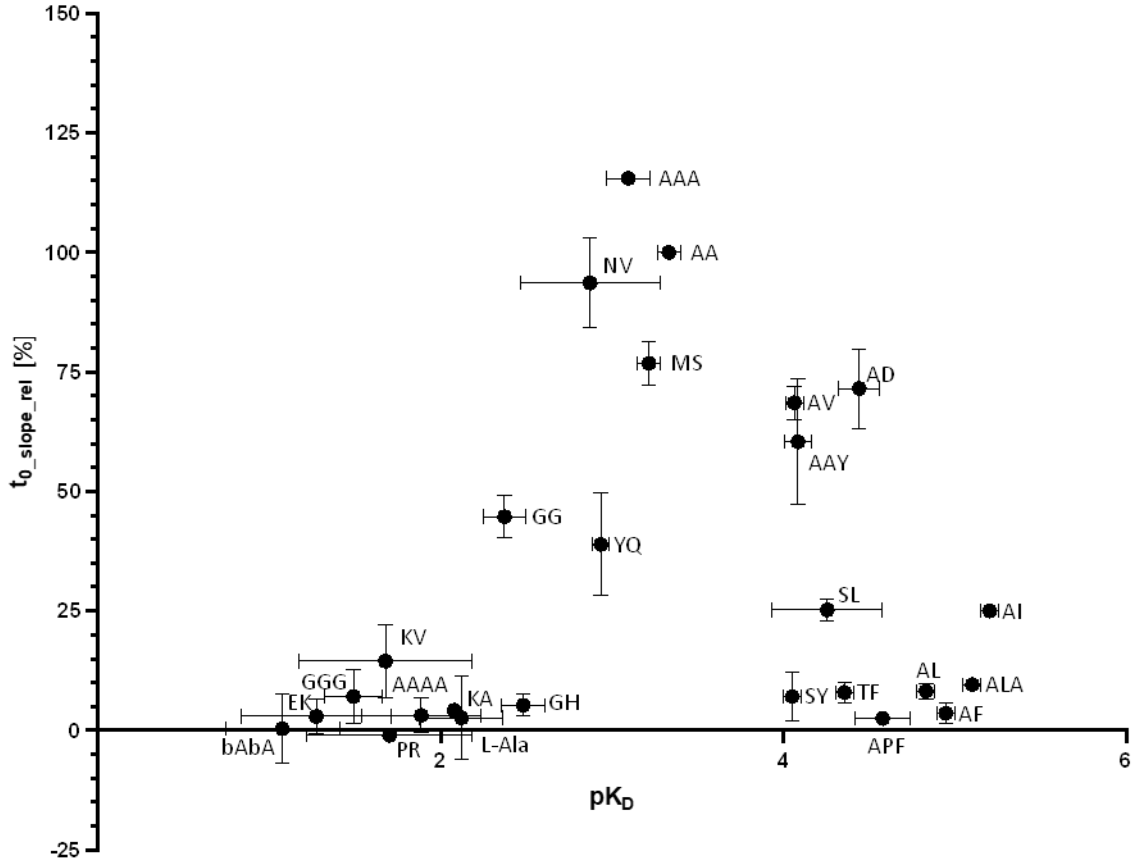

Figure 28: Correlation of affinity and transport activity for different peptides to DtpB. *Transport activity ($t_{0\_slope\_rel}$) is displayed as t_0 slope relative to the slope of AA. Affinity was determined using nanoDSF and is displayed as the negative logarithm of the K_D (pK_D). For each peptide the median of the $t_{0\_slope\_rel}$, median absolute deviation of the $t_{0\_slope\_rel}$, the mean pK_D and the standard deviation of the pK_D are shown.*

Affinity of most tested peptides to DtpB was measured using low volume differential intrinsic tryptophan scanning fluorimetry (nanoDSF) by Giada Finocchio (former member of Loew group, EMBL Hamburg). This method is based on measuring the melting temperature of the protein, which depends on its thermodynamic stability (Magnusson et al., 2019). Binding of a ligand can increase the thermal stability of a transporter, where high affinity binding of a ligand to the transporter is associated with a higher melting temperature (Magnusson et al., 2019). Figure 28 shows affinity as negative logarithm of the dissociation constant (pK_D). A higher pK_D indicates higher affinity. It can be observed that peptides with low transport activity are mainly located in the low affinity area (pK_D <2.5) and in the high affinity area (pK_D > 4.0). In between (pK_D ~2.5 to 4.0) peptides show a high proton influx, meaning they have the highest transport activity.

The setup of this liposomal uptake assay furthermore allowed determination of apparent K_M values for different peptides by measuring a range of peptide concentrations. This was done for selected di- and tripeptides showing a high transport activity of DtpB, which were AA, AAA and GG, and also for GGG. Like before, the t_0 slopes were normalised to the AA transport signal at 2.5 mM to make data comparable. Relative t_0 slopes were then plotted against the substrate concentration and the K_M and

V_{max} values were determined using the Michaelis-Menten equation (Figure 29). The individual curves for each peptide concentration in triplicates are shown in the annex (section 9.2).

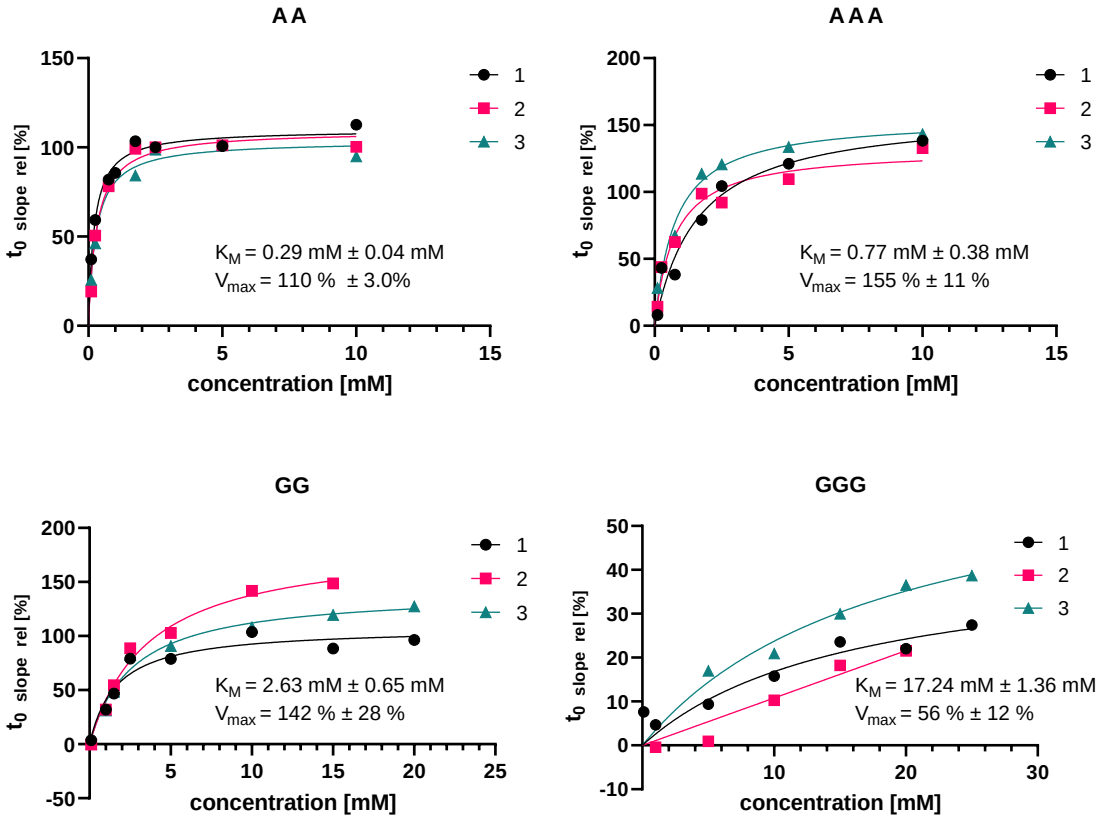

Figure 29: Uptake measurements with DtpB proteoliposomes using different concentrations of a peptide to determine the K_M value. *The peptides AA, GG, AAA and GGG were tested in triplicates using the pyranine assay with peptide concentrations ranging from 0 to 25 mM. The t_0 slopes were plotted against the concentration of the peptide. Determination of the K_M was performed using the software Prism Graphad.*

The highest apparent K_M value was observed for GGG with K_M^{app} = 17.24 mM ± 1.36 mM, where no clear saturation behaviour was observed. AA resulted in the lowest apparent K_M value of 0.29 mM ± 0.04 (Figure 29). For AAA and GG apparent K_M values of 0.77 mM ± 0.38 mM and 2.63 mM ± 0.65 mM respectively, were observed. Similar apparent V_{max} values were observed for AA, AAA and GG, with 110 % ± 3.0 %, 155 % ± 11 % and 142 % ± 28 %, respectively. The apparent V_{max} of GG was lower with 56 % ± 12 %.

Additionally, AF was tested in different concentrations for its ability of inhibiting the transporter, as this peptide has a high affinity but no transport was detected in the pyranine assay. Different concentrations of AF were mixed with a fixed AA concentration of 2.5 mM, to determine an IC_{50} value for AF. The t_0 slopes were normalised to the AA transport signal at 2.5 mM to compare data from different measurement days. Relative t_0 slopes were then plotted against the AF concentration and the IC_{50} value was determined using Prism GraphPad (Figure 30) (Prism – GraphPad, 2021).

Increasing concentrations of AF led to a decrease in transporter activity, but transport of AA was not completely inhibited by AF. For high AF concentrations the signal stops at a slope of roughly 40 % of the initial signal slope (Figure 30). The individual curves for each AF concentration in triplicates are displayed in the annex (section 9.2).

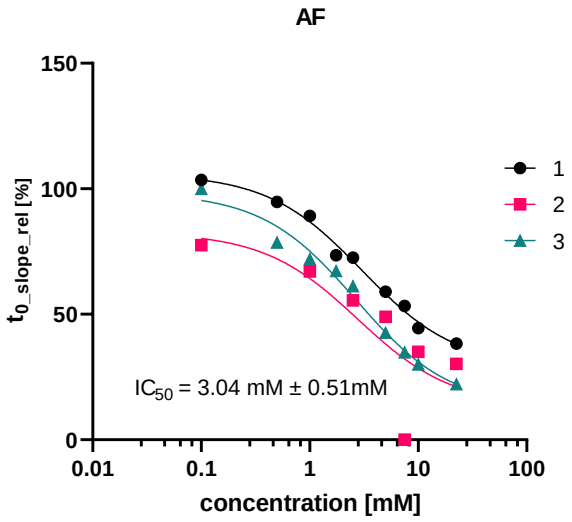

Figure 30: Uptake measurements with DtpB proteoliposomes using different concentrations of AF to examine the inhibitory effect on AA uptake. *Different concentrations of AF were mixed with 2.5 mM AA and the uptake signal was measured using the pyranine assay. The t_0 slopes were plotted against the AF concentration. Determination of the IC_{50} was performed using the software Prism GraphPad.*

4.3.2 Determining stereospecificity of LgoT and DgoT

The two transporters DgoT and LgoT, belonging to the ACS family, were tested in this project for specific uptake of sugar acids. DgoT is known to transport D-galactonate, while LgoT is a putative L-galactonate transporter (Leano et al., 2019). Stereospecificity of these transporters was evaluated in liposomal uptake assays.

The assay was performed under similar conditions as for DtpB. Measurements were done in triplicates, with 5 µg of protein per experiment, 2.5 mM substrate and 0.1 µM valinomycin. Also, buffer was used as a reference signal and galactose, a sugar, was used as a negative control. For establishment of the assay, LgoT proteoliposomes (1:60) produced by the rapid dilution method were tested for uptake of L-galactonate. Figure 31 shows a linear decrease in relative fluorescence from the beginning of the measurement on and also after addition of buffer or substrate and valinomycin. This is an indication for proton permeability of the liposomes. For this reason, reconstitution was optimised using the biobead method with the aim of a more efficient detergent removal.

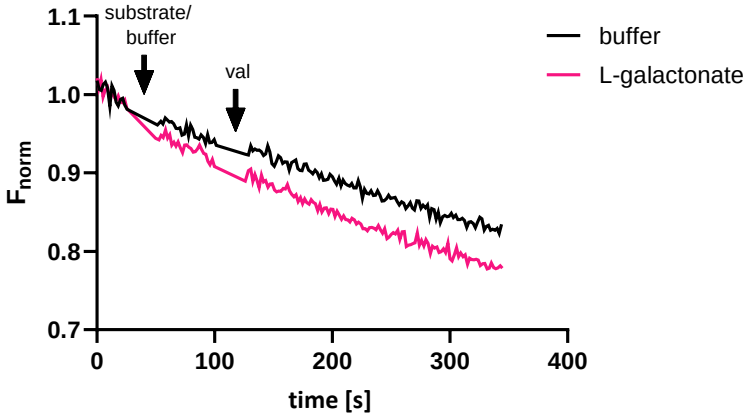

Figure 31: Uptake measurements with LgoT proteoliposomes using the pyranine assay for determination of proton influx. Reconstitution of LgoT was performed by rapid dilution and uptake was determined for buffer and L-galactonate*. The normalised fluorescence signal is plotted against the time and addition of substrate and valinomycin (val) is indicated by arrows.*

Reconstituting LgoT with the biobead method improved proton impermeability of the liposomes, as can be seen in Figure 32. Both LgoT and DgoT proteoliposomes showed a steady relative fluorescence for the buffer control, which only marginally decreased over the time course of the measurement. For LgoT a protein to lipid ratio of 1:60 was kept like for DtpB, while for DgoT it was 1:30 in accordance with Leano et al. (2019).

Transport signals for DgoT and LgoT were obtained as expected, showing the high stereospecificity of the proteins (Figure 32). While LgoT shows a relatively flat and linear transport curve for L-galactonate, DgoT shows an exponential transport curve with high amplitude for D-galactonate (Figure 32). Both transporters showed no transport activity for galactose or the other galactonate stereoisomer. The t_0 slopes of the triplicate measurements for both transporters are also shown in Figure 32. As for the DtpB data, the t_0 slopes of the buffer signal were subtracted from the transport signals, but the slopes were not normalised as no positive control was used here. The bar graphs indicate the single data points as well as the median value and median standard deviation.

The Z-factor was calculated between galactose as a negative control and the substrate of each transporter. Again, median and median absolute deviation were used, as this improves the Z-factor. The results are given in equation 16 and 17 for LgoT and DgoT, respectively.

$$Z_{LgoT} = 1 - \frac{(3\sigma_{L-galactonate} + 3\sigma_{galactose})}{|\mu_{L-galactonate} - \mu_{galactose}|} = 1 - \frac{(0.55 * 10^{-3} + 0.11 * 10^{-3})}{|1.20 * 10^{-3} - 0.03 * 10^{-3}|} = 0.44 \quad (16)$$

$$Z_{DgoT} = 1 - \frac{(3\sigma_{D-galactonate} + 3\sigma_{galactose})}{|\mu_{D-galactonate} - \mu_{galactose}|} = 1 - \frac{(1.36 * 10^{-3} + 0.88 * 10^{-3})}{|3.41 * 10^{-3} - 0.93 * 10^{-3}|} = 0.10 \quad (17)$$

The Z-factors for LgoT and DgoT in the pyranine assay are lower than the Z'-factor for the DtpB data. Both are in the range of $0 \leq Z \leq 0.5$, so these assays can be classified as acceptable assays with small separation bands.

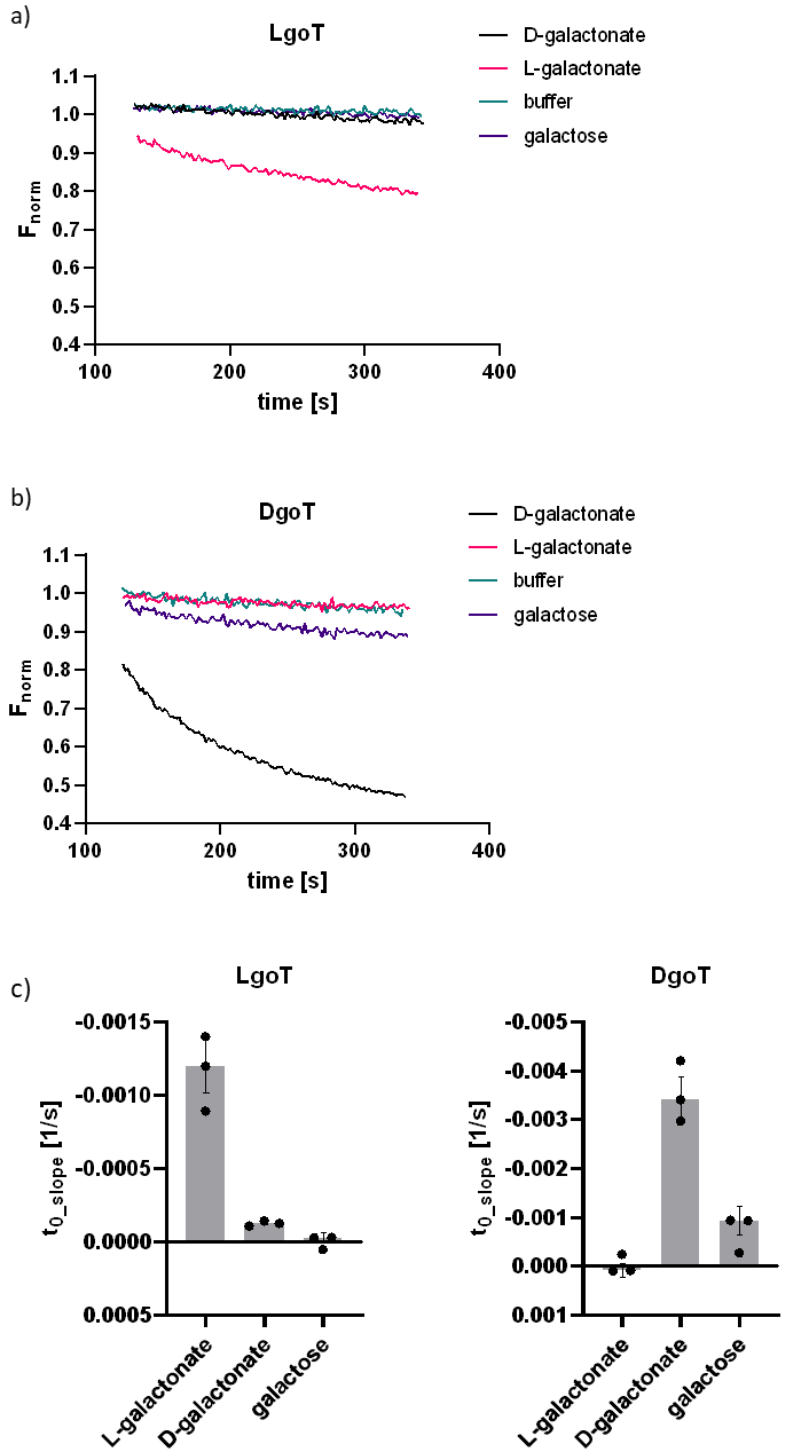

Figure 32: Determination of stereospecificity of LgoT and DgoT using the pyranine assay. *For both proteins, uptake of D-galactonate, L-galactonate and galactose was tested at a substrate concentration of 2.5 mM. A) exemplary normalised and corrected transport curves for LgoT; B) exemplary normalised and corrected transport curves for DgoT; C) overview of t_0 slopes for triplicate uptake measurements of DgoT and LgoT proteoliposomes with different substrates. The individual datapoints, the median value and the median absolute deviation are displayed for each substrate.*

The complete transport curves for single concentration measurements in triplicates are displayed in the annex (section 9.3).

In addition to the single concentration measurements, several dilutions of the transported substrate were measured for each protein in duplicates to obtain K_M values. Here, the t_0 slopes were normalised to the transport signal at 2.5 mM substrate concentration. Relative t_0 slopes were then plotted against the substrate concentration and the K_M and V_{max} values were determined using the Michaelis-Menten equation.

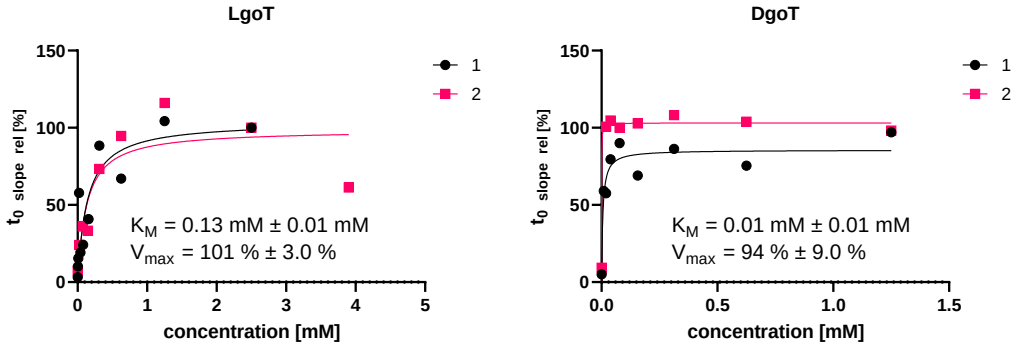

Figure 33: Determination of K_M values for uptake of D-galactonate and L-galactonate by DgoT and LgoT, respectively. *The pyranine assay was performed with proteoliposomes of each protein adding different concentrations of the respective substrate. The relative t_0 slopes were plotted against the substrate concentration. Determination of the K_M was performed using the software Prism Graphad.*

LgoT reached the maximum transport rate at 1.25 mM substrate concentration, while for DgoT this was already the case below 0.1 mM (Figure 33). For LgoT an apparent K_M of 0.13 mM ± 0.01 mM was determined for L-galactonate transport and the apparent K_M of DgoT for transport of D-galactonate was at 0.01 mM ± 0.01 mM. The V_{max} values were similar for both transporters with 101 % ± 3.0 % and 94 % ± 9.0 % for LgoT and DgoT, respectively. Transport curves at different concentrations for each substrate in duplicates are shown in the annex (section 9.4).

4.4 SSM-based assay

The SURFE^{2}R N1 technology was designed for functional assays of membrane transporters and ion channels (Bazzone et al., 2017). Vesicles like cell membranes or liposomes are immobilized on a solid supported membrane and a flux of charged molecules in or out of the vesicles is measured by electrodes (Bazzone et al., 2017). Similar to the pyranine assay, purified protein was reconstituted into liposomes to achieve controlled transport conditions. Here, a protein to lipid ratio of 1:10 was used, as this has previously been shown to be a suitable ratio, e.g. for an excitatory amino acid transporter (Qui et al., 2021). Liposomes were then diluted to 1 mg/mL lipid before adding the solution on the

sensors. As no charge or pH gradient was applied to the liposomes, substrate driven transport was measured. Therefore, a substrate concentration of 20 mM was applied to the sensors.

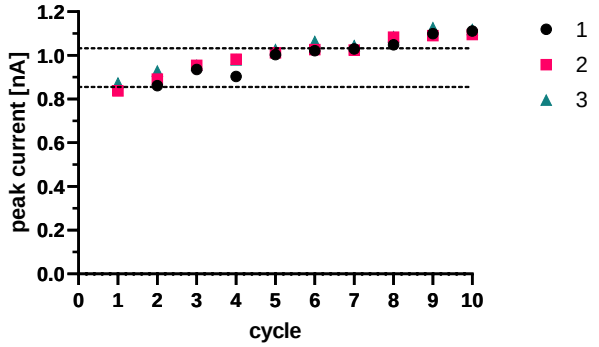

Figure 34: Stability testing of a SURFE²R sensor chip with DtpB proteoliposomes attached. *A series of 10 triplicate measurements (cycles) was performed on one sensor using 20 mM GG (activating solution) and 20 mM glycine (deactivating solution). The signal was assigned as stable as long as the observed peak current did not differ from the initial peak current by more than 20 %. This was the case for the first seven measurement cycles.*

Sensor stability was tested performing a series of 10 triplicate measurements under the same conditions on one sensor (Figure 34). Therefore, 20 mM GG were used in the activating solution and 20 mM glycine in the deactivating solution. The transport signal was assigned as stable as long as the observed mean peak current did not differ from the initial mean peak current by more than 20 % (Bazzone et al., 2017). The resulting peak currents show that the sensor was stable over seven triplicate measurements, meaning 21 single measurements could be performed on the sensor.

To avoid high artefact signals, empty liposomes were used to optimise the deactivating solution for each peptide tested. Exemplary measurements with AV in the activating solution and different amino acid combinations in the deactivating solution can be seen in Figure 35. The tested deactivating solutions contained 20 mM alanine, 20 mM valine, and 10 mM alanine mixed with 10 mM valine, respectively. Solution exchange from AV to valine induced the smallest peak current for empty liposomes, so this combination was used in the subsequent measurements.

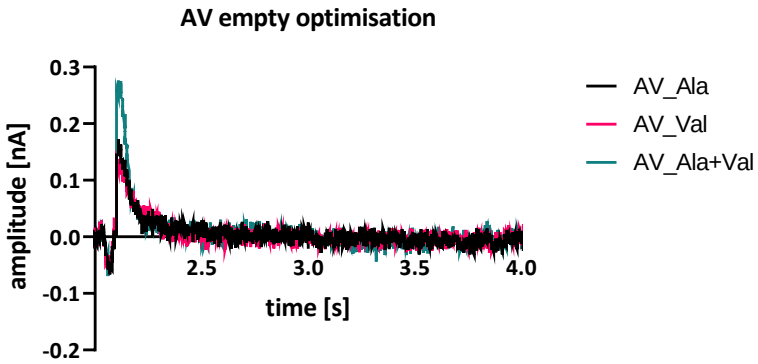

Figure 35: Control measurement for AV with empty liposomes using the SURFE²R technology. Different amino acids were tested in the deactivating solution to reduce artefact signals due to solution exchange during a measurement. *The amplitude of the change in current is displayed during rinse of the sensor with activating solution containing 20 mM AV. The three deactivating solutions contained 20 mM alanine, 20 mM valine and a mixture of 10 mM alanine and valine, respectively.*

Measurements at a single concentration were performed on two different sensors in triplicates for the peptides AA, GG, AAA, AV and AI (Figure 36). For AI, AA and AAA, alanine was used in the deactivating solution, and for GG, glycine. Every test series on one sensor was started and completed with a GG measurement to ensure sensor stability. If the GG signal deviated by more than 20 % over the course of the measurement the data from this sensor were discarded. Peak currents of triplicates from one sensor were first averaged and corrected by the average empty liposome signal and then normalised to the peak current of GG as a reference. This approach allowed to compare data between different sensors. Figure 37 summarizes the average peak currents of all tested peptides. It can be seen that all peptides tested here, induced a signal peak upon solution exchange from deactivating to activation solution, indicating proton influx into the liposomes. As no or only minor peak currents were observed for empty liposomes under the same conditions, the proton influx was DtpB specific. Highest transport activity was observed for AA, followed by AV, AI and AAA. The lowest peak current was measured for GG. The complete data set of single concentration measurements in triplicates on different sensors is depicted in the annex (section 9.5). For AA and GG, also the K_M and V_{max} values were determined using the SURFE²R N1 (Figure 38). As in the pyranine assay, various peptide concentrations were measured. Every concentration was measured in triplicates and all measurements for one peptide were performed on one sensor with stability controls included. The observed peak currents were normalised to the data point with the highest amplitude as suggested by Bazzone et al. (2017).

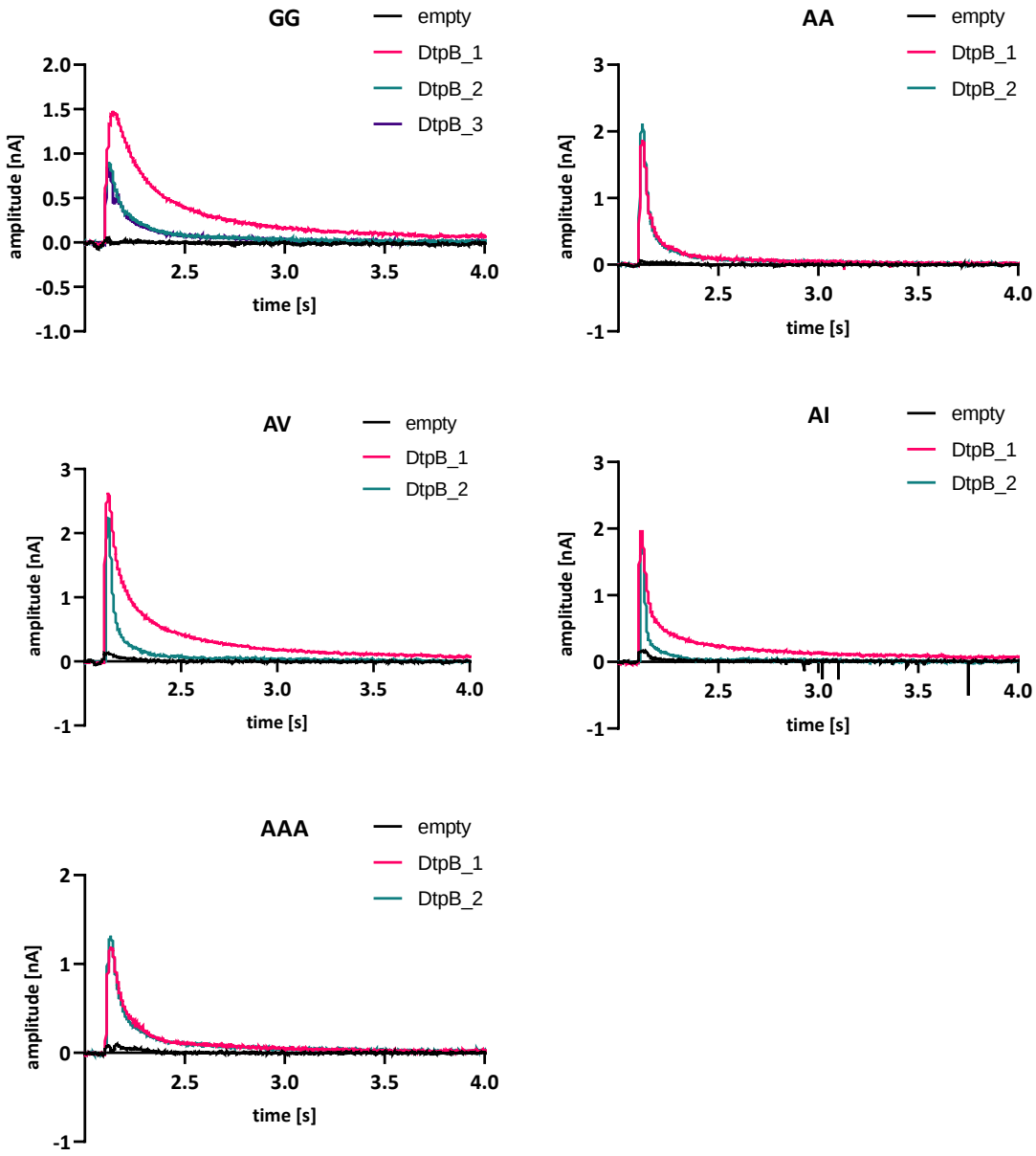

Figure 36: Uptake assays for DtpB proteoliposomes using the SURFE²R technology. The peptides GG, AA, AV, AI and AAA were tested in a concentration of 20 mM in triplicates on three different sensors *(DtpB_1, 2 and 3). For each sensor an exemplary measurement of the triplicate is shown. Also, an exemplary empty signal is displayed. The amplitude of the change in current is shown over the time the sensor was rinsed with activating solution.*

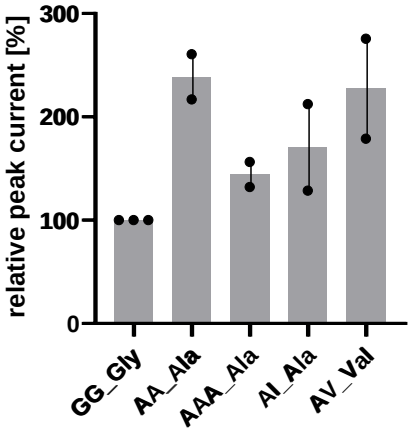

Figure 37: Overview of relative peak currents for uptake assays with DtpB proteoliposomes using the SURFE²R technology. *Uptake was tested for GG, AA, AAA, AI and AV. Each substrate was measured on two sensors in triplicates. The Figure shows median relative peak currents of both sensors (black dots) and the median (bar) and median absolute deviation (error bar).*

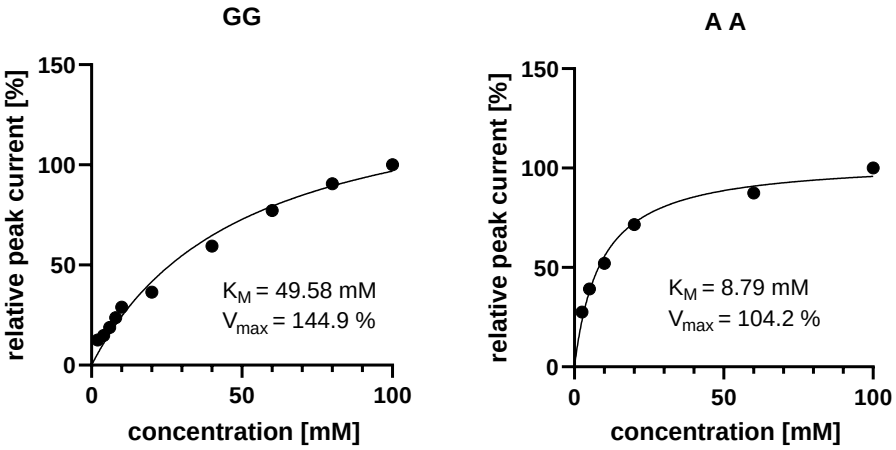

Figure 38: K_M determination for transport of AA and GG by DtpB using the SURFE²R technology. *Both peptides were measured in triplicates on one sensor in different concentrations and the respective peak currents plotted against the peptide concentration. K_M and V_{max} values were determined according to the Michaelis-Menten kinetics using Prism GraphPad.*

For GG a higher K_M value was calculated than for AA, which correlates with the results from the pyranine-based assay (Figure 29). It can be noted that the V_{max} values are very similar between pyranine- and SSM-based methods, but they cannot be directly compared because different experimental conditions and evaluation procedures were used. Section 9.6 shows the raw data for the different substrate concentration measurements.

5 Discussion

This study focused on the establishment of label-free uptake assays for functional characterisation of proton-coupled nutrient transporters. These transporters are essential for nutrient uptake into a cell and therefore play an important role in metabolism. Functional studies of these transporters contribute to deciphering the transport mechanism and substrate specificity. This information can be used in human disease research e.g., in the development of drugs specifically targeted to certain transporters to alter their activity. Also, optimising a drug molecule to be recognised by a transporter can improve absorption and bioavailability.

Most uptake assays developed in the last decades utilized radiolabelled or fluorescently labelled substrates to determine uptake into cells. Not only is the availability of labelled substrates limited but radioactive labelling also bares safety hazards. The methods studied here have the advantage of working without labelling of substrates, indirectly measuring substrate uptake by detecting proton-influx into liposomes. Two different methods were conducted to detect proton-influx, using the pH-sensitive dye pyranine and SSM-based electrophysiology. Both assays were established to test uptake by the di- and tripeptide transporter DtpB from *E. coli*. Moreover, the pyranine assay was verified for the two Anion:Cation symporters LgoT and DgoT.

5.1 Expression and purification of membrane transporters

Established protocols for expression and purification of DtpB and LgoT were used to obtain pure protein for reconstitution into liposomes. Membrane protein expression in *E. coli* C41 cells resulted in sufficient amounts of protein one day after induction of the cells, with roughly 1-2 mg pure protein per litre cell culture, which is a typical amount observed for expression of DtpB in *E. coli* (Harder, 2008). Here, some loss of protein during the purification process was observed on SDS-PAGE gels (Figure 12 and 14). IMAC on Ni-beads was successfully used to separate the protein of interest form other soluble and membrane proteins of *E. coli*, which was confirmed by SDS-PAGE (Figure 12 and 14). Subsequent SEC further indicated high homogeneity of the protein, only showing minor impurities or small amounts of aggregated protein (Figure 13 and 15). Migration of DtpB, LgoT and DgoT on SDS-PAGE gels did not exactly correlate with the theoretical molecular weights of the proteins. This is a known phenomenon for membrane proteins and might originate from detergent binding to the proteins (Rath et al, 2009). Proteins were solubilized in detergent for stabilisation, but the detergent micelle might prevent complete denaturation of the protein by SDS (Rath et al, 2009). This can lead to an altered migration behaviour on an SDS-PAGE compared to proteins not surrounded by detergent (Rath et al, 2009). Therefore, membrane proteins show a different migration behaviour than marker

proteins, which is also termed “gel shifting” (Rath et al, 2009). Function and stability of the proteins was maintained over the purification process, as demonstrated by transport activity in the subsequent uptake assays.

5.2 Liposome preparation and reconstitution

In this study, two different methods, the rapid dilution method and biobead method, were used for reconstitution of membrane transporters into liposomes. Both methods resulted in functional proteoliposomes, but some variability in reconstitution efficiency was observed independent of the protein that was used. Not for all proteoliposome batches the whole amount of protein added to the liposomes was reconstituted. The efficiency might depend on the quality of the protein batch, as highest efficiencies were observed when directly reconstituting the protein after purification without freezing it in between.

The lipid composition of POPE and POPG (3:1) formed sufficiently tight liposomes and proton impermeability could be demonstrated for empty liposomes as well as for liposomes containing protein, as already shown by previous studies (Tsai and Miller, 2013; Parker et al., 2014). In the pyranine assay, liposomes were able to maintain the membrane potential induced by valinomycin over the time course of a measurement, which was proven by addition of CCCP to empty liposomes (Figure 20). CCCP led to a high proton influx into the liposomes due to the negative inward membrane potential. LgoT proteoliposomes that were generated using the rapid dilution method showed a higher proton permeability than liposomes generated using the biobead method. A linear decrease of the relative fluorescence was observed after addition of buffer to the rapid dilution proteoliposomes (Figure 31). The reason for this might be incorporation of some remaining detergent molecules into the liposomes, which can disturb liposome formation. The biobead method removes almost all of the detergent and therefore resulted in liposomes with lower proton permeability (Rigaud and Lévy, 2003). Another advantage of this method is that reconstitution can be performed within two days, opposed to the rapid dilution method, which takes a minimum of three days.

5.3 Pyranine assay

The procedure for performing uptake assays based on encapsulating pyranine into liposomes as a reporter dye for proton influx was adapted for DtpB, LgoT and DgoT. An electrochemical gradient was generated across the liposomal membrane due to an equilibrium potential of potassium ions induced by valinomycin, as similarly used for uptake assays on other proton-coupled transporters (Parker et

al., 2014). The difference in electrical potential was at -100 mV, which is close to the typical physiological membrane potential of an *E. coli* cell (K12) starting at -140 mV.

For DtpB, uptake of a range of peptides was tested to examine specificity of the transporter and get an idea about a possible correlation between transport activity of a peptide and affinity to the binding site. LgoT and DgoT were studied with the aim of verifying the high stereospecificity of both transporters, which was demonstrated by previous studies (Leano et al. 2019, Bartels, 2020).

5.3.1 Establishing pyranine assay for DtpB

Uptake experiments with AA identified this peptide as a substrate of DtpB because proton influx into the proteoliposomes was observed. Buffer controls showed a relatively stable fluorescence for empty and DtpB liposomes and no proton influx was observed for addition of AA to empty liposomes, indicating the observed transport signal was specific to DtpB (Figure 22). The normalised curves of AA uptake showed a slight linear decrease in fluorescence upon addition of AA and then a faster exponential decrease after valinomycin was added (Figure 22). The immediate linear decrease after substrate addition, and in absence of a membrane potential, indicates some AA transport due to the substrate gradient. Presence of a membrane potential strongly increased AA uptake. The reproducibly strong transport signal and high availability of AA made it a suitable positive control for DtpB uptake assays.

However, comparison of corrected transport curves for the positive control showed some variability between the different measurement days and proteoliposomes batches (Figure 24). Curves were differing in the initial relative fluorescence and in amplitude and tau values. They ranged from exponential curves with a steep initial slope to more flat curves with faster saturation. Different initial relative fluorescence values can be caused by a slightly higher proton permeability of the liposomes, which leads to a shift in fluorescence upon substrate and valinomycin addition. As the transport signal was expressed as the relative change in fluorescence (t_0 slope) here, the initial values do not influence the final result. Variations in amplitude and tau values were reduced by setting acceptance criteria for the positive control curves. Discarding all experiments with positive control data outside these boundaries improved data quality of the assay. Furthermore, normalisation of all t_0 slopes to the t_0 slope of the respective positive control was introduced to account for the variability of the assay between different experiment days and reduce its impact on the final result. Calculation of the Z'-factor (Z' = 0.89) further underlined the quality of the assay and classified it as a suitable method for screening and identifying substrates of DtpB.

5.3.2 Substrate profile of DtpB

28 peptides were tested for uptake by DtpB in order to obtain information on the specificity of the transporter and to answer the question whether there is a correlation between affinity and transport activity of peptides. The data obtained from the pyranine assay allowed separation of peptides into transported and not transported ones. Here, all peptides that led to an exponential transport curve with an amplitude above 0.1 were characterised as transported peptides. Peptides leading to a slowly decreasing linear transport curve might be transported by DtpB with a very low turnover rate. This was not classified as transport because it can be assumed that these are not preferred substrates of DtpB, at least under the experimental conditions used here. Furthermore, transport curves with an exponential shape but amplitude below 0.1 and fast saturation (tau ≤ 50s) were also assigned to the non-transported peptides. The steep initial slope might in this case be an artifact due to valinomycin addition or generation of the membrane potential and might not indicate substrate transport, as this behaviour was also observed for some buffer control signals. Based on this classification, the peptides AAY, AD, AV, AA, MS, AAA, NV, WG, AI, YQ and GG were assigned as apparent substrates of DtpB.

Comparing the structural data of DtpB with the results of the uptake assay, it can be concluded that not all ligands of DtpB are also substrates. Structures of DtpB with 12 different peptides located in the binding site were obtained by Maxime Killer and Giada Finocchio. Of these, 10 were tested for uptake and two of them were clearly transported according to the results of the pyranine assay. Although peptides might sterically fit into the binding site of DtpB, they are not necessarily transported. They need to exhibit certain structural and chemical features, which might include position of side chains and charges, to interact with the binding site of the protein and induce transport. Regarding the affinity, K_D values for all 28 peptides were determined from nanoDSF measurements, ranging from high affinities with K_D values in the µM range (K_D = 6.26 µM ± 0.76 µM for AI) to low affinities in the mM range (K_D = 84.0 mM ± 64.2 mM for bAbA). Here, it has to be noted, that affinities in the high mM range could not be detected with a high reliability, indicated by the error for K_D of bAbA. Most peptides showing a high transport activity clustered around an affinity in the range of 0.08 mM (AAY) to 4.3 mM (GG) (Figure 28). Outside this affinity range peptides mainly showed very low or no transport activity. High affinity of a peptide to the binding site of DtpB might inhibit transport because the peptide probably does not dissociate from the protein in the inward open conformation due to the tight binding. At the same time low binding affinity might not be sufficient to induce the transport process. Based on this data, it can be suggested that there might be an optimum affinity range for peptides being transported by DtpB. However, in this uptake assay the transport signal indicates proton influx into the liposome and does not directly describe substrate uptake. Here, it is assumed that all peptides are transported with the same peptide:proton ratio. The actual ratio is not known for DtpB, but for

$PepT_{St}$ it was suggested that dipeptides might be transported with a different number of protons than tripeptides (Parker et al., 2014). Therefore, a high transport signal might originate from a high number of co-transported protons and overestimate substrate transport. Moreover, the data presented here only represents a small selection of more than 8000 possible di- and tripeptide combinations.

For selected peptides apparent K_M and V_{max} values were determined in addition to the single concentration measurements, by measuring the transport signal of a series of different substrate concentrations. The K_M describes the required substrate concentration to reach half maximum transport activity and is a measure for affinity, where a low K_M indicates high affinity (Kaput and Rodriguez, 2006). The highest apparent K_M value was determined for GGG, which did not show transport in the single concentration experiments. Transported peptides AA, AAA and GG resulted in lower apparent K_M values by one to two magnitudes, indicating a higher affinity to DtpB (Figure 29). Overall, a lower K_M correlated with a higher transport activity at 2.5 mM substrate concentration for the four peptides tested here. Only for AA and AAA this correlation was not exactly true because AAA showed the highest transport activity ($t_{0\_slope\_rel}$ = 115 %), but K_M was lower for AA (0.29 mM ± 0.04 mM) than for AAA (0.77 mM ± 0.38 mM). However, AA and AAA are very similar in transport activity as well as K_M and the error in both parameters must be taken into consideration, making this a minor anomaly from the overall trend. The standard deviation of K_M was relatively high, especially for AAA with roughly 50 % and also for GG with 25 %. This might be caused by differing temperatures inside the TECAN during the series of measurements or slight variations in the dilution of peptide stock solutions, which were prepared individually for each triplicate measurement.

The V_{max} value is the extrapolated maximum transport activity possible and was similar for AA, AAA and GG with values in a range of roughly 110 % to 155 % (GraphPad, 2020). This is a reasonable result, as V_{max} should be constant at constant protein concentration (Berg et al., 2002). Only for GGG a lower V_{max} (56 %) was measured. Possible reasons for deviations in the maximum transport activity might be discrepancies in protein concentration in the liposomes. Furthermore, no saturation was reached for GGG opposed to the other three peptides.

Another application of the pyranine assay that was tested here, is the determination of the IC_{50} of an inhibitor molecule. Here, the dipeptide AF was tested as an inhibitor because it did not induce transport activity in the single concentration measurements. At the same time AF showed a high affinity to DtpB and a structure of AF in the binding site of DtpB was available, both indicating strong binding of AF. Different concentrations of AF were mixed with 2.5 mM AA and the mixture added to the liposomes. With increasing concentrations of AF, a decrease in AA uptake was observed, pointing to an inhibition of DtpB by AF (Figure 30). However, AF was not able to completely prevent AA

transport even at high concentrations. From this result it can be concluded that AA and AF compete for the DtpB binding site, although the binding affinity is higher for AF than for AA.

5.3.3 Stereospecificity of LgoT and DgoT

For further verification of the pyranine assay, it was tested with two more transporters, DgoT and LgoT. They were examined for stereospecific uptake of D-galactonate and L-galactonate using the same methods as for DtpB. The proteoliposomes gained by the rapid dilution method for reconstitution of LgoT showed a larger proton permeability than DtpB proteoliposomes. A steady linear decrease in fluorescence was observed from the beginning of the measurement on, independently of substrate or valinomycin addition (Figure 31). This indicates solution exchange between the exterior and interior of the liposome. A reason for this might be that LgoT behaves slightly different in the liposomes than DtpB and remaining detergent might disturb liposome solidity. Impermeability of the liposomes was improved using the biobead method for reconstitution. The fluorescence signal was stable over time for empty liposomes and for buffer controls of LgoT and DgoT proteoliposomes, indicating effective detergent removal by the biobeads (Figure 32). With these proteoliposomes, specific uptake of L-galactonate by LgoT and of D-galactonate by DgoT was observed. For both transporters an exponential transport curve was observed for transport of the respective galactonate stereoisomer, but DgoT showed higher proton influx with a t_0 slope of roughly 0.0035 sec^{-1}, while for LgoT it was around 0.001 sec^{-1}. The reason for this might either be a higher turnover rate of DgoT, a differing substrate to proton ratio between D-galactonate and L-galactonate transport or the different protein to lipid ratios of the proteoliposomes. Both transporters showed no uptake of galactose or the other galactonate stereoisomer. Comparison of the t_0 slopes for all tested substances allowed clear differentiation between transported and not transported ones. Furthermore, the Z-factor analysis (Z_{LgoT} = 0.44, Z_{DgoT} = 0.10) classified the assay as suitable to distinguish between transported and not transported compounds for both proteins. Here, assay quality could be optimised in the same way it was done for DtpB, by developing acceptance criteria for the proteoliposome batches and then normalising all t_0 slopes to the slope of the positive control, but this is more important for screening of a large compound library than for testing one specific substrate.

In addition, K_M values were determined for both transporters, indicating a higher apparent K_M by one magnitude for LgoT than for DgoT. As already described for the K_M data of DtpB, a lower apparent K_M, and therefore higher affinity, correlated with a higher transport activity. Also, here the K_M values must

be treated critically, due to the high standard deviation, especially for DgoT, where it is at 100 %. This mainly originates from the very low substrate concentrations that were needed here to determine the K_M and the respectively increasing error of the assay in this range. Possibly, the sensitivity of the pyranine assay is limited in this low concentration range because decreasing the substrate concentration from 0.02 mM to 0.01 mM did not lead to a further decrease in transport activity, but the relative t_0 slope stayed constant. To reliably determine K_M for D-galactonate transport by DgoT an assay with high sensitivity in the lower µM substrate concentration range might be needed. Opposed to the K_M, the apparent V_{max} values were very similar for LgoT and DgoT with an acceptable standard deviation of maximal 10 %.

To conclude, the pyranine assay was successfully established to measure transport activity for DtpB, LgoT and DgoT. Proton influx associated with substrate uptake was detected by a decrease in pyranine fluorescence with a high reproducibility. However, it was observed that the transport signal can vary in this assay due to different reconstitution efficiencies, the quality of the protein batch or age of the proteoliposomes. Longer storage times were associated with a decreasing protein activity. Therefore, it was crucial to develop acceptance criteria and to normalise all data to the transport signal of the respective positive control signal. The relative initial slope provided an exact and universal parameter for comparison of all measurements, minimising the effect of assay variability on the result. Furthermore, the automated evaluation procedure applied for this data was able to account for the different shapes of transport curves (linear and exponential) observed from the assay. Not only can this assay be used to discriminate between transported and not transported substrates but also for determination of K_M and IC_{50} values, as demonstrated in this study. Sensitivity of the assay appears to be limited to minimal substrate concentrations in the upper µM range. Moreover, the method can be adapted for different proton-coupled transporters independently of the type of substrate.

5.4 SURFE^{2}R assay

The SURFE^{2}R assay was established for DtpB and uptake of a selection of apparent substrates, known from the pyranine assay, were tested. Here, substrate driven uptake was measured by electrogenic coupling of proteoliposomes to the gold surface of a sensor chip. Proton influx was measured as a change in current between two electrodes according to the principle of capacitive coupling. Measurements with empty liposomes showed that the use of amino acids as inert compensation for the activating solution was suitable to reduce solution exchange artefacts, as they are not transported but are similar to the peptides in structure and charge. The remaining artefact signal for empty liposomes was subtracted from the DtpB transport signal to obtain the peak current originating from

substrate uptake by DtpB. Stability of a sensor was tested by a series of measurements with GG, indicating the sensor was at least stable over 21 single measurements or seven triplicate measurements (Figure 34). Usually, a sensor can be used for up to 50 – 100 measurements and 5 – 10 different conditions (triplicates) (Bazzone et al., 2017). However, stability of a sensor depends on the transporter, on the vesicle preparation and on experimental conditions (Bazzone et al., 2017). To assure the stability of each individual sensor used here, rundown controls using 20 mM GG were applied. GG was further used as a positive control and peak currents were normalised to the GG signal to enable comparison of data from different sensors, which can vary in vesicle-SSM adsorption efficiency, affecting the current amplitude (Bazzone et al., 2017).

In the pyranine assay, an indication of substrate driven transport could be observed after addition of AA to the liposomes, as the relative fluorescence started to slightly decrease before valinomycin was added (Figure 22). From this, it was assumed that transport is generally possible without a proton gradient, which was previously shown for DtpB (Harder et al., 2008). All tested peptides showed transport activity, as was expected based on the results from the pyranine assay (Figure 36). The peak current was used as a measure for transport activity because it is proportional to the turnover rate, but no information on the absolute turnover rate could be obtained from this assay since the total number of transporters contributing to the signal was not known (Bazzone et al., 2017). In the pyranine assay, AA showed the highest transport activity of the five peptides, while in the SURFE^{2}R assay it was AV followed by AA. Also, AI showed a different transport behaviour, as it had the lowest transport activity in the pyranine assay but was close to the transport activity of AA in the SURFE^{2}R assay. The lowest transport activity of the five peptides was found for GG. From these results it can be assumed that the transporter behaves differently in presence and absence of an electrochemical potential. It might alter transport activity and selectivity of the transporter. However, it has to be taken into consideration that deviations in the transport signals between the two assays can also be caused by the different experimental settings. Different ways of detecting proton-influx were used and also buffer composition and substrate concentration were not the same. In the SURFE^{2}R assay a higher substrate concentration than for the pyranine assay was used in order to generate a sufficient substrate gradient to detect transport.

The K_M values observed from the SURFE^{2}R assay can also not directly be compared to the K_M values calculated from the pyranine assay data due to the reasons mentioned above. Still, it was shown that also here, based on the two tested peptides, a lower K_M value correlated with a higher transport activity under the applied experimental conditions.

To conclude, it can be said that this assay was suitable for examination of DtpB uptake activity in liposomes, like it was previously shown for GG in Harder et al. (2008). Here, uptake of five peptides

was verified with this method and it was shown that substrate driven transport is possible in DtpB. Compared to the pyranine assay, this method is suitable for high-throughput screening of substrates due to the high degree of automation. Several substrates can automatically be measured in triplicates in a row on one sensor and one triplicate measurement can be performed in less than 3 minutes. Furthermore, a low amount of protein and lipids is necessary for preparation of one sensor. Ideal conditions for most transporters are 0.2-5 mg/mL lipid and 0.1-1 mg/mL protein per sensor (Bazzone et al., 2017). Data quality was assured by including stability controls in a series of measurements and reducing solution exchange artefacts using a suitable inert substance in the deactivating solution.

6 Conclusion

The main aim of this study was the development of two label-free uptake assays for proton-coupled membrane transporters as an alternative for using radiolabelled or fluorescently labelled substrates. The pyranine-based uptake assay was successfully applied to identify substrates and an inhibitor of DtpB. It was shown that this assay provides a reliable tool to evaluate uptake by DtpB, if the procedure is carefully established and suitable references and quality controls are developed. The complex evaluation procedure, established by Vadim Kotov, enabled classification of the ligands into transported and not-transported ones under the assumption of a stable proton:substrate ratio. Setting acceptance criteria for reference signals further contributed to the excellent assay quality.

The relation between transport activity and affinity of peptides pointed towards an optimal K_D range from roughly 0.1 mM to 4 mM for a peptide to be transported by DtpB, but it has to be noted that this is so far only true for the experimental conditions applied here. Moreover, only a selection of peptides was tested, which does not necessarily represent the behaviour of all possible di- and tripeptide combinations. However, this data gave a first impression, indicating the K_D might be useful for prediction of transport activity.

Furthermore, stereospecificity of LgoT and DgoT was successfully demonstrated using the pyranine-assay after optimisation of the reconstitution method. Although the assay was of lower quality, differentiation of transported and not transported compounds was possible.

Apart from that, transporter kinetics for all proteins could be determined, including K_M, V_{max} and IC_{50} values. However, the variability was mostly relatively high and reproducibility could be further improved, e.g. by using a temperature-controlled system with continuous stirring of the sample to gain more stable experimental conditions.

In summary, the pyranine assay was suitable for screening different compounds and produced reproducible results, but it is not ideal for high-throughput screening, as liposome preparation was relatively time consuming and a single measurement took 5 min.

The SURFE^{2}R assay is more suitable for high-throughput screening, as sensor preparation can be performed in 2-3 hours and a single measurement typically takes less than 1 min. Furthermore, the SURFE^{2}R technique is highly automated and many compounds can be screened on one sensor in a row, without supervision by the experimenter. Transport of selected peptides by DtpB could be verified and quantified in a reproducible manner using the SURFE^{2}R assay, also here assuming a stable proton:substrate stoichiometry. Quality of this assay was assured by controlling the quality of the sensors and using empty liposomes to evaluate background signals.

7 Outlook

The biobead method has been shown to be an effective technique for detergent removal in reconstitution of membrane transporters but still variations in reconstitution efficiency were observed. It could be further optimised testing the influence of different incubation conditions, e.g. variation of incubation temperature and duration, on the reconstitution efficiency of different transporters. Also, for reproducibility of the transport data it would be advantageous to improve protein stability inside the liposomes when stored at -80 °C. For example, one could try covering the liposomes with nitrogen before freezing in order to prevent oxidation of the lipids.

Regarding the relation between transport activity and affinity of peptides to DtpB screening of more peptides would be necessary to achieve a representative result. Also, based on the data collected here, a model could be developed to predict transport activity from affinity data and selected peptides could be tested in an uptake assay to challenge and further develop the model.

Regarding the SURFE^{2}R assay, it would be interesting to establish a membrane potential across the liposomes to make this assay an even more suitable solution for high-throughput substrate screening for DtpB. Application of pH jumps is not advisable for proton-coupled transporters in the SURFE^{2}R setting because it produces large artefact signals (Bazzone et al, 2017). Therefore, valinomycin would be an alternative for membrane potential generation, preloading the liposomes with potassium ions and using a potassium-free activating solution (Bazzone et al, 2017). This was already used to show the driving force of a charge-gradient for peptide transport by PepT1 and consequently should also be applicable for DtpB (Bazzone et al, 2017).

Furthermore, the SURFE^{2}R assay can generally also be used with cells overexpressing the protein of interest or isolated cell membranes. Such experiments with DtpB could give an insight into the transport behaviour under physiological conditions and how well this correlates with the results from the liposomal experiments.

8 References

Avanti Polar Lipids (2021): 16:0-18:1 PE. Online verfügbar unter https://avantilipids.com/product/850757, zuletzt aktualisiert am 05.08.2021, zuletzt geprüft am 05.08.2021.

Avanti Polar Lipids (2021): 16:0-18:1 PG. Online verfügbar unter https://avantilipids.com/product/840457, zuletzt aktualisiert am 05.08.2021, zuletzt geprüft am 05.08.2021.

Barthmes, Maria; Bazzone, Andre (2017): SURFE2R N1 Protocols. Quickstart Guide. nanion. München.

Bazzone, Andre; Barthmes, Maria; Fendler, Klaus (2017): SSM-Based Electrophysiology for Transporter Research. In: *Methods in enzymology* 594, S. 31–83. DOI: 10.1016/bs.mie.2017.05.008.

Berg, J. M.; Tymoczko, J. L.; Stryer, L.; National Center for Biotechnology Information (2002): Biochemistry, Fifth Edition: W. H. Freeman ([NCBI bookshelf]). Online verfügbar unter https://books.google.de/books?id=TLNpAAAAMAAJ.

Cheng, Yifan (2018): Membrane protein structural biology in the era of single particle cryo-EM. In: *Current Opinion in Structural Biology* 52, S. 58–63. DOI: 10.1016/j.sbi.2018.08.008.

Daniel, Hannelore; Spanier, Britta; Kottra, Gabor; Weitz, Dietmar (2006): From bacteria to man: archaic proton-dependent peptide transporters at work. In: *Physiology (Bethesda, Md.)* 21, S. 93–102. DOI: 10.1152/physiol.00054.2005.

Drew, David; North, Rachel A.; Nagarathinam, Kumar; Tanabe, Mikio (2021): Structures and General Transport Mechanisms by the Major Facilitator Superfamily (MFS). In: *Chemical reviews* 121 (9), S. 5289–5335. DOI: 10.1021/acs.chemrev.0c00983.

Ernst, Heidi A.; Pham, Antony; Hald, Helle; Kastrup, Jette S.; Rahman, Moazur; Mirza, Osman (2009): Ligand binding analyses of the putative peptide transporter YjdL from E. coli display a significant selectivity towards dipeptides. In: *Biochemical and biophysical research communications* 389 (1), S. 112–116. DOI: 10.1016/j.bbrc.2009.08.098.

Esteras, Noemí; Adjobo-Hermans, Merel J. W.; Abramov, Andrey Y.; Koopman, Werner J. H. (2020): Visualization of mitochondrial membrane potential in mammalian cells. In: *Methods in cell biology* 155, S. 221–245. DOI: 10.1016/bs.mcb.2019.10.003.

Fedosov, Sergey N.; Brask, Jesper; Xu, Xuebing (2012): Microtitration of Free Fatty Acids in Oil and Biodiesel Samples Using Absorbance and/or Fluorescence of Pyranine. In: *J Am Oil Chem Soc* 89 (12), S. 2155–2163. DOI: 10.1007/s11746-012-2117-8.

Foucaud, C.; Poolman, B. (1992): Lactose transport system of Streptococcus thermophilus. Functional reconstitution of the protein and characterization of the kinetic mechanism of transport. In: *Journal of Biological Chemistry* 267 (31), S. 22087–22094. DOI: 10.1016/S0021-9258(18)41639-0.

Gerbeth-Kreul, Carolin; Pommereau, Antje; Ruf, Sven; Kane, John L.; Kuntzweiler, Theresa; Hessler, Gerhard et al. (2021): A Solid Supported Membrane-Based Technology for Electrophysical Screening of B0AT1-Modulating Compounds. In: *SLAS discovery : advancing life sciences R & D* 26 (6), S. 783–797. DOI: 10.1177/24725552211011180.

GraphPad (2020): GraphPad Prism 9 Curve Fitting Guide - Equation: Michaelis-Menten model. Online verfügbar unter https://www.graphpad.com/guides/prism/latest/curve-fitting/reg_michaelis_menten_enzyme.htm, zuletzt aktualisiert am 28.10.2020, zuletzt geprüft am 05.08.2021.

Guettou, Fatma; Quistgaard, Esben M.; Trésaugues, Lionel; Moberg, Per; Jegerschöld, Caroline; Zhu, Lin et al. (2013): Structural insights into substrate recognition in proton-dependent oligopeptide transporters. In: *EMBO reports* 14 (9), S. 804–810. DOI: 10.1038/embor.2013.107.

Hammond, Constance (2015): Ionic gradients, membrane potential and ionic currents. In: Cellular and Molecular Neurophysiology: Elsevier, S. 39–54.

Harder, Daniel; Stolz, Jürgen; Casagrande, Fabio; Obrdlik, Petr; Weitz, Dietmar; Fotiadis, Dimitrios; Daniel, Hannelore (2008): DtpB (YhiP) and DtpA (TppB, YdgR) are prototypical proton-dependent peptide transporters of Escherichia coli. In: *The FEBS journal* 275 (13), S. 3290–3298. DOI: 10.1111/j.1742-4658.2008.06477.x.

Hunter, John D. (2007): Matplotlib: A 2D Graphics Environment. In: *Computing in Science & Engineering* 9 (3), S. 90–95. DOI: 10.1109/MCSE.2007.55.

Jardetzky, O. (1966): Simple allosteric model for membrane pumps. In: *Nature* 211 (5052), S. 969–970. DOI: 10.1038/211969a0.

Jones, Eric; Oliphant, Travis; Peterson, Pearu; others (2001): SciPy: Open source scientific tools for Python. Online verfügbar unter http://www.scipy.org/.

Kano, K.; Fendler, J. H. (1978): Pyranine as a sensitive pH probe for liposome interiors and surfaces. pH gradients across phospholipid vesicles. In: *Biochimica et biophysica acta* 509 (2), S. 289–299. DOI: 10.1016/0005-2736(78)90048-2.

Leano, Jonathan B.; Batarni, Samir; Eriksen, Jacob; Juge, Narinobu; Pak, John E.; Kimura-Someya, Tomomi et al. (2019): Structures suggest a mechanism for energy coupling by a family of organic anion transporters. In: *PLoS biology* 17 (5), e3000260. DOI: 10.1371/journal.pbio.3000260.

Magnusson, Anders O.; Szekrenyi, Anna; Joosten, Henk-Jan; Finnigan, James; Charnock, Simon; Fessner, Wolf-Dieter (2019): nanoDSF as screening tool for enzyme libraries and biotechnology development. In: *The FEBS journal* 286 (1), S. 184–204. DOI: 10.1111/febs.14696.

McKinney, Wes (2010): Data Structures for Statistical Computing in Python. In: Stéfan van der Walt und Jarrod Millman (Hg.): Proceedings of the 9th Python in Science Conference, S. 51–56.

Miroux, B.; Walker, J. E. (1996): Over-production of proteins in Escherichia coli: mutant hosts that allow synthesis of some membrane proteins and globular proteins at high levels. In: *Journal of molecular biology* 260 (3), S. 289–298. DOI: 10.1006/jmbi.1996.0399.

Moraes, Trevor F.; Reithmeier, Reinhart A. F. (2012): Membrane transport metabolons. In: *Biochimica et biophysica acta* 1818 (11), S. 2687–2706. DOI: 10.1016/j.bbamem.2012.06.007.

Newstead, Simon (2015): Molecular insights into proton coupled peptide transport in the PTR family of oligopeptide transporters. In: *Biochimica et biophysica acta* 1850 (3), S. 488–499. DOI: 10.1016/j.bbagen.2014.05.011.

Newstead, Simon; Drew, David; Cameron, Alexander D.; Postis, Vincent L. G.; Xia, Xiaobing; Fowler, Philip W. et al. (2011): Crystal structure of a prokaryotic homologue of the mammalian oligopeptide-proton symporters, PepT1 and PepT2. In: *The EMBO journal* 30 (2), S. 417–426. DOI: 10.1038/emboj.2010.309.

Nicholls, David G.; Ferguson, Stuart J. (2013): Bioenergetics. Fourth edition. Amsterdam: Academic Press Elsevier.

Parker, Joanne L.; Mindell, Joseph A.; Newstead, Simon (2014): Thermodynamic evidence for a dual transport mechanism in a POT peptide transporter. In: *eLife* 3. DOI: 10.7554/eLife.04273.

Parker, Joanne L.; Newstead, Simon (2014): Molecular basis of nitrate uptake by the plant nitrate transporter NRT1.1. In: *Nature* 507 (7490), S. 68–72. DOI: 10.1038/nature13116.

Prism - GraphPad (2021). Online verfügbar unter https://www.graphpad.com/scientific-software/prism/, zuletzt aktualisiert am 05.08.2021, zuletzt geprüft am 05.08.2021.

PubChem (2021): L-Galactonic acid. Online verfügbar unter https://pubchem.ncbi.nlm.nih.gov/compound/L-galactonic%20acid, zuletzt aktualisiert am 20.08.2021, zuletzt geprüft am 20.08.2021.

Pyranine | Sigma-Aldrich (2021). Online verfügbar unter https://www.sigmaaldrich.com/DE/de/search/pyranine?focus=products&page=1&perPage=30&sort=relevance&term=pyranine&type=product_name, zuletzt aktualisiert am 29.07.2021, zuletzt geprüft am 29.07.2021.

Python (2019): Python Software Foundation. Online verfügbar unter http://www.python.org.

Qiu, Biao; Matthies, Doreen; Fortea, Eva; Yu, Zhiheng; Boudker, Olga (2021): Cryo-EM structures of excitatory amino acid transporter 3 visualize coupled substrate, sodium, and proton binding and transport. In: *Sci. Adv.* 7 (10), eabf5814. DOI: 10.1126/sciadv.abf5814.

Quistgaard, Esben M.; Löw, Christian; Guettou, Fatma; Nordlund, Pär (2016): Understanding transport by the major facilitator superfamily (MFS): structures pave the way. In: *Nature reviews. Molecular cell biology* 17 (2), S. 123–132. DOI: 10.1038/nrm.2015.25.

Quistgaard, Esben M.; Löw, Christian; Moberg, Per; Trésaugues, Lionel; Nordlund, Pär (2013): Structural basis for substrate transport in the GLUT-homology family of monosaccharide transporters. In: *Nature structural & molecular biology* 20 (6), S. 766–768. DOI: 10.1038/nsmb.2569.

Ramahi, A. A.; Ruff, R. L. (2014): Membrane Potential. In: Encyclopedia of the Neurological Sciences: Elsevier, S. 1034–1035.

Rath, Arianna; Glibowicka, Mira; Nadeau, Vincent G.; Chen, Gong; Deber, Charles M. (2009): Detergent binding explains anomalous SDS-PAGE migration of membrane proteins. In: *Proceedings of the National Academy of Sciences of the United States of America* 106 (6), S. 1760–1765. DOI: 10.1073/pnas.0813167106.

Reddy, Vamsee S.; Shlykov, Maksim A.; Castillo, Rostislav; Sun, Eric I.; Saier, Milton H. (2012): The major facilitator superfamily (MFS) revisited. In: *The FEBS journal* 279 (11), S. 2022–2035. DOI: 10.1111/j.1742-4658.2012.08588.x.

Rigaud, Jean-Louis; Lévy, Daniel (2003): Reconstitution of Membrane Proteins into Liposomes. In: Liposomes, Part B, Bd. 372: Academic Press (Methods in Enzymology), S. 65–86. Online verfügbar unter https://www.sciencedirect.com/science/article/pii/S0076687903720047.

Saier Lab: 2.A.1.14.33 Putative L-galactonate transporter, YjjL. Saier Lab Bioinformatics Group. Online verfügbar unter https://www.tcdb.org/aboutus.php, zuletzt geprüft am 23.07.2021.

Shi, Yigong (2013): Common folds and transport mechanisms of secondary active transporters. In: *Annual review of biophysics* 42, S. 51–72. DOI: 10.1146/annurev-biophys-083012-130429.

Sigma Aldrich (2021): Carbonyl Cyanide m-Chlorophenylhydrazone. Online verfügbar unter https://www.sigmaaldrich.com/DE/de/product/mm/215911, zuletzt aktualisiert am 06.08.2021, zuletzt geprüft am 06.08.2021.

Software, GraphPad (2020): GraphPad Prism 9 Curve Fitting Guide - Equation: Absolute IC50. Online verfügbar unter https://www.graphpad.com/guides/prism/latest/curve-

fitting/reg_absolute_ic50.htm?q=IC50, zuletzt aktualisiert am 28.10.2020, zuletzt geprüft am 05.08.2021.

Spriestersbach, Anne; Kubicek, Jan; Schäfer, Frank; Block, Helena; Maertens, Barbara (2015): Purification of His-Tagged Proteins. In: *Methods in enzymology* 559, S. 1–15. DOI: 10.1016/bs.mie.2014.11.003.

Stetsenko, Artem; Guskov, Albert (2017): An Overview of the Top Ten Detergents Used for Membrane Protein Crystallization. In: *Crystals* 7 (7), S. 197. DOI: 10.3390/cryst7070197.

Tsai, Ming-Feng; Miller, Christopher (2013): Substrate selectivity in arginine-dependent acid resistance in enteric bacteria. In: *Proceedings of the National Academy of Sciences of the United States of America* 110 (15), S. 5893–5897. DOI: 10.1073/pnas.1301442110.

Ural-Blimke, Yonca; Flayhan, Ali; Strauss, Jan; Rantos, Vasileios; Bartels, Kim; Nielsen, Rolf et al. (2019): Structure of Prototypic Peptide Transporter DtpA from E. coli in Complex with Valganciclovir Provides Insights into Drug Binding of Human PepT1. In: *Journal of the American Chemical Society* 141 (6), S. 2404–2412. DOI: 10.1021/jacs.8b11343.

Valinomycin ≥99.0% (TLC) | Sigma-Aldrich (2021). Online verfügbar unter https://www.sigmaaldrich.com/DE/de/product/sigma/94675, zuletzt aktualisiert am 29.07.2021, zuletzt geprüft am 29.07.2021.

van der Walt, Stéfan; Millman, Jarrod (Hg.) (2010): Proceedings of the 9th Python in Science Conference.

Volpe, Donna A. (2016): Transporter assays as useful in vitro tools in drug discovery and development. In: *Expert opinion on drug discovery* 11 (1), S. 91–103. DOI: 10.1517/17460441.2016.1101064.

Waskom; Botvinnik; Joel Ostblom; Maoz Gelbart; Saulius Lukauskas; Paul Hobson et al. (2020): mwaskom/seaborn: v0.10.1 (April 2020): Zenodo. Online verfügbar unter https://zenodo.org/record/3767070#.XtuDBZ9fiu1, zuletzt geprüft am 06.06.2020.

Yamamoto, Norio; Ueda, Manabu; Sato, Takuya; Kawasaki, Kengo; Sawada, Keisuke; Kawabata, Kyuichi; Ashida, Hitoshi (2011): Measurement of glucose uptake in cultured cells. In: *Current protocols in pharmacology* Chapter 12, Unit 12.14.1-22. DOI: 10.1002/0471141755.ph1214s55.

Yan, Nieng (2013): Structural advances for the major facilitator superfamily (MFS) transporters. In: *Trends in biochemical sciences* 38 (3), S. 151–159. DOI: 10.1016/j.tibs.2013.01.003.

Yan, Nieng (2015): Structural Biology of the Major Facilitator Superfamily Transporters. In: *Annual review of biophysics* 44, S. 257–283. DOI: 10.1146/annurev-biophys-060414-033901.

Zhang, Ji-Hu; Chung, Thomas D. Y.; Oldenburg, Kevin R. (1999): A Simple Statistical Parameter for Use in Evaluation and Validation of High Throughput Screening Assays. In: *Journal of Biomolecular Screening* 4 (2), S. 67–73. DOI: 10.1177/108705719900400206.

9 Annex

9.1 Single concentration measurements for DtpB in pyranine assay

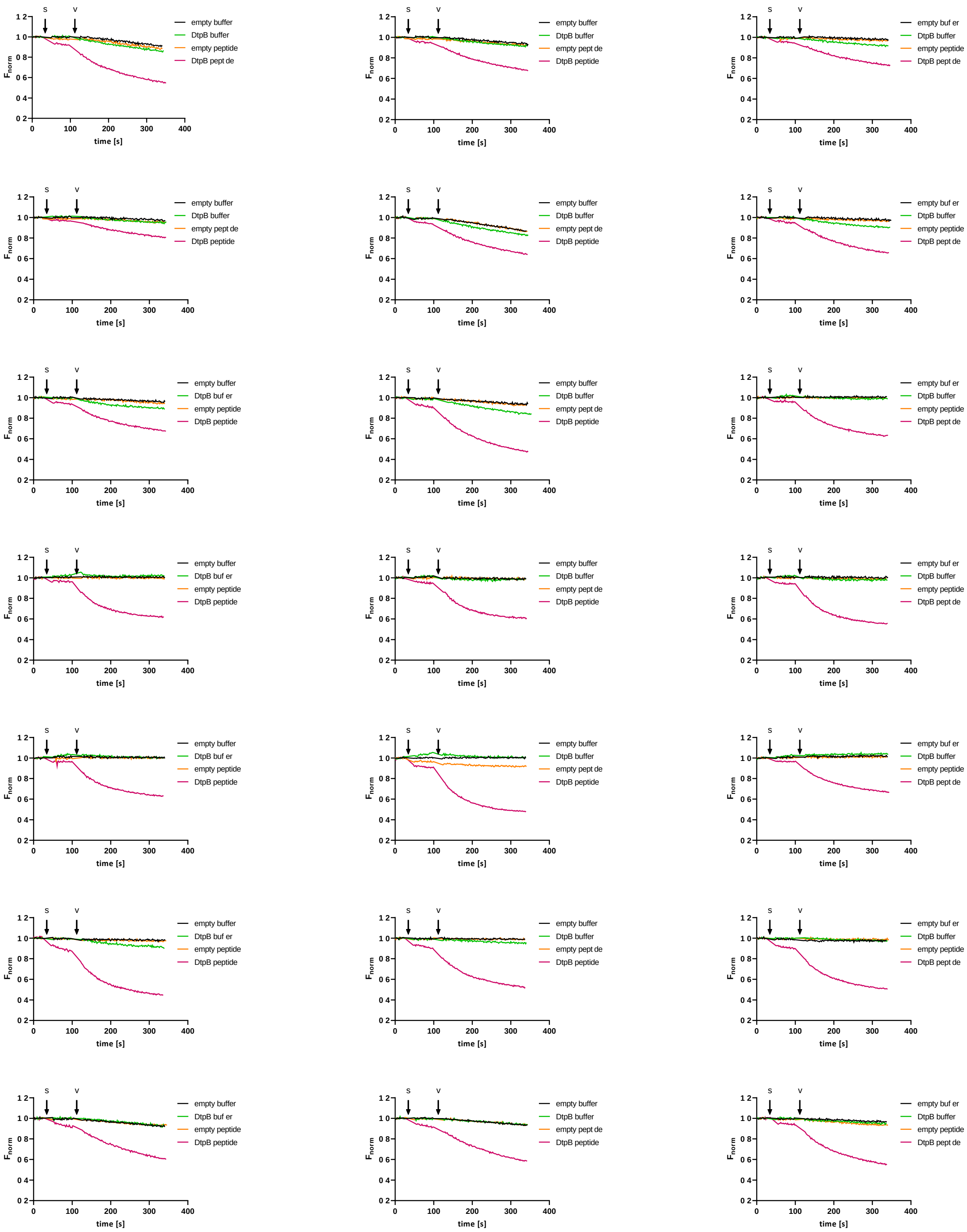

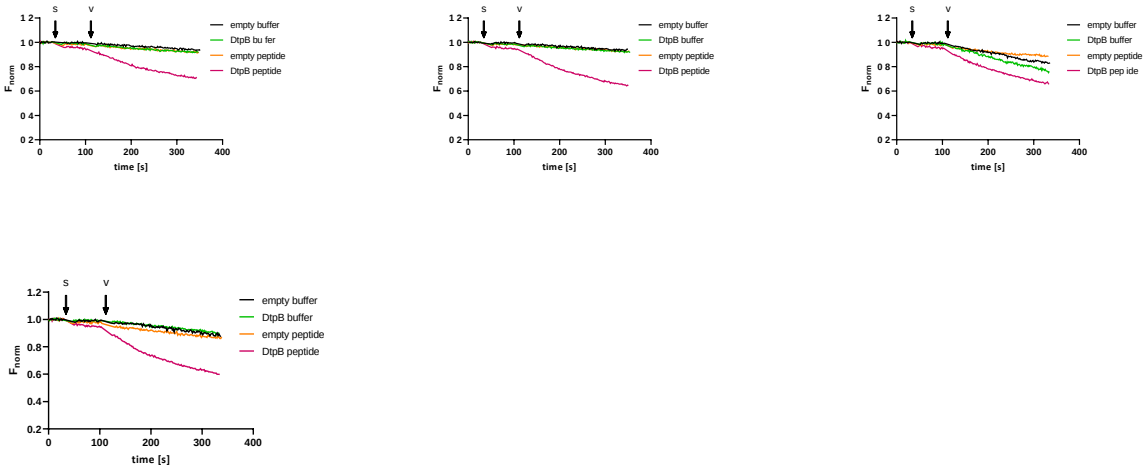

Figure 39: Overview of all transport curves for 2.5 mM AA in the pyranine-based assay using DtpB proteoliposomes. *Each plot shows the normalized fluorescence signal over the time course of the measurement for empty liposomes and DtpB proteoliposomes with addition of buffer and peptide, respectively. The time points of buffer/substrate (s) and valinomycin (v) addition are marked by arrows.*

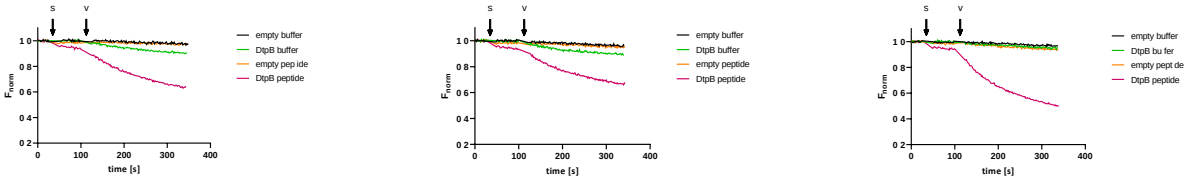

Figure 40: Overview of all transport curves for 2.5 mM AAA in the pyranine-based assay using DtpB proteoliposomes. *Each plot shows the normalized fluorescence signal over the time course of the measurement for empty liposomes and DtpB proteoliposomes with addition of buffer and peptide, respectively. The time points of buffer/substrate (s) and valinomycin (v) addition are marked by arrows.*

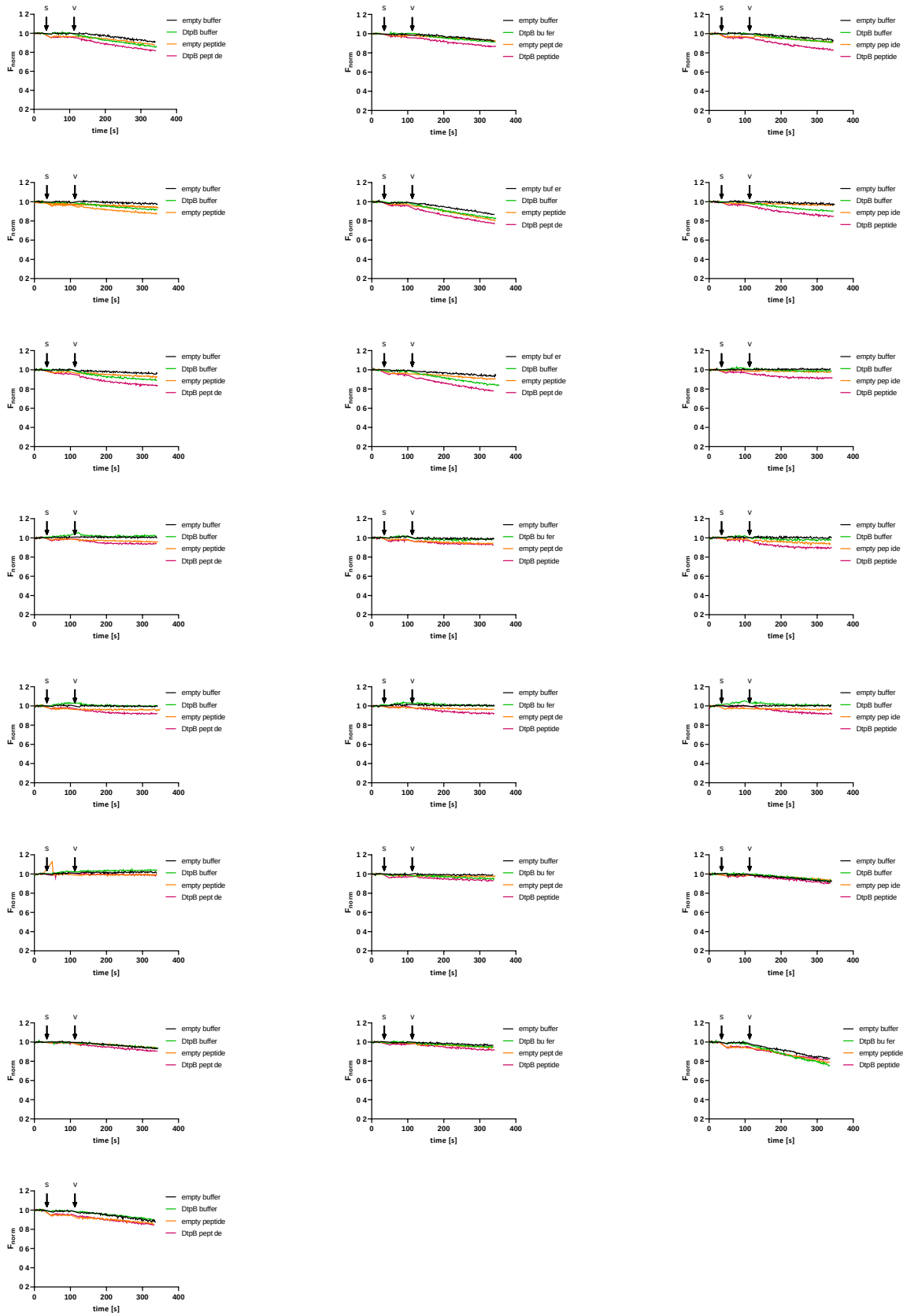

Figure 41: Overview of all transport curves for 2.5 mM AAAA in the pyranine-based assay using DtpB proteoliposomes. *Each plot shows the normalized fluorescence signal over the time course of the measurement for empty liposomes and DtpB proteoliposomes with addition of buffer and peptide, respectively. The time points of buffer/substrate (s) and valinomycin (v) addition are marked by arrows.*

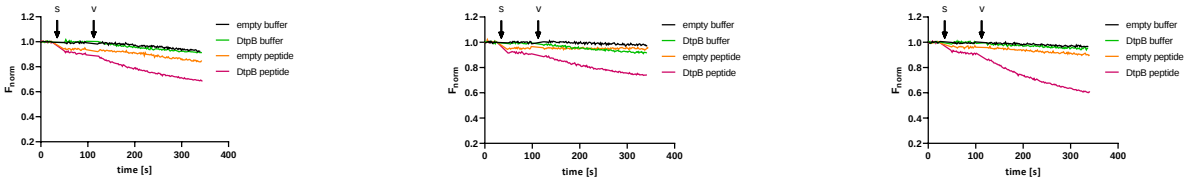

Figure 42: Overview of all transport curves for 2.5 mM AAY in the pyranine-based assay using DtpB proteoliposomes. *Each plot shows the normalized fluorescence signal over the time course of the measurement for empty liposomes and DtpB proteoliposomes with addition of buffer and peptide, respectively. The time points of buffer/substrate (s) and valinomycin (v) addition are marked by arrows.*

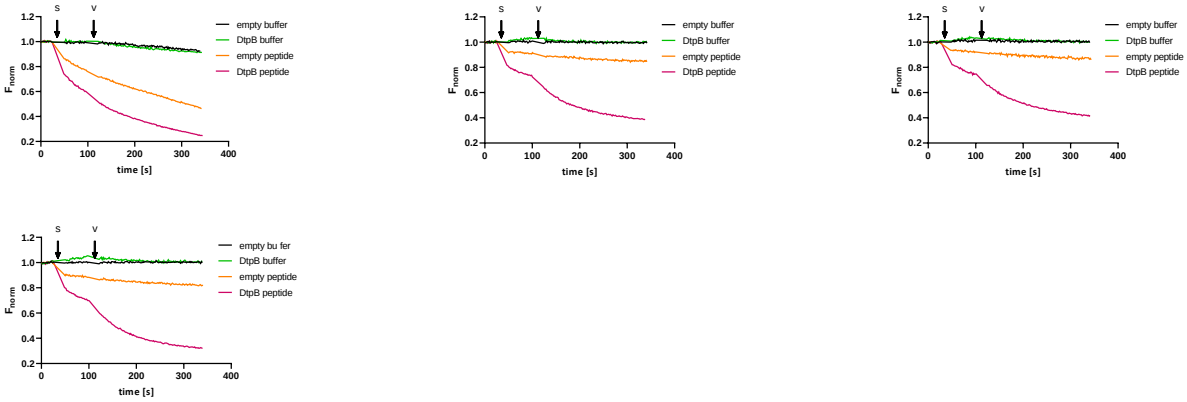

Figure 43: Overview of all transport curves for 2.5 mM AD in the pyranine-based assay using DtpB proteoliposomes. *Each plot shows the normalized fluorescence signal over the time course of the measurement for empty liposomes and DtpB proteoliposomes with addition of buffer and peptide, respectively. The time points of buffer/substrate (s) and valinomycin (v) addition are marked by arrows.*

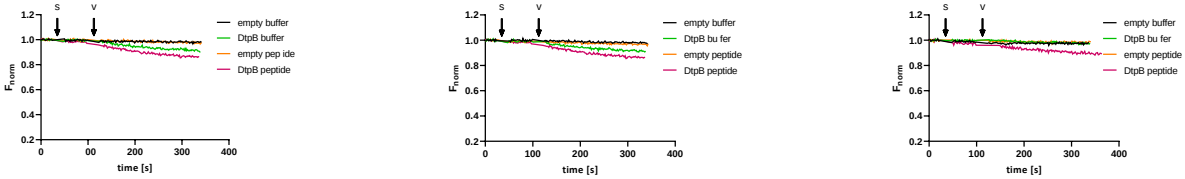

Figure 44: Overview of all transport curves for 2.5 mM AF in the pyranine-based assay using DtpB proteoliposomes. *Each plot shows the normalized fluorescence signal over the time course of the measurement for empty liposomes and DtpB proteoliposomes with addition of buffer and peptide, respectively. The time points of buffer/substrate (s) and valinomycin (v) addition are marked by arrows.*

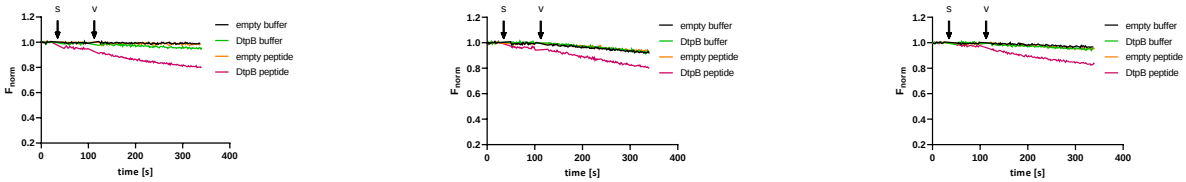

Figure 45: Overview of all transport curves for 2.5 mM AI in the pyranine-based assay using DtpB proteoliposomes. *Each plot shows the normalized fluorescence signal over the time course of the measurement for empty liposomes and DtpB proteoliposomes with addition of buffer and peptide, respectively. The time points of buffer/substrate (s) and valinomycin (v) addition are marked by arrows.*

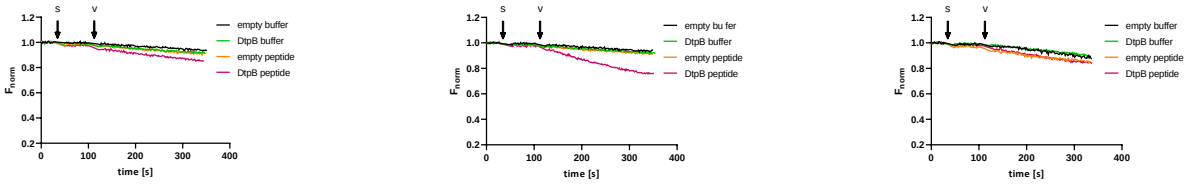

Figure 46: Overview of all transport curves for 2.5 mM AL in the pyranine-based assay using DtpB proteoliposomes. *Each plot shows the normalized fluorescence signal over the time course of the measurement for empty liposomes and DtpB proteoliposomes with addition of buffer and peptide, respectively. The time points of buffer/substrate (s) and valinomycin (v) addition are marked by arrows.*

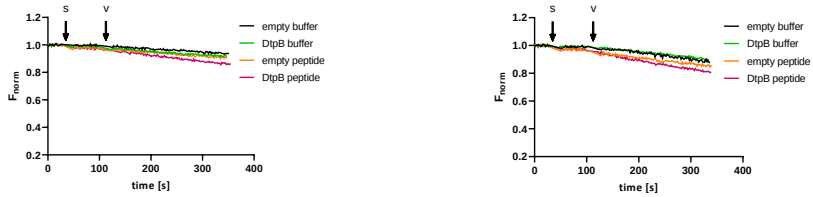

Figure 47: Overview of all transport curves for 2.5 mM ALA in the pyranine-based assay using DtpB proteoliposomes. *Each plot shows the normalized fluorescence signal over the time course of the measurement for empty liposomes and DtpB proteoliposomes with addition of buffer and peptide, respectively. The time points of buffer/substrate (s) and valinomycin (v) addition are marked by arrows.*

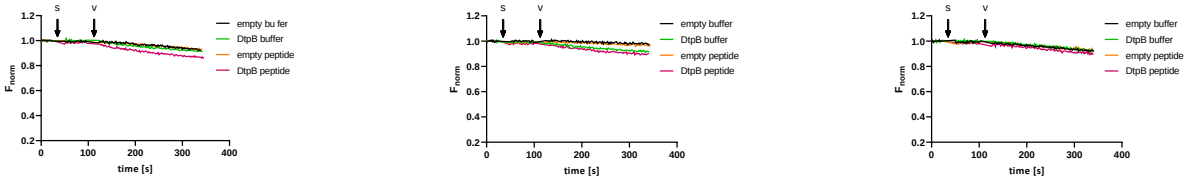

Figure 48: Overview of all transport curves for 2.5 mM APF in the pyranine-based assay using DtpB proteoliposomes. *Each plot shows the normalized fluorescence signal over the time course of the measurement for empty liposomes and DtpB proteoliposomes with addition of buffer and peptide, respectively. The time points of buffer/substrate (s) and valinomycin (v) addition are marked by arrows.*

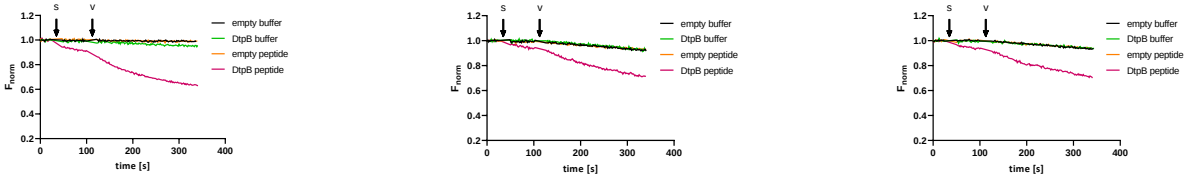

Figure 49: Overview of all transport curves for 2.5 mM AV in the pyranine-based assay using DtpB proteoliposomes. *Each plot shows the normalized fluorescence signal over the time course of the measurement for empty liposomes and DtpB proteoliposomes with addition of buffer and peptide, respectively. The time points of buffer/substrate (s) and valinomycin (v) addition are marked by arrows.*

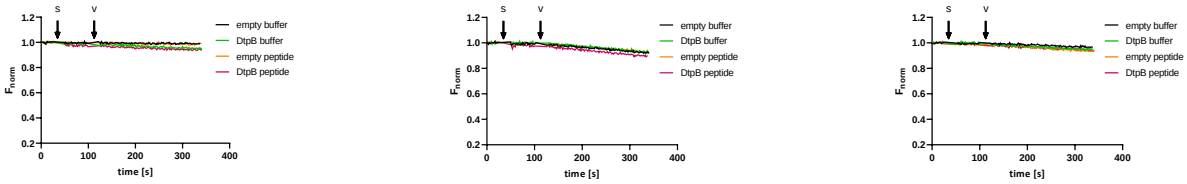

Figure 50: Overview of all transport curves for 2.5 mM AW in the pyranine-based assay using DtpB proteoliposomes. *Each plot shows the normalized fluorescence signal over the time course of the measurement for empty liposomes and DtpB proteoliposomes with addition of buffer and peptide, respectively. The time points of buffer/substrate (s) and valinomycin (v) addition are marked by arrows.*

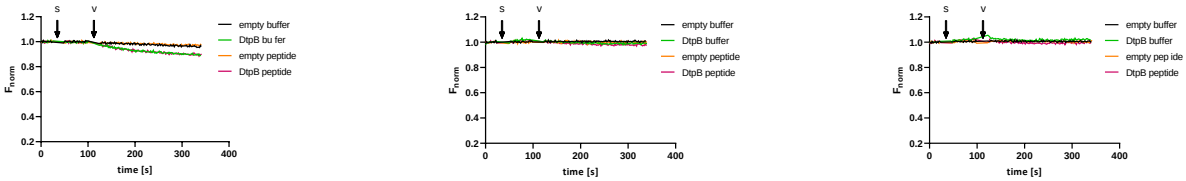

Figure 51: Overview of all transport curves for 2.5 mM bAbA in the pyranine-based assay using DtpB proteoliposomes. *Each plot shows the normalized fluorescence signal over the time course of the measurement for empty liposomes and DtpB proteoliposomes with addition of buffer and peptide, respectively. The time points of buffer/substrate (s) and valinomycin (v) addition are marked by arrows.*

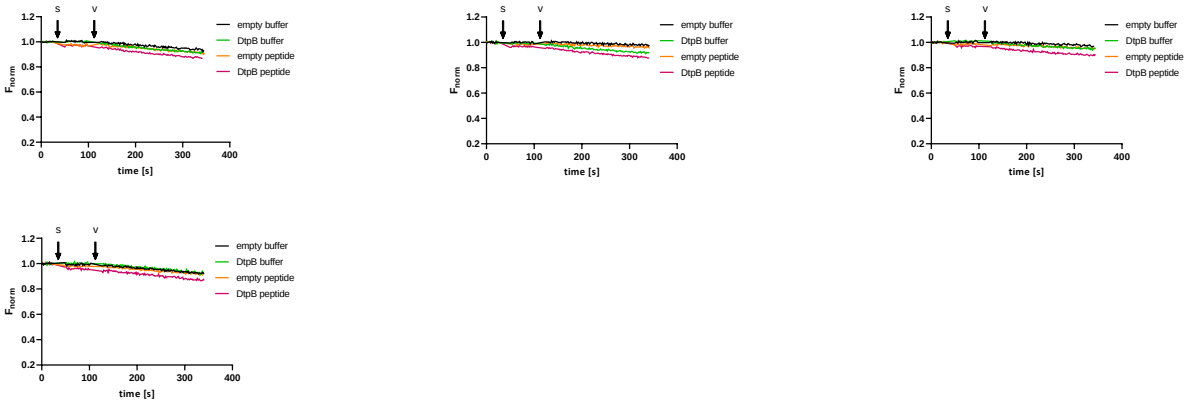

Figure 52: Overview of all transport curves for 2.5 mM EK in the pyranine-based assay using DtpB proteoliposomes. *Each plot shows the normalized fluorescence signal over the time course of the measurement for empty liposomes and DtpB proteoliposomes with addition of buffer and peptide, respectively. The time points of buffer/substrate (s) and valinomycin (v) addition are marked by arrows.*

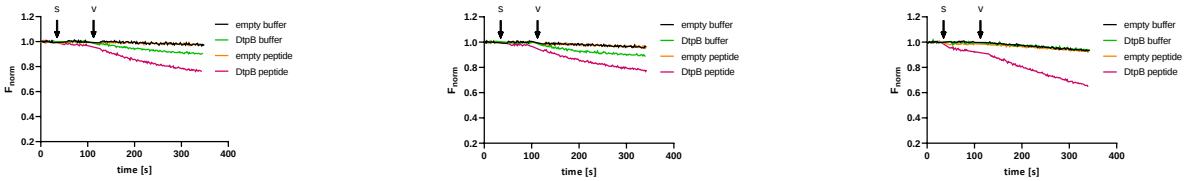

Figure 53: Overview of all transport curves for 2.5 mM GG in the pyranine-based assay using DtpB proteoliposomes. *Each plot shows the normalized fluorescence signal over the time course of the measurement for empty liposomes and DtpB proteoliposomes with addition of buffer and peptide, respectively. The time points of buffer/substrate (s) and valinomycin (v) addition are marked by arrows.*

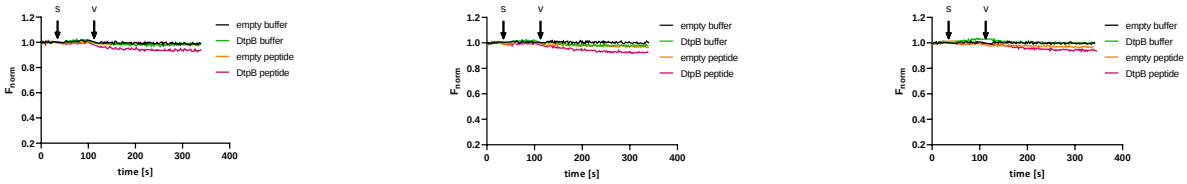

Figure 54: Overview of all transport curves for 2.5 mM GGG in the pyranine-based assay using DtpB proteoliposomes. *Each plot shows the normalized fluorescence signal over the time course of the measurement for empty liposomes and DtpB proteoliposomes with addition of buffer and peptide, respectively. The time points of buffer/substrate (s) and valinomycin (v) addition are marked by arrows.*

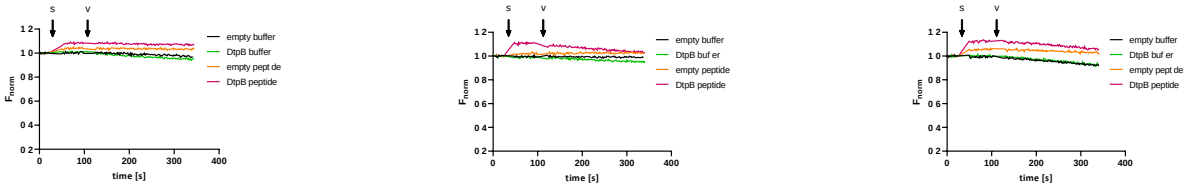

Figure 55: Overview of all transport curves for 2.5 mM GH in the pyranine-based assay using DtpB proteoliposomes. *Each plot shows the normalized fluorescence signal over the time course of the measurement for empty liposomes and DtpB proteoliposomes with addition of buffer and peptide, respectively. The time points of buffer/substrate (s) and valinomycin (v) addition are marked by arrows.*

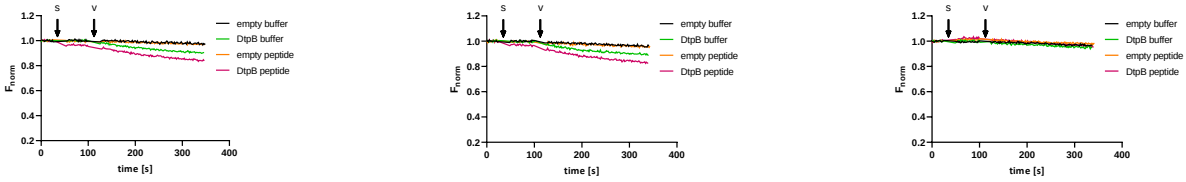

Figure 56: Overview of all transport curves for 2.5 mM KA in the pyranine-based assay using DtpB proteoliposomes*. Each plot shows the normalized fluorescence signal over the time course of the measurement for empty liposomes and DtpB proteoliposomes with addition of buffer and peptide, respectively. The time points of buffer/substrate (s) and valinomycin (v) addition are marked by arrows.*

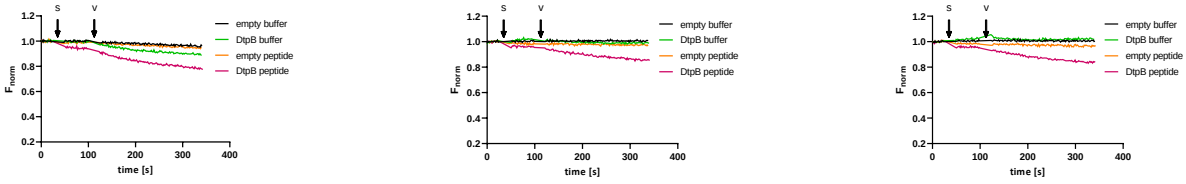

Figure 57: Overview of all transport curves for 2.5 mM KV in the pyranine-based assay using DtpB proteoliposomes. *Each plot shows the normalized fluorescence signal over the time course of the measurement for empty liposomes and DtpB proteoliposomes with addition of buffer and peptide, respectively. The time points of buffer/substrate (s) and valinomycin (v) addition are marked by arrows.*

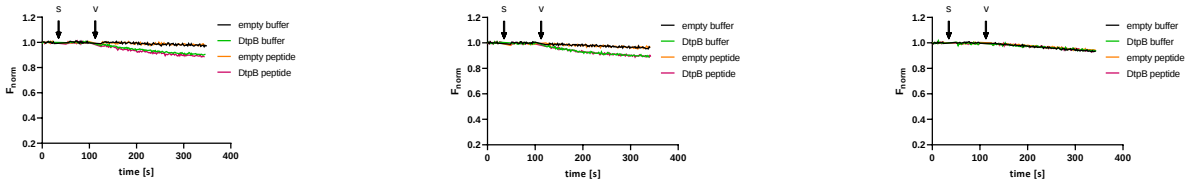

Figure 58: Overview of all transport curves for 2.5 mM L-Ala in the pyranine-based assay using DtpB proteoliposomes. *Each plot shows the normalized fluorescence signal over the time course of the measurement for empty liposomes and DtpB proteoliposomes with addition of buffer and peptide, respectively. The time points of buffer/substrate (s) and valinomycin (v) addition are marked by arrows.*

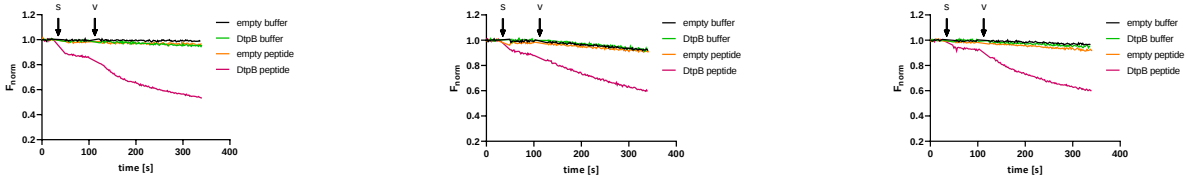

Figure 59: Overview of all transport curves for 2.5 mM MS in the pyranine-based assay using DtpB proteoliposomes. *Each plot shows the normalized fluorescence signal over the time course of the measurement for empty liposomes and DtpB proteoliposomes with addition of buffer and peptide, respectively. The time points of buffer/substrate (s) and valinomycin (v) addition are marked by arrows.*

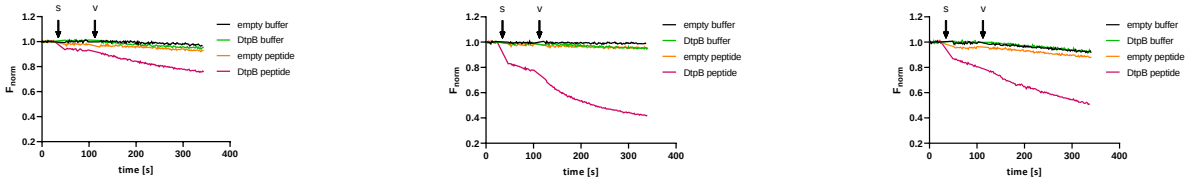

Figure 60: Overview of all transport curves for 2.5 mM NV in the pyranine-based assay using DtpB proteoliposomes. *Each plot shows the normalized fluorescence signal over the time course of the measurement for empty liposomes and DtpB proteoliposomes with addition of buffer and peptide, respectively. The time points of buffer/substrate (s) and valinomycin (v) addition are marked by arrows.*

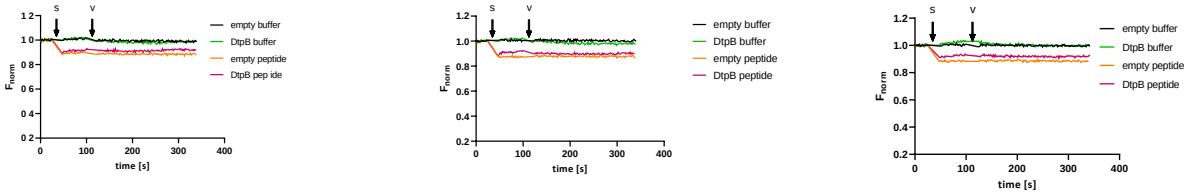

Figure 61: Overview of all transport curves for 2.5 mM PR in the pyranine-based assay using DtpB proteoliposomes. *Each plot shows the normalized fluorescence signal over the time course of the measurement for empty liposomes and DtpB proteoliposomes with addition of buffer and peptide, respectively. The time points of buffer/substrate (s) and valinomycin (v) addition are marked by arrows.*

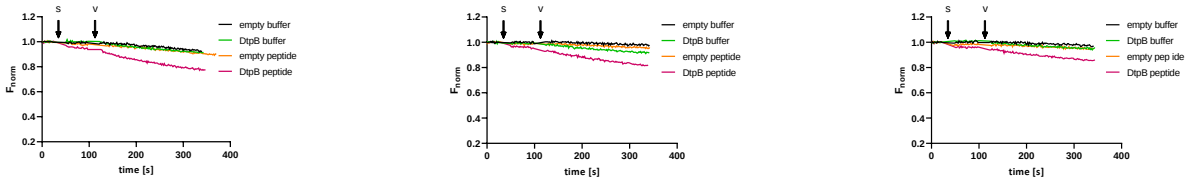

Figure 62: Overview of all transport curves for 2.5 mM SL in the pyranine-based assay using DtpB proteoliposomes. *Each plot shows the normalized fluorescence signal over the time course of the measurement for empty liposomes and DtpB proteoliposomes with addition of buffer and peptide, respectively. The time points of buffer/substrate (s) and valinomycin (v) addition are marked by arrows.*

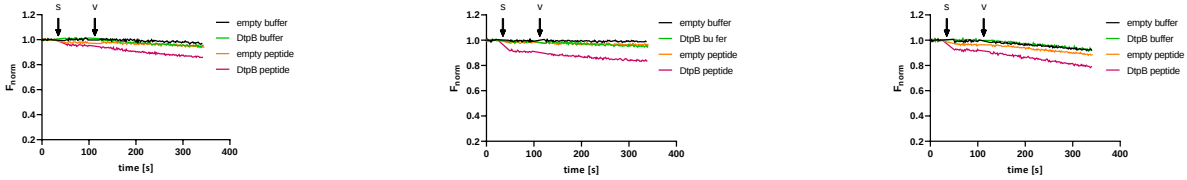

Figure 63: Overview of all transport curves for 2.5 mM SY in the pyranine-based assay using DtpB proteoliposomes. *Each plot shows the normalized fluorescence signal over the time course of the measurement for empty liposomes and DtpB proteoliposomes with addition of buffer and peptide, respectively. The time points of buffer/substrate (s) and valinomycin (v) addition are marked by arrows.*

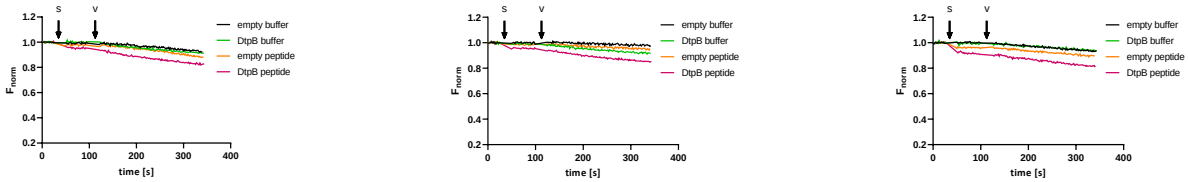

Figure 64: Overview of all transport curves for 2.5 mM TF in the pyranine-based assay using DtpB proteoliposomes. *Each plot shows the normalized fluorescence signal over the time course of the measurement for empty liposomes and DtpB proteoliposomes with addition of buffer and peptide, respectively. The time points of buffer/substrate (s) and valinomycin (v) addition are marked by arrows.*

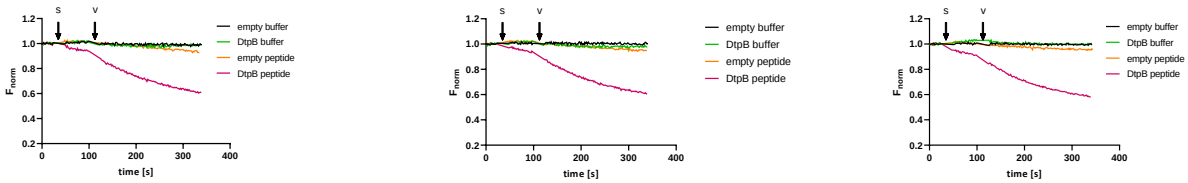

Figure 65: Overview of all transport curves for 2.5 mM WG in the pyranine-based assay using DtpB proteoliposomes. *Each plot shows the normalized fluorescence signal over the time course of the measurement for empty liposomes and DtpB proteoliposomes with addition of buffer and peptide, respectively. The time points of buffer/substrate (s) and valinomycin (v) addition are marked by arrows.*

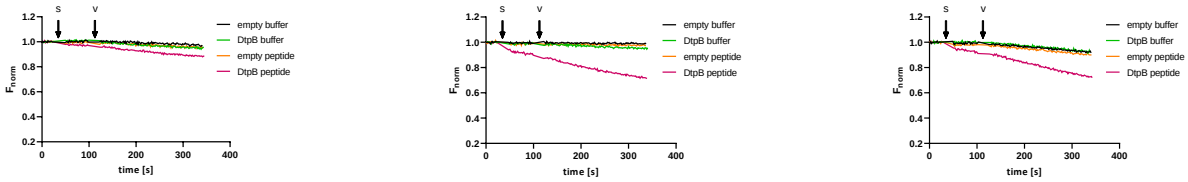

Figure 66: Overview of all transport curves for 2.5 mM YQ in the pyranine-based assay using DtpB proteoliposomes. *Each plot shows the normalized fluorescence signal over the time course of the measurement for empty liposomes and DtpB proteoliposomes with addition of buffer and peptide, respectively. The time points of buffer/substrate (s) and valinomycin (v) addition are marked by arrows.*

9.2 Determination of kinetic parameters of DtpB in pyranine assay

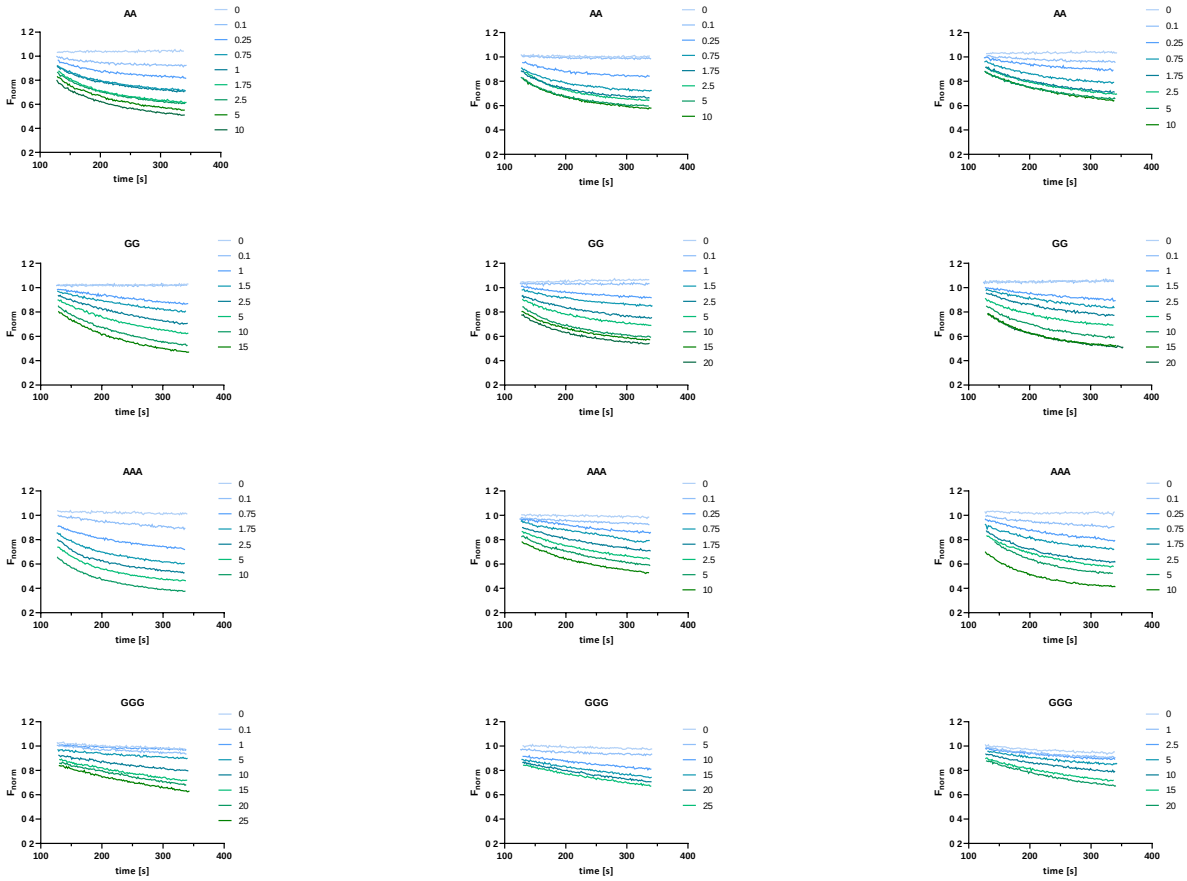

Figure 67: Transport curves for estimation of K_M and V_{max} of different peptides for transport by DtpB, measured using the pyranine assay. *For each peptide triplicate measurements are displayed and each graph shows the normalised and corrected curves for different peptide concentrations.*

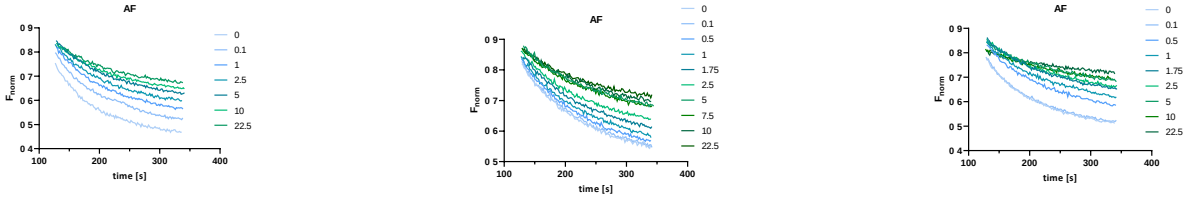

Figure 68: Transport curves for estimation of IC_{50} of AF for inhibition of DtpB, measured using the pyranine assay. *For each of the triplicates one graph is shown, displaying the normalised and corrected transport curves for different concentrations of AF mixed with 2.5 mM AA.*

9.3 Single concentration measurements for LgoT and DgoT in pyranine assay

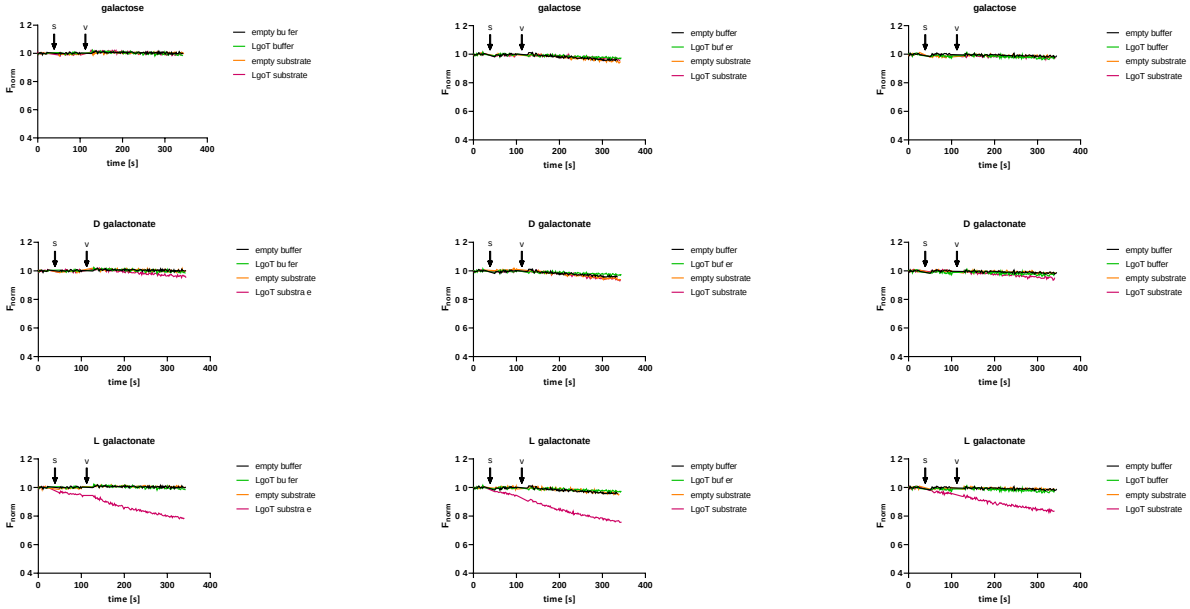

Figure 69: Overview of all transport curves for 2.5 mM galactose, D-galactonate and L-galactonate in the pyranine-based assay using LgoT proteoliposomes. *Each plot shows the normalized fluorescence signal over the time course of the measurement for empty liposomes and LgoT proteoliposomes with addition of buffer and substrate, respectively. The time points of buffer/substrate (s) and valinomycin (v) addition are marked by arrows.*

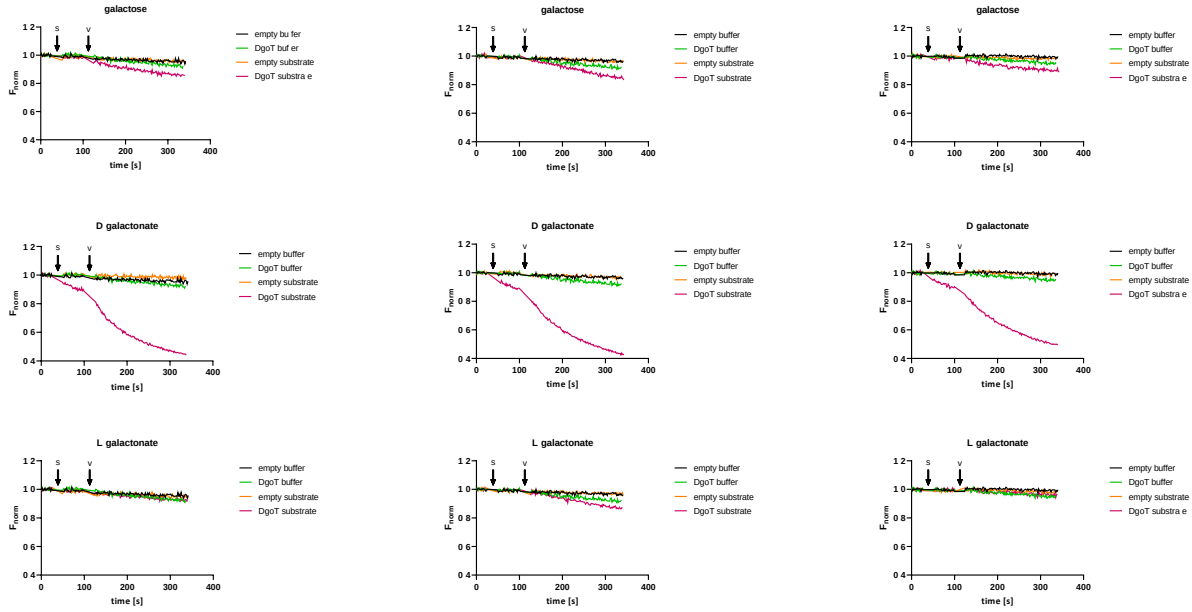

Figure 70: Overview of all transport curves for 2.5 mM galactose, D-galactonate and L-galactonate in the pyranine-based assay using DgoT proteoliposomes. *Each plot shows the normalized fluorescence signal over the time course of the measurement for empty liposomes and DgoT proteoliposomes with addition of buffer and substrate, respectively. The time points of buffer/substrate (s) and valinomycin (v) addition are marked by arrows.*

9.4 Determination of kinetic parameters of LgoT and DgoT in pyranine assay

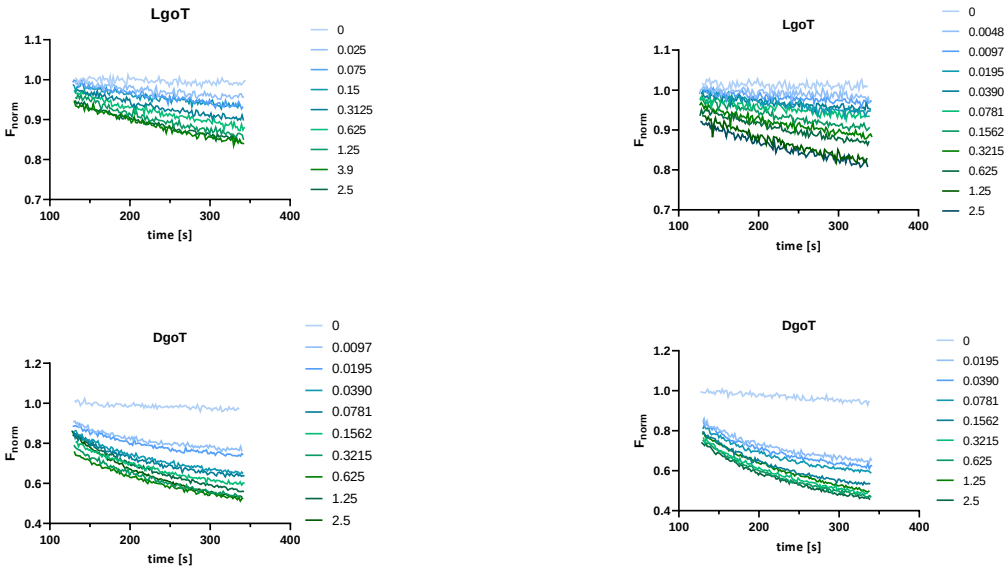

Figure 71: Transport curves for estimation of K_M and V_{max} of L-galactonate (top) and D-galactonate (bottom) for transport by LgoT and DgoT, respectively, measured using the pyranine assay. *For each peptide triplicate measurements are displayed and each graph shows the normalised and corrected curves for different peptide concentrations.*

9.5 Single concentration measurements for DtpB in SURFE^{2}R assay

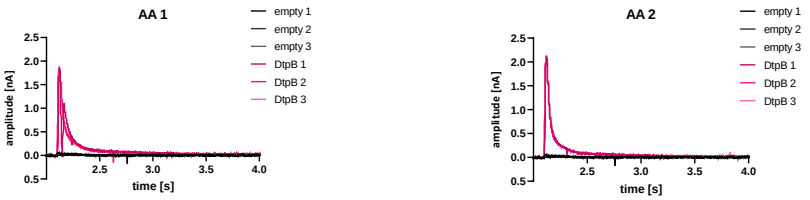

Figure 72: Overview of all transport curves for 20 mM AA in the SURFE²R assay using DtpB proteoliposomes. *Each plot shows the change in current over the time course of the measurement for empty liposomes and DtpB proteoliposomes with addition of substrate, in triplicates. Triplicates were performed on two different sensors.*

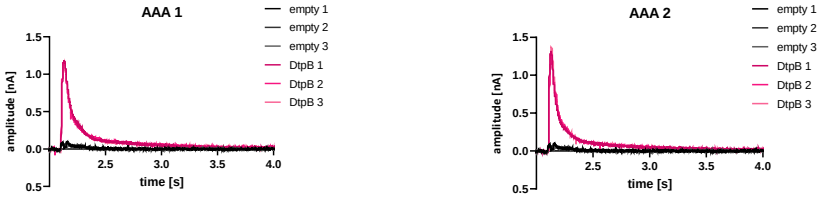

Figure 73: Overview of all transport curves for 20 mM AAA in the SURFE²R assay using DtpB proteoliposomes. *Each plot shows the change in current over the time course of the measurement for empty liposomes and DtpB proteoliposomes with addition of substrate, in triplicates. Triplicates were performed on two different sensors.*

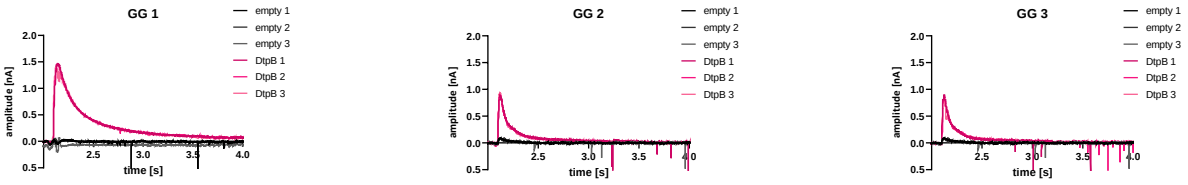

Figure 74: Overview of all transport curves for 20 mM GG in the SURFE²R assay using DtpB proteoliposomes. *Each plot shows the change in current over the time course of the measurement for empty liposomes and DtpB proteoliposomes with addition of substrate, in triplicates. Triplicates were performed on two different sensors.*

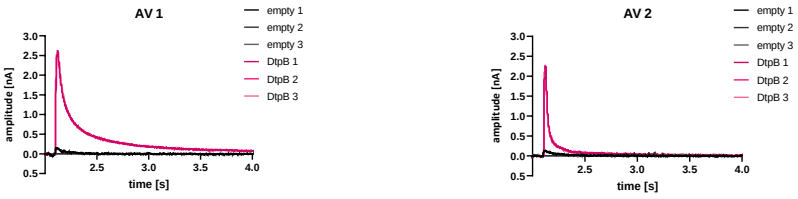

Figure 75: Overview of all transport curves for 20 mM AV in the SURFE²R assay using DtpB proteoliposomes. *Each plot shows the change in current over the time course of the measurement for empty liposomes and DtpB proteoliposomes with addition of substrate, in triplicates. Triplicates were performed on two different sensors.*

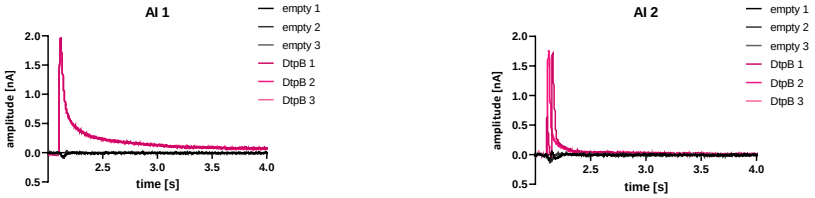

Figure 76: Overview of all transport curves for 20 mM AI in the SURFE²R assay using DtpB proteoliposomes. *Each plot shows the change in current over the time course of the measurement for empty liposomes and DtpB proteoliposomes with addition of substrate, in triplicates. Triplicates were performed on two different sensors.*

9.6 Determination of kinetic parameters of DtpB in SURFE²R assay

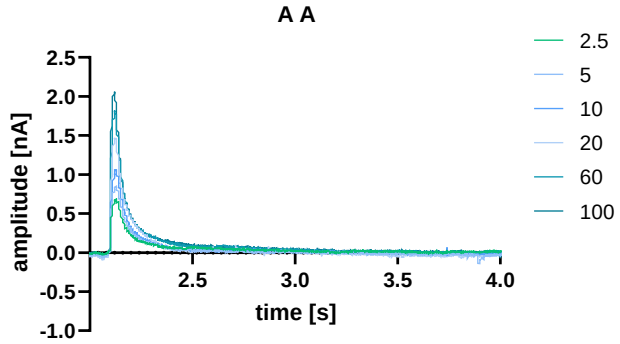

Figure 77: Transport curves for estimation of K_M and V_{max} of AA for transport by DtpB, measured using the SURFE²R assay. *Each AA concentration was measured in triplicates on one sensor. The plot displays the change in current over the time course of the measurements for each AA concentration.*

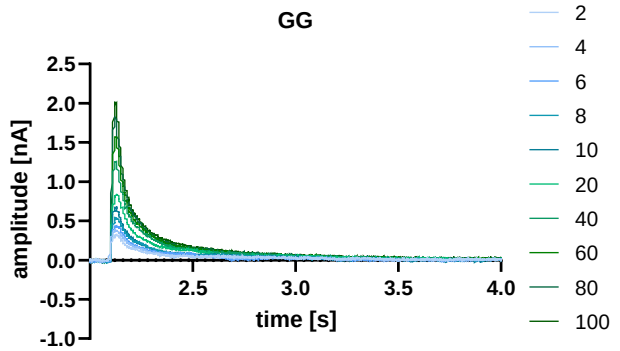

Figure 78: Transport curves for estimation of K_M and V_{max} of GG for transport by DtpB, measured using the SURFE²R assay. *Each GG concentration was measured in triplicates on one sensor. The plot displays the change in current over the time course of the measurements for each GG concentration.*

10 Declaration of Authorship

Hereby, I declare that I have composed the presented thesis independently on my own and without any other resources than the ones indicated. All thoughts taken directly or indirectly from external sources are properly denoted as such.

Date Signature: Josi Steinke